Regulation of mesenchymal stromal cell culture in 3D collagen and NiTi scaffolds by inflammatory and biomechanical factors

Inauguraldissertation

zur
Erlangung der Würde eines Dr. sc. med.
vorgelegt der
Medizinischen Fakultät
der Universität Basel
von

Waldemar Hoffmann

Tschujskur, Kirgisien

Basel, 2016

Genehmigt von der Medizinischen Fakultät

auf Antrag von:

Prof. Dr. Bert Müller (Fakultätsverantwortlicher)

Prof. Dr. Ivan Martin (Dissertationsleiter)

Prof. Dr. Michael de Wild (Korreferent)

Prof. Dr. Marcy Zenobi-Wong (Externe Expertin)

Basel, den 29. August 2014

(Datum der Zulassung durch die Fakultät)

………………………………..

Dekanin/Dekan

(Prof. Dr. med. Th. Gasser)

The value of an idea lies in the

using of it.

Thomas A. Edison

During my time as a PhD Student many people supported me in the scientific field. Moreover, I enjoyed the "distractions", which helped to recharge my batteries whenever necessary. Therefore I would like to thank: the "BIWlers" (**Bianca, Elena, Joe, Karin, Marius, and Simon**) for our hiking weekends; the "Andros gang" (**Adam and his family, Ben, Paul, Prasad, and Sinan**) for the wonderful time on the lovely Greek island.

I especially want to mention the support and encouragement I received from **Ben and Nora**, **Kathrin and Nico**, **Sandra**, and **Adam**, who always stood beside me.

For the support, their love and their unconditional back up during all the ups and downs I thank my parents (**Alfred** and **Irene**), my siblings (**Anna** und **Karl-Heinz**) and my extended family.

And last, but by no means least, I would like to wholeheartedly thank my wife and love of my life **Katharina** for her sustained encouragement, strong belief into my person, keen support and for taking the load off me whenever necessary!

"Our greatest weakness lies in giving up.
The most certain way to succeed is always to try just one more time."

Thomas A. Edison

Table of contents

General

Introduction

A.   Bone structure and properties

1. Function

Bone, the main supporting system of vertebrates, is defined as a "rigid body tissue consisting of cells embedded in an abundant, hard intercellular material. The two principal components of this material, collagen and calcium phosphate, distinguish bone from such other hard tissues as chitin, enamel, and shell. Bone tissue makes up the individual bones of the human skeletal system and the skeletons of other vertebrates." (*Encyclopedia Britannica*)

In more detail, bone is a highly vascularized and mineralized connective tissue, which together with cartilage, tendons and ligaments constitutes the skeletal system. The functions of bone in mammals include (i) structural support for mechanical actions as locomotion, (ii) protection of vital organs and soft tissues, (iii) site of hematopoiesis (Taichman 2005), and (iv) reservoir of calcium and phosphate (Clarke 2008).

Bone is a specialized bi-phasic connective tissue with nonhomogeneous, anisotropic mechanical properties. The two phases consist of organic (30 wt-%) and inorganic (60 wt-%) components and are completed by 10 wt-% of water. The distinct composition and structure of bone leads to functionally adapted mechanical properties as ductility, brittleness and viscoelasticity. Moreover, the ultimate compressive and tensile strengths of bone are in the range of 100-200 MPa and 50-130 MPa, respectively (Keaveny et al. 2004; Weiner & Wagner 1998).

2. Bone anatomy

2.1. Anatomical structure

Bone is classified according to its gross anatomy into flat, long, short or irregular bones. The principle function of flat bones, e.g. skull, pelvis, scapula, is either extensive protection of underlying tissues and organs or the provision of large surface in order to facilitate muscle and tendon attachment. Flat bones are composed of a three-layered structure with two thin layers of compact bone enclosing an in thickness variable layer of cancellous bone. The void within the cancellous bone is filled with bone marrow giving rise to most of the red blood cells in adults (Clarke 2008).

Long bones are found in the limbs consisting of a diaphysis (body or shaft) and two extremities. The diaphysis has a cylindrical shape, with a central cavity named medullary canal. As for flat bones, the medullary canal is filled with bone marrow. The wall of the diaphysis consists of dense, compact bone getting spongier towards the medullary cavity. The extremities of long bones are expanded in order to allow for both articulation and muscular attachment. They consist of cancellous bone covered by a thin layer of compact bone. The development of the extremities is initiated by separate ossification centers termed epiphysis. Long bones, as for example the femur, are curved in two planes accounting for their high strength (Gray et al. 1973).

Examples for short and irregular bones include the patellae and the vertebrae, respectively.

2.2. Hierarchical structure

The bone tissue is build up in a hierarchical structure comprised of up to seven levels of organization (Figure 1). As for all biological substances, the building blocks of bone are amino acids in the form of polypeptide strands. Collagen molecules (tropocollagen) are mainly consisting of the amino acid glycine. Tropocollagen is a subunit of larger collagen aggregates (collagen fibrils) and is made up of three polypeptide strands organized in a triple helix. Each collagen molecule is arranged parallel with the other molecules head to tail. This arrangement leaves a gap of approximately 40 nm between each molecule. This gap is the starting point for mineralization, which further extends to other intramolecular spaces leading to mineralized collagen fibrils arranged in fibril arrays. The ceramic crystalline-type mineral consists of spindle- or plate-shaped crystals of carbonated
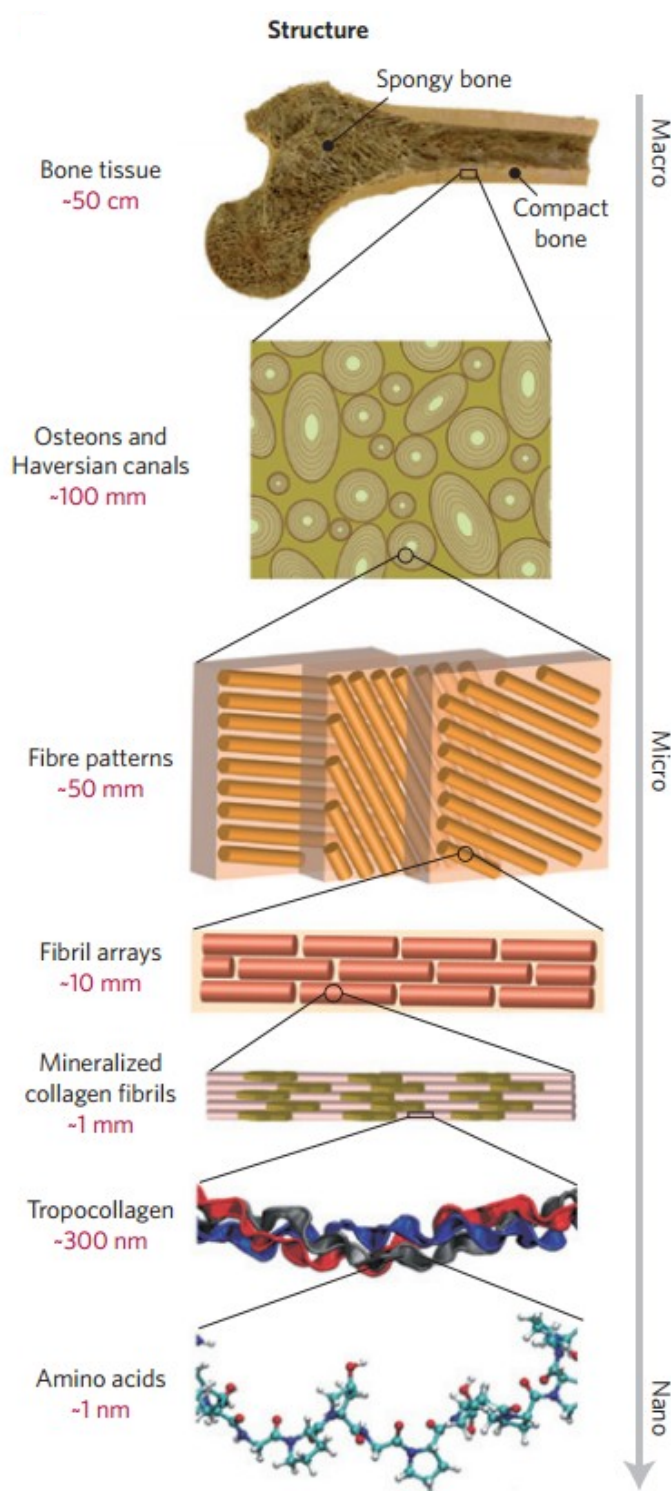
Figure 1 The seven levels of bone hierarchy (Ritchie 2011).

hydroxyapatite $(Ca_{10}(PO_4)_6(OH)_2)$. In order to facilitate the high tensile and compressive strength of bone, fibril arrays are stacked in a non-parallel manner giving rise to distinct structure as osteons (cylindrical motifs of fibril arrays), the Haversian canals (HC, longitudinal canal within an osteon) and the Volkmann canals (transversal canals connecting HC) (Keaveny et al. 2004) (Figure 2).

Besides the structural components of bone, organic components are important for the maintenance and the function of bone. Solely 2% of the organic fraction is made up by cells (osteoblasts, osteocytes, osteoclasts), growth factors [e.g. fibroblast growth factors (FGFs), platelet-derived growth factors (PDGFs), transforming growth factor-beta (TGF-β) and bone morphogenic proteins (BMPs)] and cytokines [e.g. Interleukin 1-beta (IL-1b), Interleukin 6 (IL-6), tumor necrosis factor (TNF)] (de Vernejoul et al. 1993). About 90% of the organic extracellular matrix (ECM) is composed of type-I collagen fibrils. The remaining fraction composes proteoglycans and non-collagenous proteins, such as bone sialoprotein II (BSP), osteocalcin (OC), and osteopontin (= bone sialoprotein I, OP) (Manolagas & Jilka 1995; Post et al. 2010).
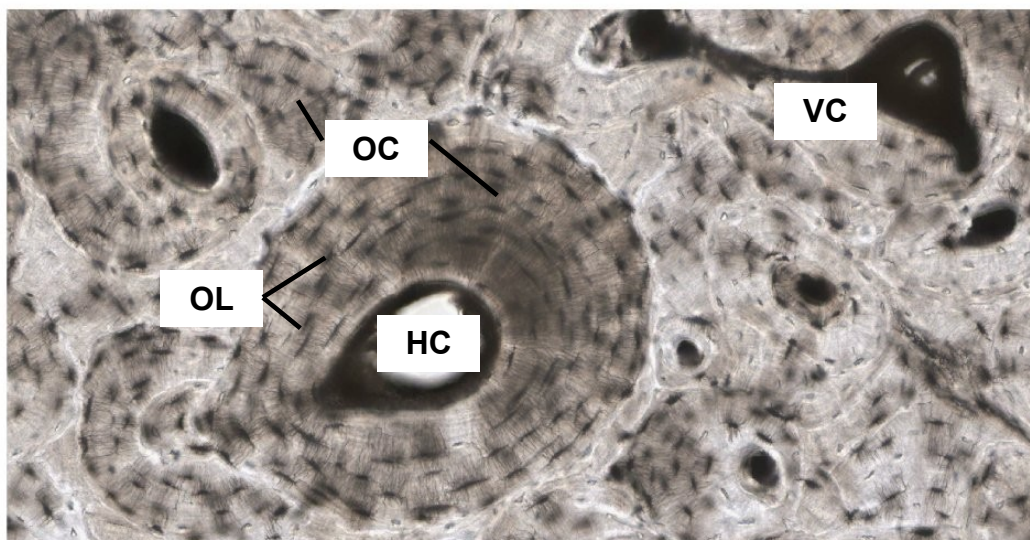
Figure 2 The osteon units of bone.
The osteon is made up of osteocyte lacunae (OL), osteocyte canaliculi (OC), Haversian canals (HC) and Volkmann canals (VC) (OpenStax College 2014).

The major cell types in the bone tissue are osteoblasts, osteocytes and osteoclasts. Osteoblasts are bone forming cells derived from local pluripotent mesenchymal stromal cells (MSC). These MSC are originating from either the bone marrow or the periosteum. The functions of osteoblasts include synthesis and secretion of non-mineralized bone matrix containing alkaline phosphatase, type-I collagen, osteonectin and osteocalcin and the regulation of osteoclast function. Lining the bone surface, osteoblasts are gradually entrapped in the bone matrix that they secrete resulting in a dramatic decrease of their metabolic activity. These entrapped, stellate-shaped cells are fully differentiated mature bone cells (osteocytes) (Bonewald 2011; Knothe Tate et al. 2004). Osteocytes are the most abundant cell type in bone tissue accounting for about 90% of cells in the mature skeleton. Inter-osteocytic communication and the communication between osteocytes and bone lining cells are carried out with the help of the well-developed canalicular network consisting of extended cytoplasmic processes. Though osteocytes are relatively inert cells, they are involved in the maintenance of bone, the homeostasis of calcium and phosphorous as well as signal transmission via their processes (Knothe Tate et al. 2004; Noble 2008; Bonewald 2011).

Osteoclasts originate from hematopoietic cells of the macrophage lineage. Through the fusion of monocyte progenitors they form mature multinuclear cells. The main function of osteoclasts is resorption of bone (Nordin & Frankel 2001). The well organized and orchestrated interplay of the previously describe cell types is crucial for bone homeostasis, remodeling and repair.

3. Bone formation

In the early stages of embryonic development, the embryo's skeleton consists of hyaline cartilage. By the sixth or seventh week of embryonic life, the actual process of bone development begins. Bone formation or ossification during the fetal stage of development occurs by two distinct processes: *intramembranous ossification* and *endochondral ossification*.

3.1. Intramembranous ossification

Intramembranous ossification occurs during formation of the flat bones of the skull, the flat part of the clavicle and during primary fracture healing. In this ossification process, compact and spongy bone is formed by direct bone matrix deposition. The process begins through condensation of MSC, which then differentiate into osteoblasts (Figure 3a). The osteoblasts secrete type-I collagen fibrils that make up the osteoid. The osteoid, an uncalcified matrix, calcifies within a few days through the deposition of mineral salts forming calcified bone matrix (Figure 3b). During the next step, trabeculae are formed through the random creation of osteoids around blood vessels. Simultaneously, the periosteum is formed through condensation of the blood vessels surrounding the bone (Figure 3c). Lastly, the development of red bone marrow and compact bone through thickening of the trabeculae occurs (Figure 3d).

Intramembranous ossification is a process that begins during fetal development and continues throughout adolescence. At birth, the skull, the sutures of the skull and clavicles are not fully ossified allowing for deformation of the skull and shoulders during passage through the birth canal (Karaplis 2008; Franz-Odendaal 2011).
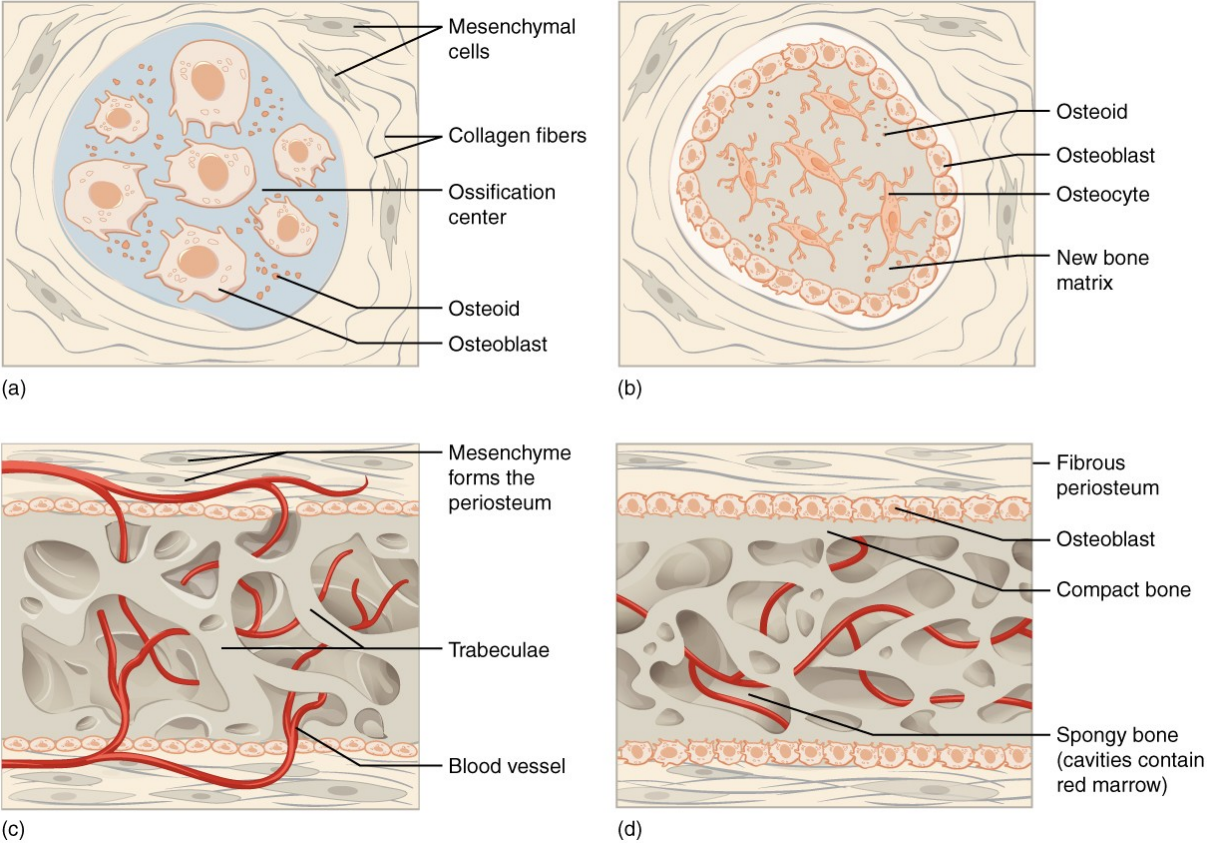
Figure 3 Intramembranous ossification.

(a) Mesenchymal stromal cell condensation and osteogenic differentiation. (b) Osteoid formation. (c) Trabeculae and periosteum formation. (d) Compact bone and bone marrow develops (Browne 2013).

3.2. Endochondral ossification

Endochondral ossification occurs in most of the bones, especially in long bones, in vertebrates and during secondary (non-rigid) fracture healing. During this process, hyaline cartilage is subsequently replaced by bone. The cartilage intermediate serves as a template in terms of size and shape (Kronenberg 2003). Endochondral ossification begins with the development and growth of the cartilage "model" through condensation of mesenchymal cells and their subsequent differentiation into chondrocytes (Figure 4a). Due to low oxygen conditions, chondrocytes differentiate further into hypertrophic chondrocytes and start to mineralize their surrounding matrix. Through the mineralized matrix nutrients can no longer reach the chondrocytes leading to cell death and the disintegration of the surrounding matrix (Figure 4b). Blood vessels invade the resulting spaces carrying osteogenic and osteo- and chondroclastic cells, thereby forming the primary ossification center. At the same time transformation of the perichondrium towards the periosteum is initiated leading to the formation of the periosteal collar (Figure 4c). During this ossification step, cartilage continues to grow and chondrocytes proliferate at the ends of the bone (epiphysis) increasing bone length (Figure 4d). This process occurs along with the replacement of cartilage by bone in the diaphysis leaving cartilage remanence at the joint surfaces (articular cartilage). Additionally, the epiphyseal growth plate remains between the diaphysis and epiphysis. The same sequence of events occurs in the epiphyseal regions leading to secondary ossification centers (Figure 4e). Lastly, the creation of the epiphysis is finalized including the joint surface and the epiphyseal (growth) plate (Figure 4f) (Gawlitta et al. 2010; Mackie et al. 2008; Mackie et al. 2011).
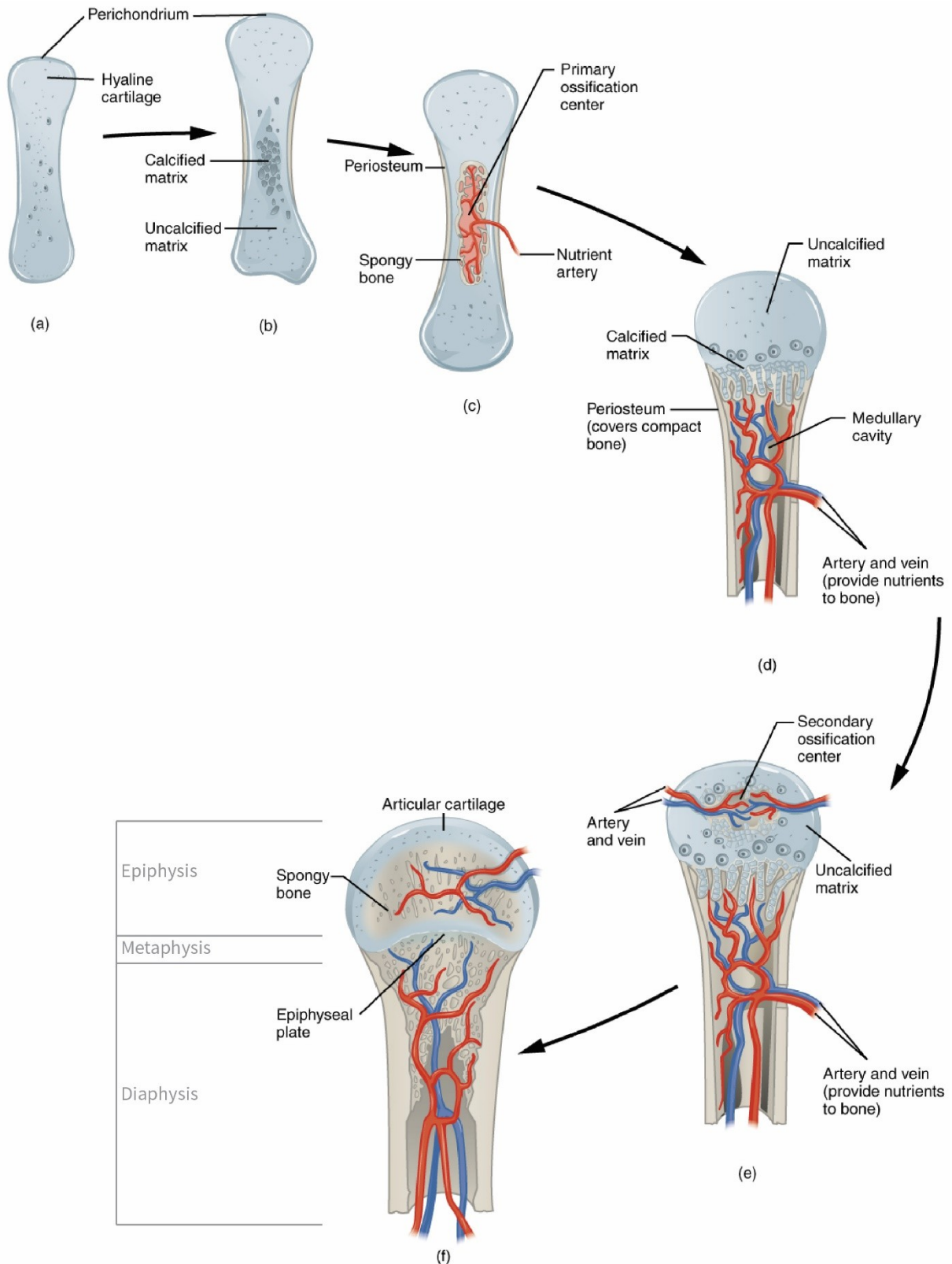
Figure 4 Endochondral ossification.

(a) Mesenchymal stromal cell condensation and chondrogenic differentiation. (b) Cartilage calcification and perichondrium formation. (c) Vascular invasion and formation of primary ossification center. (d) Cartilage growth at the ends of the bone. (e) Secondary ossification centers develop. (f) articular cartilage and epiphyseal plate remain uncalcified (Browne 2013).

4. Bone remodeling

Bone is a dynamic tissue that is remodeled in response to the mechanical forces, a phenomenon described by Wolff's Law (Wolff 1892). This phenomenon is a balanced process of bone resorption and formation, which is choreographed spatially and temporally. Tight coupling of these processes is required to maintain the skeleton (Hauge et al. 2001). A key trigger of bone remodeling is the local mechanical environment. In particular load bearing induces fluid shear stress within the canalicular network, which leads to an onset of osteocyte signaling and therewith either an activated or repressed bone formation by osteoblasts (Chen et al. 2010). These facts suggest that mechanical stimuli are among the most potent factors acting in the processes of bone remodeling (Chen et al. 2010). Ultimately bone remodeling is mediated by the cells related to the bone tissue: osteocytes, being the putative mechanosensors; osteoblasts, depositing new bone matrix; osteoclasts, resorbing fatigue bone matrix; and their progenitors (osteoblasts, mesenchymal stromal cells and mononuclear cells, respectively) (Figure 5).

© 2013 Encyclopædia Britannica, Inc.
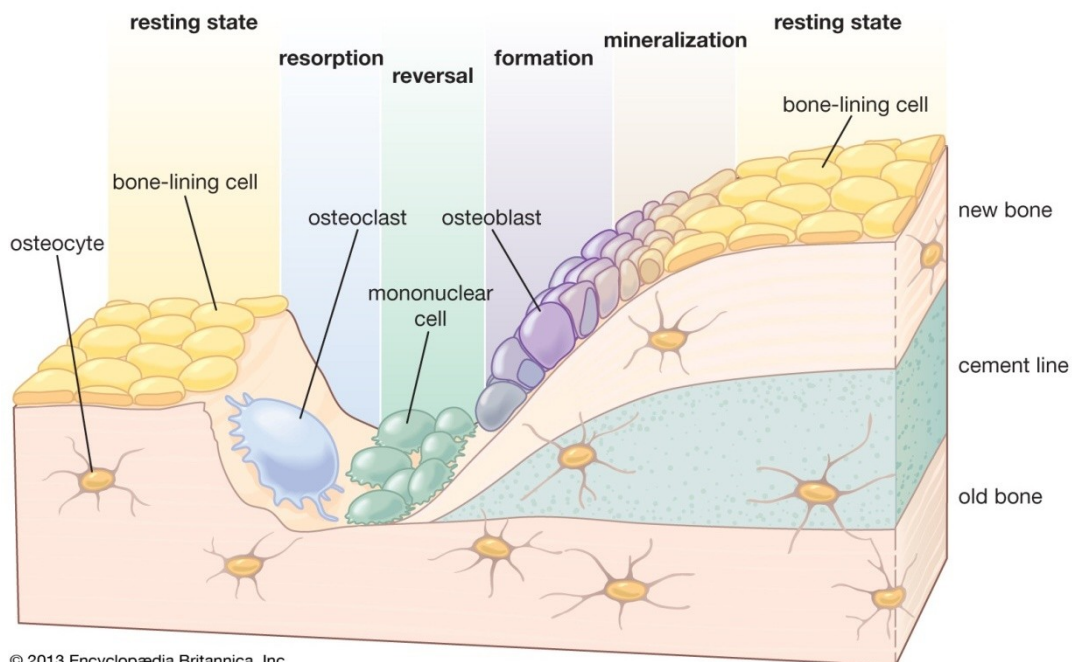
Figure 5 Bone remodeling phases (Anon 2014).

B.   Bone fracture healing

Fracture healing is a natural, physiological process leading to the repair of bone fractures. It is a highly orchestrated sequence recapitulating the processes of bone formation. Unlike soft tissue healing, which leads to scar formation, bone fracture healing results in functional tissue regeneration (Gerstenfeld et al. 2003; Behonick et al. 2007; Marsell & Einhorn 2011). As for bone formation, fracture healing occurs in two distinct processes: *primary* and *secondary* fracture healing. Stable fractures (interfragmentary strain <2%) heal along the primary (direct) fracture healing process (Shapiro 1988), whereas the majority of fractures heals along the secondary (indirect) fracture healing process.

1. Primary fracture healing

Primary fracture healing directly aims at re-establishing the anatomically correct and biomechanically competent lamellar bone structure with minimal or no formation of a fracture callus. This attempt is solely functioning when the ends of fractured bone are in direct contact and an intact vasculature is available (Sfeir et al. 2005). Due to this fact, primary healing occurs only after rigid surgical fixation or unicortical fractures (partial fracture of the bone). The process of primary fracture healing is initiated and lead by a cutting cone comprising osteoclasts resorbing bone fragments at the tip of the cone followed by osteoblasts laying down new bone matrix (Marsell & Einhorn 2011).

2. Secondary fracture healing

Secondary fracture healing is a process that resembles certain aspects of skeletal development and growth following the endochondral route. The process is generally divided into 4 phases (Figure 6): a) hemorrhage and inflammation; b) soft callus

formation; c) hard callus formation; d) callus remodeling (Sfeir et al. 2005; Schindeler et al. 2008). These phases are not strictly separated; instead there is often a significant overlap between them. The key features of secondary fracture healing are ossification of the cartilaginous (soft) callus and its complete remodeling leading to full regeneration and re-establishment of the bone functionality (Gerstenfeld et al. 2003).
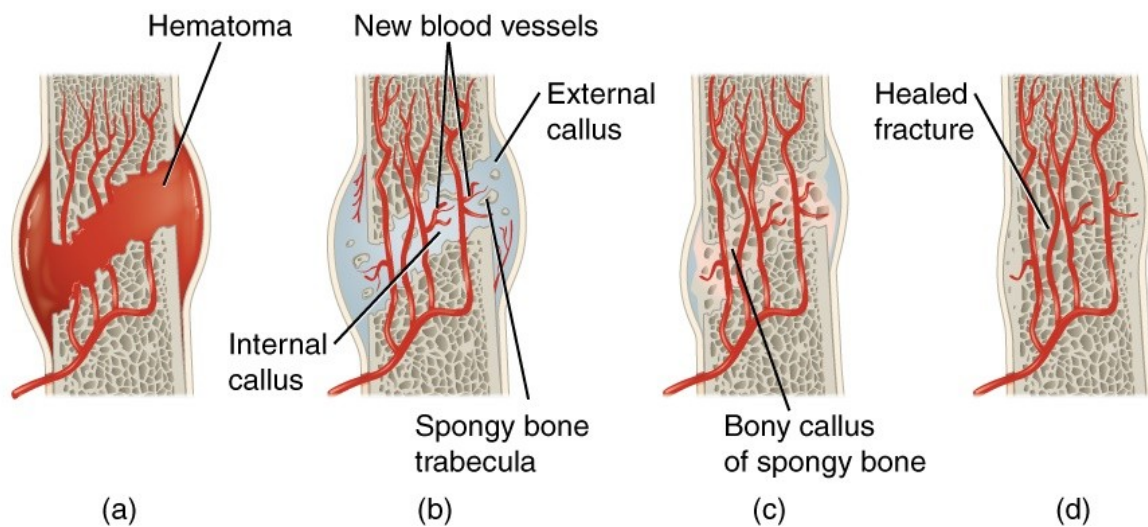
Figure 6 Secondary fracture healing.
(a) Hemorrhage and inflammation. (b) Soft callus formation. (c) Hard callus formation.
(d) Callus remodeling (OpenStaxCollege 2014).

a) Hemorrhage and inflammation

A fracture leads to the disruption of the local tissue integrity including the vasculature, soft tissues and the bone marrow. The bleeding develops into a hematoma, which activates platelets, plasma components, macrophages, and other inflammatory cells. These cells secrete cytokines (interleukin-1 (IL-1), IL-6, IL-11 and IL-18) and growth factors (e.g. transforming growth factors-β (TGF- β), tumor necrosis factor-α (TNF-α)) and thereby enable the migration and invasion of multipotent MSC into the granulation tissue (Figure 6a) (Gerstenfeld et al. 2003; Sfeir et al. 2005; Schindeler et

al. 2008). Furthermore, hypoxia induces angiogenesis through the hypoxia inducible factor 1 alpha (HIF1α) pathway (Wang et al. 2007; Wan et al. 2008).

b) Soft callus formation

Due to fracture instability, a soft callus, both internally and externally, is formed within 2 weeks post fracture. Mesenchymal progenitors are activated by signaling molecules (e.g. IL-6, TNFα) and recruited to the fracture site (Raheja et al. 2011). The sources of osteoprogenitors are mainly the bone marrow and the periosteum, but also include the circulation, the vasculature, and surrounding local tissues. The recruited cells differentiate towards osteoblasts and chondrocytes and deposit ECM. The semi-rigid callus provides mechanical stability and -as for endochondral bone formation- depicts a template for the bony callus formed in the subsequent phase. The chondrocytes replace the granulation tissue by a synthesized cartilaginous matrix mainly consisting of type-II collagen. As soon as the entire granulation tissue is replaced, chondrocytes undergo hypertrophy, mineralize the cartilaginous template, and undergo apoptosis. Following, the mineralized soft callus is vascularized through invasion of vascular endothelial cells and capillary ingrowth (Figure 6b) (Sfeir et al. 2005; Schindeler et al. 2008).

c) Hard callus formation

This phase demonstrates the most active period of osteogenesis. Osteoblasts reach their maximal activity and in collaboration with other cell types gradually replace the mineralized cartilaginous template with unordered, woven bone matrix. Due to the stability gained through the mineralization of the internal callus, the external callus is resorbed. To ensure full maturation of osteoblasts an increased oxygen tension is required. Therefore vascularization of the callus is crucial in order to develop the formation of a hard callus (Figure 6c) (Sfeir et al. 2005; Schindeler et al. 2008).

  d) Callus remodeling

The final phase of the secondary fracture healing process aims at the entire remodeling of the woven bone towards cortical and/or trabecular bone. It resembles the bone remodeling process including the involvement of osteoblasts and osteoclasts in a spatially and temporally choreographed manner (Figure 6d) (Sfeir et al. 2005; Schindeler et al. 2008).

3. Parameters affecting bone fracture healing

Bone fracture healing is a highly complex and tightly regulated process. It is influenced by many factors including mechanical stability (severity and location of fracture), environmental cues (vascularization, availability of growth factors and cytokines), nutrient supply, and medication. The key process within the progression of fracture healing is callus remodeling (Schindeler et al. 2008). During the process of fracture healing numerous cell types (e.g. osteoblasts, MSC, chondrocytes, inflammatory cells, macrophages, etc.) are actively involved and are responding to the given environmental cues. These cues comprising biochemical [e.g. insulin-like growth factor (IGF)-I, IGF-II, TGF-β, IL-1β, IL-6 (Caetano-Lopes et al. 2011; Lange et al. 2010)] and biomechanical (deformation of formed tissue, fluid flow, biophysical loads) signals control tissue differentiation, cell proliferation, ECM synthesis as well as tissue remodeling within the fracture callus (Schmidmaier et al. 2003; Ethier & Simmons 2007).

The presence and timing of the regulatory system of biochemical cues direct the healing processes during the different stages of bone fracture healing. The signaling molecules involved are classified into three groups: pro-inflammatory cytokines, TGF-β superfamily and other growth factors, and angiogenic factors (Dimitriou et al. 2005; Tsiridis et al. 2007). The pro-inflammatory cytokines (e.g. IL-1, Il-6, TNF-α) are

secreted by macrophages, other inflammatory cells, and by cells of mesenchymal origin during the initial stages of fracture healing. Besides their function in the recruitment of inflammatory cells, cytokines play a crucial role in the regulation of ECM synthesis, stimulation of neo-vascularization and homing of MSC (Dimitriou et al. 2005; Tsiridis et al. 2007). The members of the TGF-β superfamily (e.g. TGF-β, IGF-I and –II, platelet-derived growth factor (PDGF), bone morphogenetic proteins (BMPs), etc.) are involved in the regulation of proliferation and differentiation of MSC towards chondrocytes and osteoblasts (Bostrom et al. 1995; Dimitriou et al. 2005; Phillips 2005) and are known to accelerate bone fracture healing (IGF-I, (Shen et al. 2002)]. Moreover, BMPs may depict key molecules within the signaling cascade linking mechanical forces with biological responses (Sato et al. 1999; Rauch et al. 2000). Angiogenic factors (e.g. vascular endothelial growth factors (VEGFs), angiopoetin-1 and -2, HIF-1α) are the key mediators of the fracture site vascularization (Dimitriou et al. 2005).

Bone fragments, independent of the method of fracture fixation, experience a certain degree of motion when loads are applied determining the morphological structures of the fracture healing process. The "interfragmentary strain theory" relates the tissue response to the mechanical environment and defines the interfragmentary strain as "the ratio of the relative displacement of the fracture ends versus the initial gap width". This theory is an oversimplification of the actual biomechanical processes and biological responses. At the same time it depicts the basis for the understanding of the influence of biophysical stimuli on the process of fracture healing. **The mechanical environment of fractures such as interfragmentary strain and rigidity of fixation has been shown to play an important role in the processes of fracture healing and tissue differentiation** (Chao & Inoue 2003). Additionally, it has been demonstrated that mechanical stimulation of fractures can induce/trigger

their healing or alter the biological pathways involved. Crucial mechanical loading-related parameters comprise: strain amplitude, frequency, stimulation pattern (loading and resting phases), fracture geometry, and direction of loading (Rand et al. 1981; Goodship & Kenwright 1985; Aro et al. 1991; Claes et al. 1997; Park et al. 1998; Rubin et al. 2001). These parameters have been studied both *in vitro* (Démarteau et al. 2003; Matziolis et al. 2006; Sun et al. 2010; Lujan et al. 2011; Puetzer et al. 2012) and *in vivo* (Park et al. 1998; Hente et al. 2004; Willie et al. 2010). Nevertheless, some studies correlated local mechanical environments and their effects on tissue differentiation or fracture healing patterns with the tissue differentiation theories (Claes & Heigele 1999) using finite element modeling (FEM) (Prendergast 1997; Lacroix 2000; Loboa et al. 2005; Lacroix et al. 2002). These studies emphasize the complex processes occurring during fracture healing. In 1999, Claes and Heigele (Claes & Heigele 1999) hypothesized the following relations between strains in a fracture site and the outcome obtained during fracture healing (Figure 7): small strains and small hydrostatic pressures < ±0.15 MPa lead to direct bone formation, compressive hydrostatic pressures > 0.15 MPa lead to chondrogenesis and therefore endochondral ossification, and all other stimuli lead to connective tissue or fibrocartilage formation. However, more recently (2004) Smith-Adaline et al. (Smith-Adaline et al. 2004) demonstrated that intermittent tensile strains promote endochondral ossification and compressive strains promote intramembranous ossification. These studies, upon others, emphasize that effects induced through biophysical processes during fracture healing are not entirely understood.
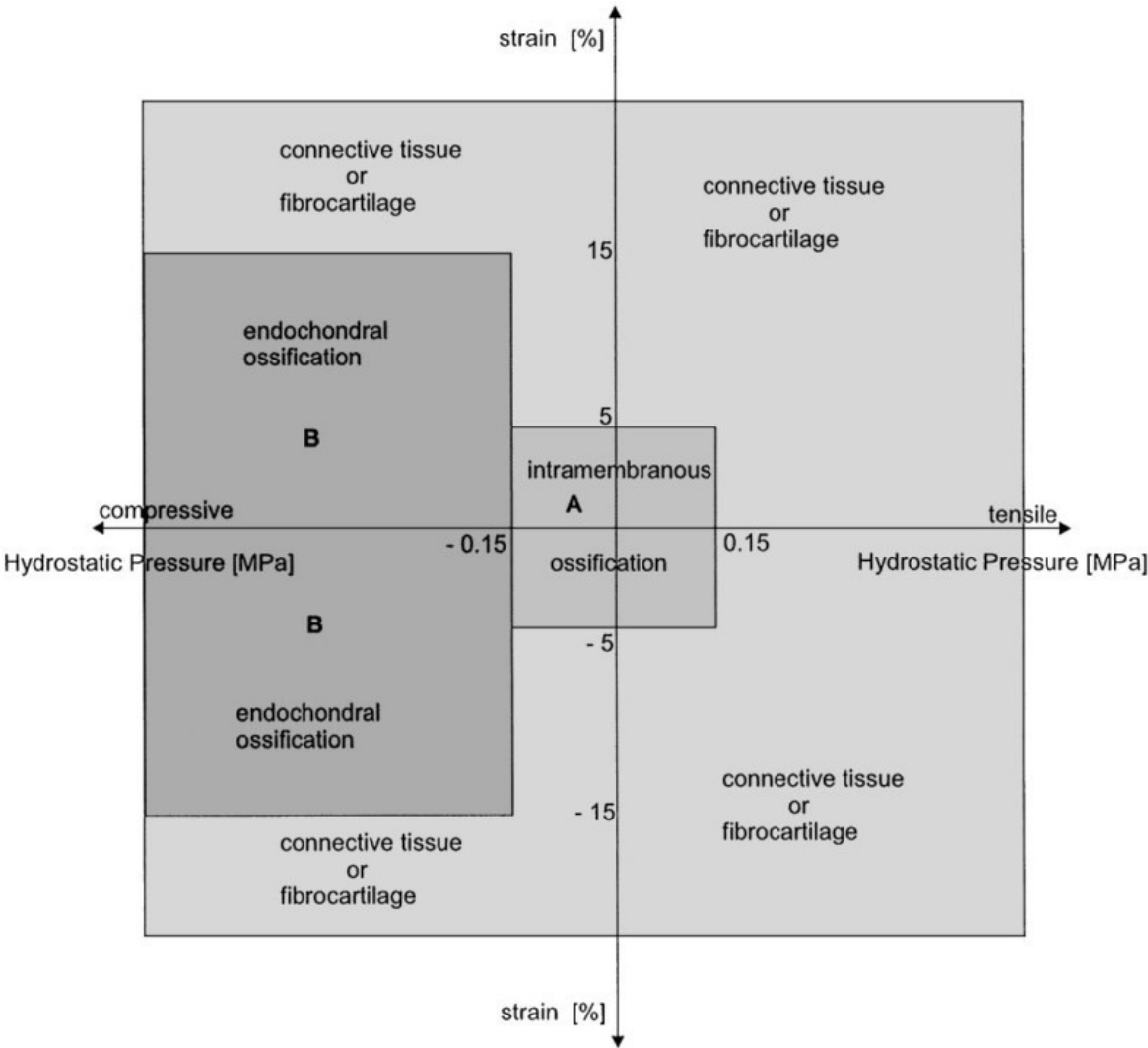
Figure 7 Hypothesis-based correlations between mechanical conditions and types of tissues generated in a fracture callus. Adopted from (Claes & Heigele 1999).

C.   Tissue Engineering

The origin of Tissue Engineering (TE) can be traced to Y.C. Fung, a pioneer in the fields of biomechanics and bioengineering. In 1985 he submitted a proposal to the American National Science Foundation for an engineering research center to be entitled "Center for the Engineering of Living Tissues". Nevertheless, the understanding of TE as a unifying concept for a broad range of interdisciplinary fields of research can be dated back to the publication of a review paper by Robert Langer and Joseph P. Vacanti in 1993. Since then tissue engineering has been defined as "an interdisciplinary field that applies the principles of engineering and the life sciences toward the development of biological substitutes that restore, maintain, or improve tissue function" (Langer & Vacanti 1993).

The general principle of TE includes the combined utilization of biomaterials, (stem) cells and signals (e.g. growth factors, mechanical stimuli), the so called "tissue engineering triad" (Lanza et al. 2000). This triad is used in several combinations and variations following the tissue engineering paradigm (Figure 8).

Autologous cells, mainly MSC, are harvested from patient's bone marrow, adipose or other tissue. They are capable of *in vitro* differentiation into the mesodermal cell lineages, like osteoblasts, chondrocytes and adipocytes. The MSC are cultured *in vitro* in monolayer cultures expanding them towards a sufficient amount of cells. The expanded MSC are further cultured on three-dimensional constructs, termed scaffolds, and additional stimuli including biochemical (growth factors, small molecules, etc.) and biomechanical (shear, compression, etc.) ones, are applied. These stimuli prime the MSC towards a desired lineage forcing them to differentiate and maturate. During this process a tissue specific extracellular matrix is deposited

and the hybrid cell-ECM-scaffold construct develops towards a functional graft. The engineered, functional graft is used as an "autologous" implant for the patient.
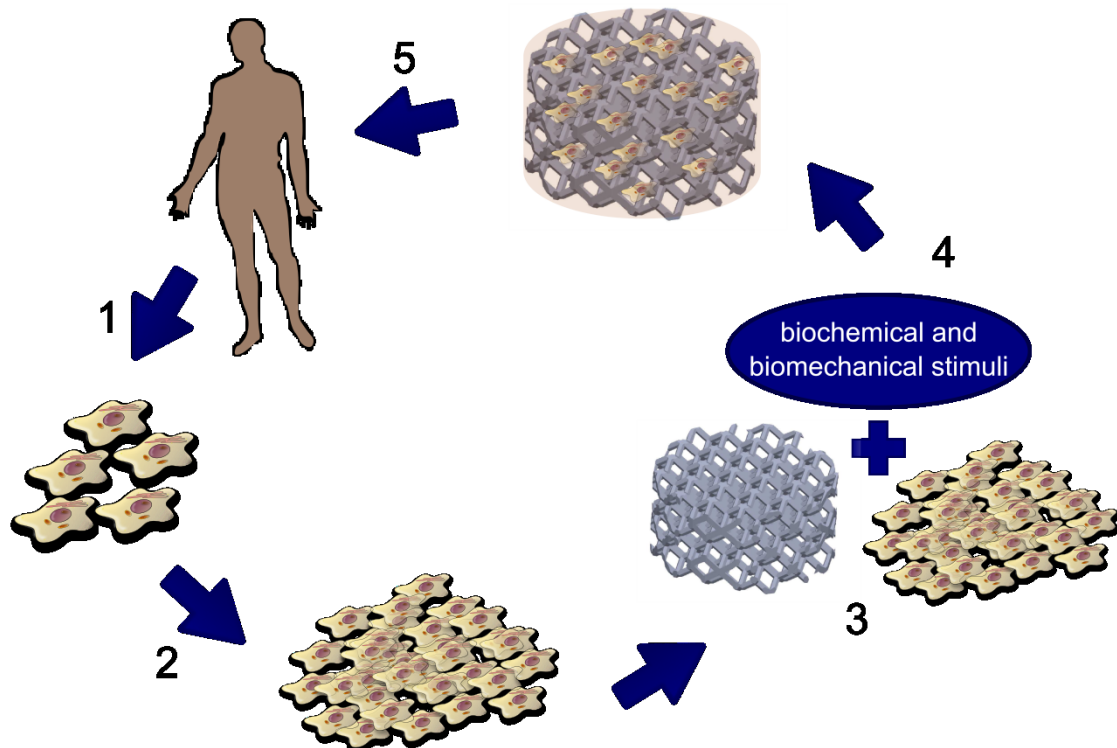
Figure 8 Tissue engineering paradigm.
Autologous (stem) cells are harvested (1) and expanded (2) *in vitro*. Reaching a sufficient cell number, cells are seeded onto a 3D scaffold (3). Further *in vitro* culture including biochemical as well as biomechanical stimuli leads to tissue formation and maturation (4). Finally, the obtained graft is implanted into the patient (5).

Bone tissue engineering (BTE) aims at the development of alternatives to the conventional bone grafting procedure via *in vitro* generation of engineered, functional bone substitutes. When bone repair mechanisms fail, bone grafting has been shown to be a highly potent alternative. Bone grafting is a procedure in which bone from a different location is harvested in order to bridge the gap and to stimulate bone formation at the fracture site. The graft can be of several origins: autologous (patient's own bone), allogeneic (bone from other humans), xenogeneic (bone from other species) or synthetic (biomaterial). Each of the mentioned origins of the bone

graft holds certain advantages (mechanical strength of the graft, availability, quality, etc.) and disadvantages (transmission of diseases, donor site morbidity, etc.).

Following the tissue engineering paradigm, constructs based on autologous cells and synthetic biomaterials ideally could replace autologous bone grafts (van Gaalen et al. 2008). However, BTE-derived products are just starting to enter clinical applications due to several limitations and challenges, such as lacking sufficient vascularization at the defect site, lacking FDA approval, and cost-effectiveness (Amini et al. 2012).

1. Biomaterials

The first reported application of "biomaterials" dates back to 3000 B.C. In ancient Egypt linen threads have been used to close wounds (surgical suture). The first dental implant, a shell shaped to fill the defect, was placed according to carbon dating in 900 A.D. It was implanted in Europe and was found to be properly integrated into the surrounding bone (Bobbio 1972; Gentleman et al. 2009).

According to the American National Institute of Health biomaterials can be defined as "any substance or combination of substances, other than drugs, synthetic or natural in origin, which can be used for any period of time, which augments or replaces partially or totally any tissue, organ or function of the body, in order to maintain or improve the quality of life of the individual" (NIH Consens Statement 1982). Nevertheless, this definition lacks the fact that biomaterials have to be biocompatible, i.e. show the ability to perform with an appropriate host response in a specific situation (Williams 1999). The possible host tissue reactions are used to classify biomaterials: (i) bio-tolerant materials (no adverse host reaction, mostly fibrous encapsulation), (ii) bio-active materials (trigger a desired, positive biochemical host response) and (iii) bio-inert materials (no biochemical response occurs) (Bergmann & Stumpf 2013).

Nowadays, biomaterials are used for many applications including long- and short-term implants, sensors, scaffolds for tissue engineering, and surgical tools and auxiliary material (e.g. tubes, blood bags, etc.). Biomaterials can be derived from natural components or synthesized using a variety of chemical approaches. Table 1 summarizes the biomaterial classes and their applications in the biomedical field (Ratner et al. 1996).

Table 1 Classification of biomaterials (Ratner et al. 1996)

Class of biomaterial	Properties of class	Examples & applications
Metals	mechanically strong, excellent electrical and thermal conductivity, though, ductile; may corrode, very dense, may cause allergies	stainless steel, Ti, Ti-based alloys (Ti6Al4V), gold, etc.; joint replacements, bone plates and screws, used in orthopedics, oral & maxillofacial or cardiovascular surgery and as surgical tools, etc.
Polymers	resilient, easy to fabricate; may degrade, deform with time, mechanically weak, may provoke inflammatory response	poly-ether-ether-ketone (PEEK), polyester, polyurethane (PUR); sutures, facial prosthesis, joints, blood vessels, etc.
Ceramics, glasses and glass-ceramics	very biocompatible, inert, strong in compression; brittle, non-resilient, difficult to manufacture	calcium phosphates, circonia, aluminum oxides; femoral head of hip replacement, coating of dental and orthopedic implants
Natural materials	biocompatible, geometry and composition mimics *in situ* environment; may be immunogenic, difficult to manufacture and to maintain constant quality	Proteins (silk, collagen, fibrinogen, etc.), polysaccharides (cellulose, glycosaminoglycan (GAG), etc.), polynucleotides (DNA, RNA) ; sutures, bone substitute, heart valves, etc.
Bioresorbable materials	resilient, easy to fabricate; deform with time, mechanically weak	polylactide (PLA), polyglycolide (PGA), polycaprolcatone (PCL), beta-tri-calcium phosphate (β-TCP), magnesium; sutures, drug delivery device, adhesion prevention
Composites	strong, tailor-made; difficult to manufacture, biocompatibility	wire, particle or fiber reinforced composites; bone cements, joint implants, heart valves
Biologically functionalized materials	biological "activation" of inert biomaterials; difficult to manufacture	immobilized enzymes, antibodies, lipids, substrates; cancer treatment, improvement of osseointegration (BMP immobilization), etc.

As for the materials, a high degree of versatility exists for their manufacturing, cleaning and sterilization procedures. In the following paragraph, a short description of the additive manufacturing process in particular of biomaterials will be given.

Additive manufacturing or 3D printing (3DP) is known since the 1980s. Nevertheless, it has traditionally been used during product development to manufacture concept prototypes ("rapid prototyping") prior to production. However during the last years there has been increased interest to adopt the technology as a full-scale manufacturing solution. The technology fabricates 3D objects in a bottom-up, additive manner using digital computer aided design (CAD) (Chua et al. 2010). In contrast to conventional methods (e.g. drilling, milling, turning, etc.), where material is removed (subtractive processes), 3DP deposits material or fuses powdered material in successive steps, where thin layers finally build-up a solid 3D object. Depending on the materials used (metals, ceramics, polymers) different methods/technologies are applied to solidify the powders. These technologies include *fused deposition molding* (FDM, polymer and eutectic metals), *electron beam free-form fabrication* (EBF, metal alloys), *direct metal laser sintering* (DMLS, metal alloys), *electron-beam melting* (EBM, titanium alloys), *selective laser sintering* (SLS, thermoplastic, ceramic and metallic powders), *selective laser melting* (SLM, Figure 9, titanium alloys, stainless steel, aluminum), *stereo-lithography* (SLO, photopolymers) and others (Wong & Hernandez 2012). These techniques are recently employed for the production of complex-shaped, anatomically inspired scaffolds for TE applications. A thorough review regarding rapid-prototyping techniques used to fabricate scaffolds was published by Abdelaal and Darwish in 2013 (Abdelaal & Darwish 2013).
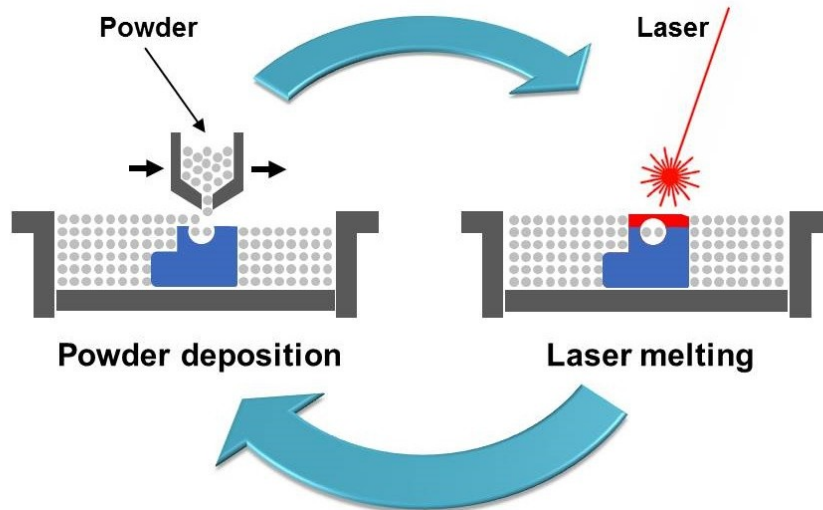
Figure 9 Selective laser melting (Protoshape 2014).

Selective laser melting (SLM), is an additive manufacturing technique that allows manufacturing prototypes using 3D CAD files. Briefly, a powder layer is selectively melted using a focused high energy laser. A consecutive powder layer is deposited. The process is repeated until the part is finalized.

In order to overcome bone grafting-related issues, synthetic materials such as hydroxyapatite (HA) (Elsinger & Leal 1996), tri-calcium phosphate (TCP) (Habibovic et al. 2006) and their combination bi-calcium phosphate (BCP) (Daculsi et al. 1989) have been used clinically and for BTE-applications. Though calcium phosphate ceramics (e.g., HA and TCP) are mostly used for bone tissue engineering applications due to their osteoinductive and osteoconductive properties (Albrektsson & Johansson 2001; Salgado et al. 2004; Rezwan et al. 2006; Hutmacher et al. 2007), they generally lack tensile strength. This is required for initial load bearing and primary implant stability. Moreover, as bulk material, ceramics do not match the mechanical properties of the surrounding bone, limiting their application to non-load bearing situations or requiring long periods of immobilization during bone healing.

In this thesis, two distinct biomaterials have been used to engineer bone or bone-like tissues and to overcome the previously mentioned limitations.

The first scaffold, Optimaix® (Matricel GmbH, Herzogenrath, Germany), is a "natural material" based on faunal collagen. The collagen scaffold is cross-linked with 1-Hydroxy-2,5-pyrrolidindion (NHS) and 1-Ethyl-3-(3 -dimethylaminopropyl)-carbodiimid (EDC) in order to adjust biodegradability. This scaffold is used as an *in vitro* model of a soft callus in bone fracture healing (secondary healing), following three weeks of chondrogenic induction of the MSC seeded scaffold.

As a second scaffold a metallic biomaterial has been used. It is manufactured from pre-alloyed powder of the shape memory alloy nickel-titanium (NiTi) using selective-laser-melting (Bormann et al. 2012). Metallic alloys allow for tuning material and mechanical properties towards specific medical needs (e.g., Young's modulus). Especially, NiTi alloys have -for a metal- particularly low Young's moduli (in the range of bone), are pseudo-elastic and have a high damping capacity (de Wild et al. 2014). The design of a scaffold is essential for its correct interaction with cells and its *in vivo* functionality (Lacroix et al. 2009). Here the scaffold geometry was designed according to geometrical specifications allowing for cell colonization and vascularization. These structural parameters include a well-defined porosity and interconnectivity to enable mass transport and vessel ingrowth, pore sizes adapted to the targeted tissue (Yeong et al. 2004), mechanical integrity, the possibility for mechanotransduction (i.e. elasticity and force transmission through the scaffold), and the feasibility to produce these structures within complex three- dimensional anatomical shapes (Hollister 2005; Rauh et al. 2011).

General Introduction

1.1. Wound healing around implants/biomaterials

Biomaterials and implants initiate a well-defined but complex process of biomaterial/host interaction upon placement into a biological environment (Stanford & Schneider 2004). These processes follow a similar cascade as is seen in secondary fracture healing and wound healing. They consist of the following phases: (i) hemostasis, (ii) inflammatory phase, (iii) proliferative phase and (iv) remodeling phase (Davies 2003).

(i) Hemostasis

Right after implant placement, various plasma proteins (e.g. fibrin) are adsorbed onto the biomaterial surface. During hemostasis platelets are activated and start releasing growth factors (PDGF, TGF-β, FGF, etc.), which act as chemoattractants (Postlethwaite et al. 1987) for fibroblasts and MSC and stimulators for their cell division and differentiation. During the formation of the blood clot a random fibrin network is secreted adhering to the biomaterial surface. This network will guide MSC migration towards the implant surface in the later phases of wound healing.

(ii) Inflammatory phase

During the inflammatory phase the site of implantation is cleaned up by polymorphonuclear leukocytes (PML), which release reactive oxygen species (ROS) to kill bacteria (Segal 2005). Simultaneously, PML release collagenase, elastase and monocyte chemotactic protein (MCP-1). Finally, recruited macrophages migrate to the implant site, eliminate bacteria and debris (created during implant placement), and release pro-inflammatory cytokines and proteases.

(iii) Proliferative phase

During the previous phases many cytokines and growth factors have been released, which initiate the synthesis and secretion of ECM components such as collagens,

28

elastin and proteoglycans by MSC. Due to hypoxia within the implant site, the migration of perivascular cells towards the implant site is initiated and neo-vascularization occurs (Pugh & Ratcliffe 2003). Furthermore, first osteoclastic bone resorption activity is occurring, which leads to the reduction of primary implant stability and the release of BMPs, TGF-β and PDGF. These factors initiate the differentiation of MSC towards osteoblasts, which produce woven bone matrix and thereby reestablish implant stability.

(iv)   Remodeling phase

During the remodeling phase, osteoclasts and osteoblasts synergistically remodel woven into lamellar bone coordinated by osteocytes.

This highly orchestrated sequence of events occurring during wound healing is influenced by many factors. These factors include implant related parameters, such as the interrelated surface characteristics (surface chemistry, roughness and topography), growth and systemic factors, mechanical loading and the health status of the patient (Anil & Anand 2011).

2. Mesenchymal stem or stromal cells

Mesenchymal stem or stromal cells depict an optimal cell source for TE applications given their high potential to differentiate along several lineages within the germ layer. "Stem cells are defined as resting cells cable of asymmetric cell division to allow both self-renewal (preventing depletion of the stem cell pool) and the production of progeny cells that start proliferation and differentiation (generating one or more tissue types)" (Aubin 1998; Bianco et al. 2001; Muschler & Midura 2002). Those properties are also referred to as 'stemness' (Jukes et al. 2008). Due to this properties stem cells can provide potentially an unlimited - because in theory immortal - cell source, which can be differentiated into a desired cell type. Stem cells are divided into two main groups: embryonic and adult or somatic stem cells. Adult stem cells are undifferentiated cells replenishing dying cells and regenerating damaged tissues. They can be found in various regions of the human body such as liver, muscle, spleen, bone marrow, adipose tissue, placenta or the umbilical cord (Pittenger et al. 1999). Embryonic stem cells are responsible for the fetal development and growth and can be isolated from the inner cell mass of blastocysts.

To obtain functional cells specialized to fulfill a certain purpose, cells have to undergo cellular differentiation, a process by which a cell acquires specialized characteristics needed to become a tissue cell (gain of specific function), at the expense of cellular plasticity. During the development of an organism multiple steps of differentiation occur to form a complex system of tissues and different cell types out of a single zygote. Not only during embryogenesis, but also in adult organisms differentiation is a common process, particularly adult stem cells are dividing and thereby creating fully differentiated daughter cells (asymmetric division). This process occurs during tissue repair and physiological cell turnover. Cells are dramatically changed during

differentiation, characterized through for example changes in size, shape, metabolic activity or responsiveness to signals. These changes are due to highly-controlled and environmental-driven modifications in their gene expression profiles (Pittenger et al. 1999).

Bone substitutes derived from neat biomaterials lack a crucial component available in bone grafts: the cellular compartment. Therefore, BTE aims at recapitulating bone grafts through the utilization of several cell types (i.e. osteoblasts, progenitors, etc.) in combination with biomaterials to engineer bone tissues or substitutes, which contribute actively to the bone repair mechanism. Such engineered tissue are generated to ensure limitless supply of bone substitutes and barred disease transmission (Amini et al. 2012).

3. Signals

As the third component of the TE triad, this chapter focuses on signals exerted towards MSC (e.g. growth factor, mechanical stimulus, etc.). Regulated growth factor/hormone release and growth factor homeostasis are key triggers during embryonic development and organogenesis. Therefore, using defined and controlled mixtures of growth factors can create a refined and controlled approach to tissue regeneration applications.

Generally, growth factors are hormones regulating cellular activity. These regulatory effects can either stimulate or inhibit cellular proliferation, differentiation, migration, adhesion, apoptosis, and gene expression (Tabata 2001). Moreover, growth factors are secreted proteins that exert their effects on neighboring cells (paracrine) or the growth factor-producing cell itself (autocrine). The effect occurs through the interaction with specific receptors on the cell surface. Various cell types can produce the same growth factors that can act on multiple cell types (pleiotropism) with similar or various effects. Moreover, the same biological effect can be induced through different growth factors (redundancy). The efficacy of a growth factor on cells is concentration-dependent and occurs at picomolar to nanomolar concentrations (Ferrara & Gerber 2001). Moreover, growth factors can initiate the up- or downregulation of the number of cell surface receptors.

The activity of secreted growth factors is regulated through their binding to matrix molecules or soluble carrier molecules thereby affecting activity and stabilization. Furthermore, the cellular response is influenced through the location and temporal expression of growth factors. Insulin-like growth factors (IGFs), bone morphogenetic proteins (BMPs), fibroblast growth factors (FGFs), and vascular endothelial growth factors (VEGFs) are examples for secreted soluble growth factors. Besides regulating

growth factors, the accessibility or bioavailability of receptors is controlled by sequestering growth factors (also known as latency) within the interstitium or in the circulation (Rifkin et al. 1999). For example, IGF-I and IGF-II (Mohan & Baylink 2002), transforming growth factor-beta (TGF-β) (Rifkin et al. 1999; Nunes et al. 1997), and BMPs (Balemans & Van Hul 2002) are linked to specific binding proteins that impede the growth factor-receptor interaction through soluble and insoluble growth factor-binding protein complexes. Moreover, platelet-derived growth factor (PDGF) (LaRochelle et al. 1991), FGF (Sahni et al. 1998) and VEGF (Sahni & Francis 2000) can bind to specific extracellular matrix molecules leading to an immobilization and inactivation of the growth factors. Their specific functions and applications within the field of TE are summarized in table 2.

Table 2 Representative growth factors in (B)TE (adopted from(Jeffrey et al. 2005)).

Growth factor	Putative function(s)	(TE) applications
BMPs	Bone, liver development, embryonic development	Spinal fusion, fracture healing, dental and craniofacial reconstruction
TGF-β	Bone formation and resorption, growth arrest, metastasis, chondrocyte differentiation	Intervertebral disc regeneration, arthritis
IGFs	Embryonic and neonatal growth, bone matrix mineralization, cartilage development and homeostasis	Cartilage, bone, tendon
FGFs	Embryonic development, wound healing, bone and cartilage formation, enhancement of blood vessels	Bone, blood vessels
VEGFs	Angiogenesis, vessel remodeling and repair, vasodilatation, bone formation	Bone, blood vessels
PDGF	Bone formation, osteoblast chemotaxis	Ligament and tendon, bone, periodontal

Besides biochemical stimuli, biomechanical stimuli have significant effects on the morphology, cell density, and differentiation of MSCs. These effects are dependent on the type, magnitude, and frequency of the applied stimulation (Maul et al. 2011). MSC differentiation can be triggered through biophysical signals (e.g. externally applied forces, manipulation of the substrate rigidity, topography or geometry of ECM patterning), which are sufficient to direct stem cell fate, if combined with minimal or suboptimal biochemical induction. Moreover, biophysical induction can also work in synergy with soluble biochemical cues (Yim & Sheetz 2012). For example, shear stress has been demonstrated to upregulate the expression of endothelial cell-related markers and downregulate smooth muscle-related markers in MSCs (Dong et al. 2009). Further examples are listed in table 3, highlighting the broad field of applications for TE using mechanical stimulation.

Table 3 MSC responses to mechanical stimuli (adopted from (Yim & Sheetz 2012)).

Cell type	Mechanical stimulus	Cellular response
MSC	Application of forces (cyclic/static), increase in cell area, increase in substrate rigidity, random nano-topography	Osteogenic differentiation
	Decrease in cell area, decrease in substrate rigidity, inhibition of RhoA pathway	Chondrogenic/adipogenic differentiation
	Application of force (e.g., cyclic strain), intermediate substrate rigidity	Myogenic/smooth muscle cell differentiation
	Soft substrate rigidity, anisotropic (line) topography	Neurogenesis
ASC	Intermediate substrate rigidity	Myogenic differentiation
	RhoA pathway inhibitor	Chondrogenic differentiation
Embryonic stem cells	Anisotropic (line) topography	Neuronal differentiation
	Pillar topography	Osteogenic differentiation

D. Bioreactors for Tissue Engineering

According to the *Oxford Dictionary* "bioreactors" are defined as "an apparatus in which a biological reaction or process is carried out, especially on an industrial scale". The main functions of bioreactors are to guarantee controlled environmental conditions (e.g. pH, CO_2 – and oxygen levels, temperature) and controlled nutrition and waste removal during the biological process. In order to meet regulatory specifications of a product (reproducibility, safety, and quality) bioreactors are optimized in terms of automation, reliability, and reproducibility. In the context of tissue engineering, bioreactors provide the possibility to control and standardize cell cultures and therefore optimize the development of tissue substitutes (Wendt et al. 2008).

1. Perfusion bioreactors

Bioreactors in tissue engineering are essential for *in vitro* cultivation and maturation of engineered tissues. Homogenous cell seeding, enhanced mass transport and physiological mechanical loading depict key functions of bioreactor systems in the field of TE. Perfusion bioreactors have been demonstrated to improve cell seeding (Wendt et al. 2003; Wendt et al. 2006) and accomplish optimal mass transport of nutrients throughout a cell seeded scaffold overcoming diffusion limitations (Martin et al. 1999). Particularly during cell seeding the performance of a perfusion bioreactor system leads to a more efficient and effective seeding when compared to the "static seeding" (Vunjak-Novakovic et al. 1999). The perfusion of a cell seeded scaffold depicts physiological conditions including shear stress, enhancing cellular osteogenesis and mineralization (Gomes et al. 2003). These systems have been used in many applications underlining their enormous potential in terms of improved proliferation and differentiation capacity as well as mineralized matrix deposition by

osteoblasts (Bancroft et al. 2002; Goldstein et al. 2001; Sikavitsas et al. 2005),
enhanced ECM synthesis by chondrocytes (Davisson et al. 2002; Wendt et al. 2006),
and the possibility of construct up-scaling (Santoro et al. 2010). Finally, perfusion
systems enable online-monitoring of metabolites or environmental parameters using
online biosensors (Santoro et al. 2011; Janssen et al. 2006). Several types of
perfusion bioreactors have been developed for (B)TE applications (Figure 10),
including spinner flask (SF), rotating wall vessel (RWV), rotating bed system (RBS),
hollow-fiber and direct perfusion bioreactors (Rauh et al. 2011; Martin et al. 2004).
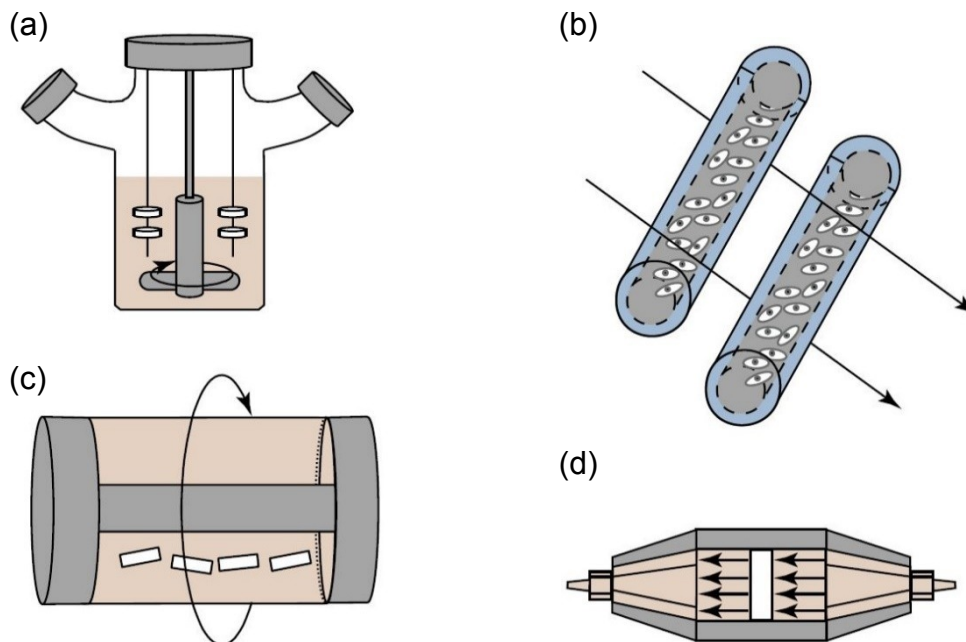
Figure 10 Perfusion bioreactor systems (Martin et al. 2004).

Representative perfusion bioreactor systems for TE applications. (a) Spinner flask bioreactors have
been used for cell seeding into 3D scaffolds and subsequent culture. (b) Hollow-fiber bioreactors
are used to enhance mass transfer during the culture of highly metabolic and sensitive cell types
such as hepatocytes. (c) Rotating-wall vessels provide a dynamic culture environment. (d) Direct
perfusion bioreactors in which medium flows directly through the pores of a scaffold.

2. Mechanical bioreactors

The human body and its organs and tissues are exposed to complex biomechanical cues, such as dynamic strains, stresses, fluid flows, electrical currents and hydrostatic pressures. These physiological forces are known to play a crucial role in *in vivo* cell physiology. Also *in vitro,* many studies have been carried out underlining the enormous potential to improve or accelerate the generation of functional tissues. The appropriate stimulus needed in order to engineer a curtain tissue depends on the mechanical, biological, biochemical and structural characteristics of the native tissue (Alvarez-Barreto & Sikavitsas 2007). Using bioreactor systems capable to apply one or more physiological loading regimes, it has been shown that mechanical conditioning *in vitro* can stimulate ECM production (Démarteau et al. 2003), improve structural organization (Niklason et al. 1999), direct cell differentiation (Knothe Tate et al. 2008; Matziolis et al. 2011; Altman et al. 2002), enhance specific tissue function (Sun et al. 2010), and affect signal pathways (Sanchez et al. 2009; Rubin et al. 2006). The systems used include bioreactors applying pulsatile fluid flow [vascular grafts, heart valves (Niklason & Langer 1997; Thompson et al. 2002)], hydrostatic pressure [vascular structures, cartilage (Niklason & Langer 1997; Thompson et al. 2002; Mizuno et al. 2002)], cyclic strain [blood vessels, bone, ligaments and tendons (Seliktar et al. 2000; Neidlinger-Wilke et al. 1994; Winter et al. 2003)], compression [cartilage, bone (Démarteau et al. 2003; Sittichokechaiwut et al. 2010; Rath et al. 2008; Matziolis et al. 2011; Jagodzinski et al. 2008)], shear [cartilage (Schätti et al. 2011)], electrical current [bone healing (Yonemori et al. 1996; Brighton et al. 2001)] and the combination of several stimuli [e.g. shear and compression (Sun et al. 2010; Shahin & Doran 2012; Yusoff et al. 2011)]. These studies emphasize that mechanical loading/conditioning of engineered tissues has the potential to improve construct generation and to lead to more physiological-like engineered tissues. Nevertheless,

the understanding about the exact mechanisms driven by various forces (i.e. shear, tension, compression and pressure) and loading regimes remain unclear. Additionally, the spatial and temporal development of engineered tissues plays a crucial role in defining the appropriate mechanical stimuli. Cell-scaffold and cell-ECM interactions vary during the maturation process of the tissue and therefore adaptation of the loading regimes during construct development might be necessary (van der Meulen & Huiskes 2002).

E.   Thesis outline

Mechanical stimuli are among the most potent factors acting in the processes of remodeling during bone fracture healing and bone development. Exploring the benefits of rapid-prototyping, shape-memory-alloys and mechanical loading, this thesis aims at the development of an *in vitro* model for endochondral ossification specifically aiming at the introduction of mechanical loading as a potent factor to modulate the endochondral process.

<u>Chapter 1</u>: *Interleukin-1β modulates endochondral ossification by human adult bone marrow stromal cells*

Inflammatory cytokines, which are present in the environment of the fracture site, are important modulators of fracture healing. During endochondral ossification interleukin-1β (IL-1β) is a key-cytokine. In this chapter, the effect of IL-1β on glycosaminoglycan (GAG) production and BMP-2 expression during chondrogenesis and ECM calcification during the hypertrophic phase of *in vitro* cultures is studied. Moreover, the effect of IL-1β treated hypertrophic constructs undergoing remodeling upon *in vivo* implantation is assessed. Taking the modulating effects on endochondral ossification of Interleukin-1β into account, a synergistic effect in combination with mechanical loading can be hypothesized.

<u>Chapter 2</u>: *Novel perfused compression bioreactor system as an in vitro model to investigate fracture healing*

With the purpose of applying mechanical loads on cartilage templates depicting an *in vitro* model of the soft callus during fracture healing, we developed a compression bioreactor system capable of applying defined physiological deformations. The system was fully validated ensuring its performance reliability in long-term cultures.

Mechanically loaded, engineered tissues exhibit a higher degree of maturation as compared to unloaded tissues. Therefore the combination of the compression bioreactor system with cell seeded collagen-based constructs is exploited to gain deeper insight into the process of load-assisted hypertrophic differentiation. This will converge in an improved *in vitro* model of hypertrophic cartilage and therefore facilitate the optimization of our fracture healing model.

Chapter 3: *Rapid prototyped porous NiTi scaffolds as bone substitutes*

In order to obtain primary implant stability and high mechanical strength, selective laser melting (SLM)-based NiTi constructs are foreseen to be utilized as a backbone for hypertrophic cartilage templates. Initially, we demonstrated high biocompatibility of NiTi- based constructs. Thereafter, MSC adhesion, proliferation and differentiation along the osteogenic lineage were obtained on two-dimensional constructs using suitable biochemical stimulators. Porous three-dimensional NiTi scaffolds cultured in a standardized perfusion bioreactor system allow for adhesion and proliferation of MSC in the same degree as observed on two-dimensional constructs. In combination with appropriate biochemical stimulators, we were able to differentiate progenitor cells towards committed cells with both osteoblastic and chondroblastic phenotype facilitating the mimicry of both routes of ossification, i.e. intramembranous and endochondral. Therefore, considering the adhesion, proliferation, and differentiation capacity of MSC on SLM-NiTi, this study as well presents the possibility to utilize 3D NiTi scaffolds as a cell-free implant material for bone repair. *In vivo*, small numbers of MSC from the blood or bone marrow in the repair site could infiltrate the scaffold, adhere to its surface and proliferate. This could result in the colonization of the scaffold, subsequent differentiation of MSC down the osteogenic linage, and ultimately lead to accelerated osseointegration of the implant.

This thesis focuses on revealing the influences of the inflammatory and biomechanical environment on fracture calluses *in vitro*. Here, the established *in vitro* fracture callus model (Scotti et al. 2010; Mumme et al. 2012, chapter 1) was further developed through the introduction of mechanical loading, applied through a novel compression bioreactor system (chapter 2). This enables to study the effects of physiological mechanical loads on fracture calluses (engineered endochondral constructs). In order to benefit from these studies, load-bearing NiTi-reinforced endochondral constructs have been intended for orthotopic *in vivo* implantation aiming at the development of NiTi-based mechanically active implants. Consequently, chapter 3 provides evidences for the potential of SLM-NiTi as a scaffold material for bone tissue engineering applications (i.e., *in vitro* engineering of osteogenic grafts) as well as regenerative medicine approaches (i.e., as a cell-free implant material).

Chapter I

Interleukin-1β modulates

endochondral ossification by human

adult bone marrow stromal cells

INTERLEUKIN-1β MODULATES ENDOCHONDRAL OSSIFICATION
BY HUMAN ADULT BONE MARROW STROMAL CELLS

Marcus Mumme[1,§], Celeste Scotti[1,§], Adam Papadimitropoulos[1], Athanas Todorov[1], Waldemar Hoffmann[1],
Chiara Bocelli-Tyndall[1,2], Marcel Jakob[1], David Wendt[1], Ivan Martin[1,*] and Andrea Barbero[1]

[1]Departments of Surgery and of Biomedicine, University Hospital Basel, Hebelstrasse 20, 4031 Basel, Switzerland
[2]Deparment of Rheumatology, University of Basel, Felix Platter Spital, Burgfelderstrasse 101, 4012 Basel,
Switzerland

§These authors contributed equally to the manuscript

Abstract

Inflammatory cytokines present in the milieu of the fracture site are important modulators of bone healing. Here we investigated the effects of interleukin-1β (IL-1β) on the main events of endochondral bone formation by human bone marrow mesenchymal stromal cells (BM-MSC), namely cell proliferation, differentiation and maturation/remodelling of the resulting hypertrophic cartilage. Low doses of IL-1β (50 pg/mL) enhanced colony-forming units-fibroblastic (CFU-f) and -osteoblastic (CFU-o) number (up to 1.5-fold) and size (1.2-fold) in the absence of further supplements and glycosaminoglycan accumulation (1.4-fold) upon BM-MSC chondrogenic induction. In osteogenically cultured BM-MSC, IL-1β enhanced calcium deposition (62.2-fold) and BMP-2 mRNA expression by differential activation of NF-κB and ERK signalling. IL-1β-treatment of BM-MSC generated cartilage resulted in higher production of MMP-13 (14.0-fold) *in vitro*, mirrored by an increased accumulation of the cryptic cleaved fragment of aggrecan, and more efficient cartilage remodelling/resorption after 5 weeks *in vivo* (i.e., more TRAP positive cells and bone marrow, less cartilaginous areas), resulting in the formation of mature bone and bone marrow after 12 weeks. In conclusion, IL-1β finely modulates early and late events of the endochondral bone formation by BM-MSC. Controlling the inflammatory environment could enhance the success of therapeutic approaches for the treatment of fractures by resident MSC and as well as improve the engineering of implantable tissues.

Keywords: Mesenchymal stem cells; tissue engineering; chondrogenesis; osteogenesis; endochondral ossification.

*Address for correspondence:
Ivan Martin
Institute for Surgical Research and Hospital Management
University Hospital Basel, Hebelstrasse 20,
CH-4031 Basel, Switzerland
                    Telephone Number: 41-61-265-2384
                         FAX Number: 41-61-265-3990
                           E-mail: imartin@uhbs.ch

Introduction

Fracture healing is a finely orchestrated process which recapitulates bone development and typically results in functional tissue regeneration (Gerstenfeld *et al.*, 2003; Behonick *et al.*, 2007; Marsell and Einhorn, 2011). Inflammation plays a crucial role in promoting and directing several aspects of bone regeneration (e.g., vascularisation, cell recruitment, cartilaginous callus production) and involves secretion of tumour necrosis factor-α (TNF-α); interleukin-1 (IL-1), IL-6, IL-11 and IL-18 (Gerstenfeld *et al.*, 2003). Importantly, the typical expression pattern of TNF-α and IL-1, the two master regulators of inflammation in fracture healing, is bimodal, with a peak within the first 24 hours which ends after 7 days, and a second peak after 4 weeks, with some variability, depending of the age of the patient (Cho *et al.*, 2002; Gerstenfeld *et al.*, 2003; Lange *et al.*, 2010). Briefly, the purpose of the first peak is to promote cell recruitment into the haematoma and vascularisation, while the second peak regulates cartilaginous callus remodelling (Cho *et al.*, 2002; Gerstenfeld *et al.*, 2003).

Even though the literature is controversial, numerous clinical studies indicate that the use of nonsteroidal anti-inflammatory drugs (NSAID), frequently used for postoperative pain control, may increase the risk of delayed fracture healing (Giannoudis *et al.*, 2000; Burd *et al.*, 2003; Bhattacharyya *et al.*, 2005). Moreover, several studies in different animal models indicated that a long-acting NSAID therapy is more deleterious than a short-acting NSAID treatment (Krishak *et al.*, 2007; O'Conner *et al.*, 2009; Ochi *et al.*, 2011). Taken together, these results highlight a key role of inflammation in influencing the processes of fracture healing.

Most fractures heal by indirect fracture healing, which consists of a combination of endochondral ossification, leading to formation of a cartilaginous callus, and intramembranous ossification, which results in formation of a periosteal callus. However, the key feature of this process is the remodelling and ossification of the cartilaginous callus (Gerstenfeld *et al.*, 2003). The interaction of a tissue undergoing the endochondral route with inflammatory signals is a crucial process to be investigated. Most *in vitro* studies assessed the effects of inflammatory cytokines on either osteogenic or chondrogenic differentiation capacity of mesenchymal stromal cells (MSC). In particular, IL-1β and TNF-α stimulation has been shown to enhance the extent of mineralisation and expression of osteoblast-related genes during MSC culture in osteogenic medium

(Ding *et al.*, 2009; Hess *et al.*, 2009; Cho *et al.*, 2010), and to inhibit MSC chondrogenesis in a dose-dependent manner (Wehling *et al.*, 2009). However, no study has yet reported on the role of inflammatory cytokines on the different phases of proliferation, differentiation and maturation/remodelling of an endochondral tissue, based on human bone marrow MSC (BM-MSC) *in vitro* or *in vivo*.

With the final goal of identifying specific tissue repair processes regulated by IL-1β during endochondral/ perichondral bone formation, we studied the effects of IL-1β on (i) proliferation and commitment of BM-MSC; (ii) osteogenic and chondrogenic differentiation of BM-MSC; (iii) maturation/remodelling of the BM-MSC-generated cartilage tissue during *in vitro* and (iv) *in vivo* endochondral bone formation. Since *in vivo* BM-MSC are typically exposed to a hypoxic environment (Das *et al.*, 2010), the effects of IL-1β during osteogenic and chondrogenic culture were also investigated at different oxygen percentages (19 %, 5 % and 2 %).

Materials and Methods

Cell harvest
Human bone marrow aspirates were harvested from 7 individuals (all male, mean age: 36.7 years, range: 24-49 years) during routine iliac crest bone grafting, in accordance with the rules of the local ethical committee (University Hospital Basel) and after informed consent was obtained.

BM-MSC culture
BM-MSC were isolated from bone marrow aspirates as previously described (Braccini *et al.*, 2005). Nucleated cells were counted after staining with Crystal Violet 0.01 % (Sigma-Aldrich, St. Louis, MO, USA) and seeded in culture dishes at a density of 4.5×10^3 cells/cm^2 for the clonogenic culture or in culture flasks at a density of 1.7×10^5 cells/cm^2 for the expansion of BM-MSC.

Clonogenic culture
Cells were cultured for 2 weeks in alpha-MEM (minimal essential medium) (Gibco/Life Technologies, Carlsbad, CA, USA) supplemented with 10 % foetal bovine serum, 1 mM sodium pyruvate, 100 mM HEPES buffer, 100 U/ mL penicillin, 100 μg/mL streptomycin, and 0.29 mg/ mL L-glutamine (complete medium) with IL-1β (Sigma-Aldrich) (0, 50 or 1000 pg/mL) in the presence or not of 5 ng/mL fibroblast growth factor-2 (FGF-2) in a humidified incubator at 37 °C with 5 % CO$_2$ with medium changes twice a week.

Expansion of BM-MSC
Cells were cultured for two passages in complete medium supplemented with 5 ng/mL FGF-2 as described earlier (Frank *et al.*, 2002).

Osteogenic differentiation
Osteogenic differentiation was induced in 2D cultures using a defined medium (osteogenic medium) as previously

described (Frank *et al.*, 2002). Briefly, BM-MSC were seeded in 6- or 12-well plates at a density of 3×10^3 cells/ cm^2 in alpha-MEM supplemented with 10 % foetal bovine serum (FBS), 10 mM β-glycerophosphate (Sigma-Aldrich), 10 nM dexamethasone (Sigma-Aldrich) and 0.1 mM L-ascorbic acid-2-phosphate (Sigma-Aldrich) and cultured for 2 or 3 weeks, with medium changes twice per week. IL-1β at different concentrations (i.e., 0, 10, 50, 100, 250 and 1000 pg/mL) was added at the beginning of the experiment and at each medium change. Cell layers were cultured for 3 weeks in a humidified incubator at 37 °C with 5 % CO$_2$ and 19 % oxygen or in a "Sci-tive" Workstation (Ruskinn Technology, Pencoed, South Wales, UK), to maintain constant hypoxic conditions (i.e., 5 % and 2 % oxygen). Medium was changed twice per week.

BM-MSC from three donors were used to study whether inhibition of NF-κB or ERK modulates IL-1β osteogenic responses. BM-MSC were grown for 7 days in 12-well plates with the last three days without FGF-2. Confluent layers were then supplemented with 50 nM pyrrolidine dithiocarbamate (PDTC, NF-κB inhibitor, Sigma-Aldrich) or 10 μM UO126 (MEK/ERK inhibitor, Sigma-Aldrich) (Cho *et al.*, 2010) while in osteogenic medium. After 3 hours IL-1β (50 pg/mL) was added to selected wells and maintained only for the first three days. Cells were then cultured in osteogenic medium (without IL-1β and inhibitors) for an additional 11 days. Control wells were cultured in osteogenic medium without inhibitors and/ or IL-1β for the entire 14 days. U0126 was dissolved in dimethyl sulphoxide (DMSO) at a stock concentration of 10 mM. DMSO 1:1000 supplemented to the cells as control was observed not to modulate osteogenic differentiation.

Chondrogenic differentiation
Chondrogenic differentiation was induced in 3D pellet cultures using a defined serum-free medium (chondrogenic medium), as previously described (Jakob *et al.*, 2001). Briefly, BM-MSC were resuspended in Dulbecco's modified Eagle's medium (DMEM) containing 4.5 mg/ mL D-glucose, 0.1 mM non-essential amino acids, 1 mM sodium pyruvate, 100 mM HEPES buffer, 100 U/mL penicillin, 100 μg/mL streptomycin, and 0.29 mg/mL L-glutamine supplemented with ITS+1 (10 μg/mL insulin, 5.5 μg/mL transferrin, 5 ng/mL selenium, 0.5 mg/mL bovine serum albumin, 4.7 μg/mL linoleic acid (Sigma-Aldrich), 0.1 mM ascorbic acid 2-phosphate (Sigma-Aldrich), 10 ng/ mL TGFβ 1 (R&D Systems, Minneapolis, MN, USA) and 10^{-7} M dexamethasone (Sigma-Aldrich). Aliquots of 4×10^5 cells/0.5 mL were centrifuged at 1,200 rpm for 5 min in 1.5 mL polypropylene conical tubes (Sarstedt, Numbrecht, Germany) to form spherical pellets. IL-1β at the concentrations described above was added at the beginning of the experiment and at each medium change. Pellets were cultured under different oxygen percentages as previously described.

Endochondral priming in vitro
BM-MSC were cultured in type I collagen meshes (Ultrafoam®, Davol, Warwick, RI, USA) at a density of 40×10^6 cells/cm^3 in chondrogenic medium. After 3 weeks, cartilaginous tissues were cultured for an

additional 2 weeks in a serum-free hypertrophic medium without TGF-β 1, supplemented with 50 nM thyroxine, 10 mM β-glycerophosphate, 10^{-8} M dexamethasone, and 0.1 mM L-ascorbic acid-2-phosphate (Scotti *et al.*, 2010). Endochondral primed constructs were then analysed or implanted ectopically in nude mice (as described below).

Endochondral bone formation in vivo
Constructs cultured for 5 weeks *in vitro* were implanted subcutaneously in the back of nude mice (CD-1 nu/nu, athymic, 6- to 8-week old females) (4 samples/mouse), following approval by the local veterinary authorities, and retrieved after 5 or 12 weeks. The *in vivo* experiment was performed with BM-MSC from only one human donor, previously selected out of 7 independent preparations based on the capability to generate hypertrophic cartilage *in vitro*.

Analytical methods
CFU-f and CFU-o
After 2 weeks of clonogenic culture, dishes were rinsed with phosphate-buffered saline (PBS) and stained for alkaline phosphatase (AP) using the 104-LL kit (Sigma Diagnostics, St. Louis, MO, USA). The number of AP positive colonies (with more than 32 cells/colony) was counted by three independent investigators to estimate the fraction of colony forming units osteoblastic (CFU-o). The same dishes were then stained with 1 % methylene blue (MB) and the total number of MB positive colonies (AP positive or negative, with more than 32 cells/colony) were counted to estimate CFU-fibroblastic (CFU-f). The diameter of the MB positive colonies was measured using the UTHSCSA ImageTool 3.0 software.

Histological staining, immunohistochemistry and in situ hybridisation (ISH)
Chondrogenic pellets and constructs were fixed in 4 % paraformaldehyde for 24 h at 4 °C, dehydrated in an ethanol series and embedded in paraffin. Sections (5 μm thick) were stained for safranin-O, alcian blue, haematoxylin and eosin (H&E) (J.T. Baker Chemical, Phillipsburg, N.J., USA), alizarin red and Masson's trichrome. Immunohistochemical analyses were performed using primary antibodies against Osterix (Abcam, Cambridge, UK), Osteocalcin (EMD Millipore, Billerica, MA, USA), MMP13 (Abcam) and aggrecan cryptical epitope-DIPEN (MD Biosciences, St Paul, MN, USA) (Scotti *et al.*, 2010). Upon rehydration in a graded ethanol series, sections were digested according to the manufacturer's instructions. The immunobinding was detected with biotinylated secondary antibodies and by Vectastain ABC (Vector Labs, Burlingame, CA, USA) kit. The red signal was developed with Fast red kit (Dako Cytomation; Dako, Glostrup, Denmark), with haematoxylin counterstaining. Negative controls were performed during each analysis by omitting the primary antibodies. Osteogenically cultured layers were washed twice with PBS, fixed for 10 min in 4 % formalin and stained with alizarin red 2 %. Hydroxyapatite deposits in osteogenically cultured layers were stained using the Osteoimage Mineralisation Assay (Lonza, Walkersville, MD, USA), following the manufacturer's instructions. Quantification of safranin O positive areas (21 slides, 10 samples, total

7.35 cm²) and bone marrow content in Masson's trichrome staining (20 slides, 10 samples, total 7 cm²) was performed with ImageJ 1.46d (National Institutes of Health, Bethesda, MD, USA) using thresholding and manual selection. ISH for human Alu repeats was performed as previously published (Scotti *et al.*, 2010).

Immunofluorescence images
Samples after *in vivo* culture were fixed in 4 % paraformaldehyde (Sigma-Aldrich), decalcified with EDTA (Sigma-Aldrich) solution, embedded in OCT and snap frozen in liquid nitrogen. Sections (20 μm thick) were incubated with the primary antibodies anti CD31 (PECAM-1; BD Pharmingen, Franklin Lakes, NJ, USA). When needed, a secondary antibody labelled with Alexa Fluo 546 (Invitrogen/Life Technologies, Carlsbad, CA, USA) was chosen and DAPI was used as nuclear staining. Fluorescence images were acquired using a Zeiss (Oberkochen, Germany) LSM-510 confocal microscope. The percentage of area infiltrated by vessels (CD31) was calculated on cross sections of the implant excluding the outer fibrotic capsule ($n = 6$ per experimental group) with ImageJ 1.46d (National Institutes of Health) using thresholding and manual selection.

Quantification of glycosaminoglycan (GAG) and DNA contents
Chondrogenic pellets and constructs were digested in proteinase K (1 mg/mL proteinase K in 50 mM Tris with 1 mM EDTA, 1 mM iodoacetamide, and 10 mg/mL pepstatin A) for 16 h at 56 °C. The GAG content of the cartilaginous tissues as well as in the supernatant harvested after each media change was determined spectrophotometrically using dimethylmethylene blue, with chondroitin sulphate as standard (Farndale *et al.*, 1986). The DNA content of constructs and cell layers (lysed with 0.01 % sodium dodecyl sulphate, SDS) was measured using the CyQuant cell proliferation assay kit (Molecular Probes, Eugene, OR, USA) and used to normalise the GAG content.

Quantification of calcium
Osteogenically cultured layers and constructs following hypertrophic culture were lysed with 0.5 N HCl. For quantification of calcium deposition, cell layers were harvested and analysed using the RANDOX (Crumlin, Co. Antrim, UK) CA 590 according to the manufacturer's protocol.

Quantification of VEGF and MMP13
VEGF and MMP13 protein levels were determined according to manufacturer in total protein lysates collected from constructs cultured for 5 weeks (Quantikine, human VEGF and human pro-MMP13, R&D Systems).

Quantitative real-time RT-PCR
Total RNA was extracted from cells using TRIzol (Invitrogen/Life Technologies), treated with DNAse and retrotranscribed into cDNA, as previously described (Frank *et al.*, 2002). Real-time reverse transcriptase-polymerase chain reaction (RT-PCR; 7300 Applied Biosystems/Life
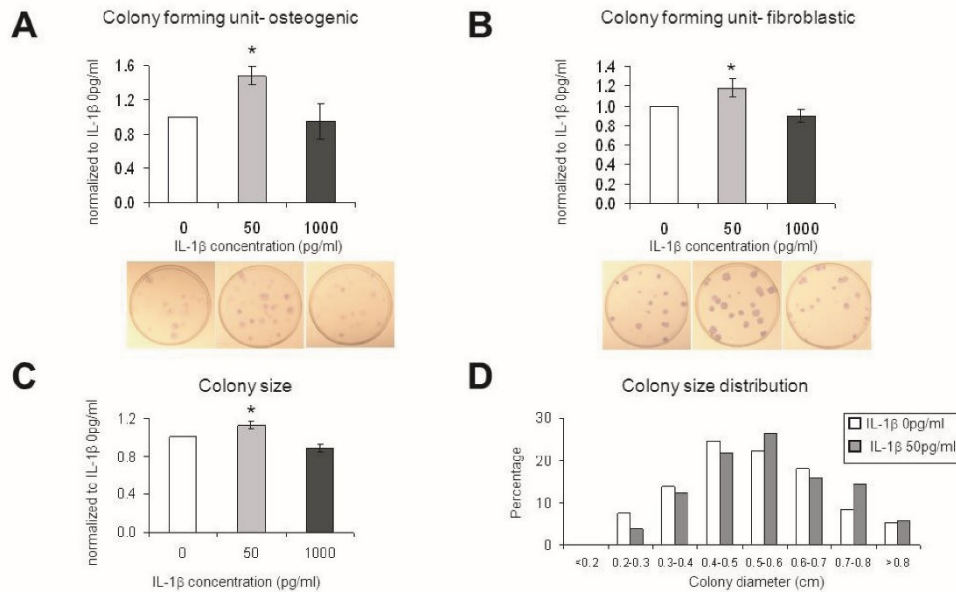
Fig. 1. Effects of IL-1β during clonal culture of human bone marrow stromal cells (BM-MSC). (**A**) Colony forming unit (CFU) -osteoblastic (quantification upper graph, representative colonies stained for alkaline phosphatase, bottom) and (**B**) CFU-fibroblastic (quantification upper graph, representative colonies further stained with methylene blue, bottom). (**C**) Quantification of colony size. $n = 3$ experiments with cells from 3 different donors, 3 plates/donor analysed. Values are mean ± SD, * = $p < 0.05$ from IL-1β 0 pg/mL. (**D**) Colony size distribution of a BM-MSC donor.

Technologies) was performed as previously described (Barbero *et al.*, 2003) to quantify expression levels of mRNA of genes expressed in cartilage (collagen type II), hypertrophic cartilage (collagen type X) in undifferentiated mesenchymal tissues and/or bone (type I collagen, bone sialoprotein, osteocalcin, bone morphogenetic protein (BMP)-2), as well as of genes involved in ECM remodelling, apoptosis and cell proliferation (MMP-13, caspase 3 and Ki-67), using human specific primers and probes. For each sample, the Ct value of each target sequence was subtracted from the Ct value of the reference gene (glyceraldehyde-3-phosphate dehydrogenase, GAPDH), to derive ΔCt. The expression level of each target gene was calculated as $2^{\Delta Ct}$.

Microtomography
Microtomography (μCT) was performed on constructs at different *in vivo* time points, after fixation in formalin and storage in PBS. μCT data were acquired using a SkyScan 1174 table top scanner (SkyScan, Kontich, Belgium) with unfiltered X-rays at an applied voltage of 32 kV and a current of 800 μA. Transmission images were acquired for a 360° scan rotation with an incremental rotation step size of 0.4°. Reconstruction was made with a modified Feldkamp algorithm at an isotropic voxel size of 6.26 μm. Threshold-based segmentation and 3D measurement analyses (bone mineral density and volume) were performed using the CT-Analyser program (SkyScan

NV), as previously described (Papadimitropoulos *et al.*, 2007). 3D rendering of the structures was performed using the commercial software VGStudio MAX 1.2.1. (Volume Graphics, Heidelberg, Germany).

Statistical analysis
For each experiment and donor, at least triplicate specimens were assessed and the values presented as mean ± standard deviation of measurements. For the dose response experiments, repeated measures ANOVA was performed using a linear mixed-effects model with a *post-hoc* Dunnett comparison to baseline, corrected for multiple comparisons. This computation was performed with R v. 2.14.2 and the packages "nlme" and "multcomp". Differences between experimental groups were otherwise assessed by two-tailed Wilcoxon tests and considered statistically significant with $p < 0.05$ (Sigma Stat software, SPSS, IBM, Amonk, NY, USA).

Results

Effect of IL-1β on the clonogenicity and proliferation of BM-MSC
We first investigated whether supplementation of IL-1β during the culture of bone marrow cells affected their (i) clonogenicity, (ii) osteogenic commitment in the absence of differentiating factors, and (iii) proliferation. Freshly
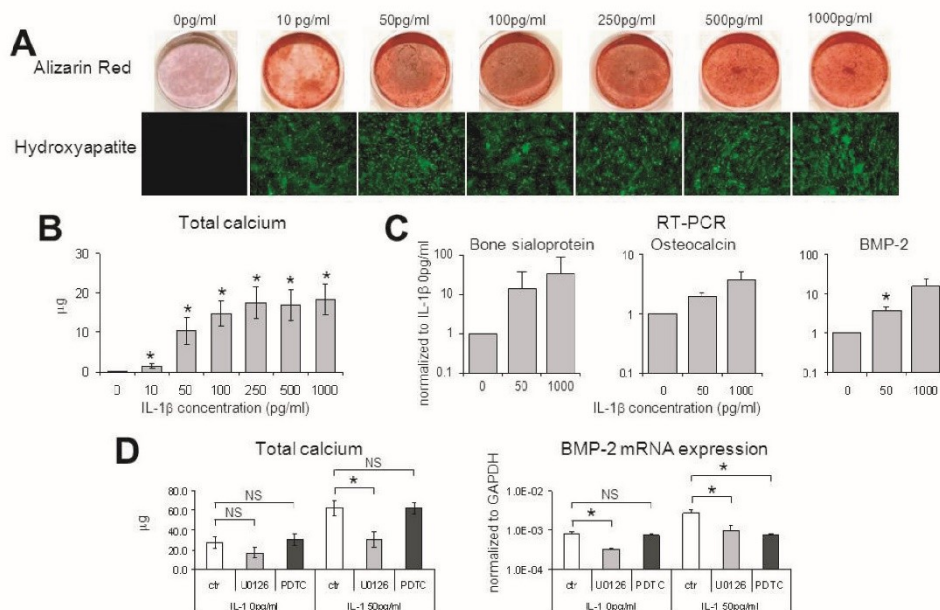
Fig. 2. Effects of IL-1β on the osteogenic differentiation of human bone marrow stromal cells (BM-MSC). (**A**) Representative alizarin red (top) and hydroxyapatite-specific fluorescence (bottom) staining and (**B**) total calcium contents of osteogenically cultured BM-MSC. (**C**) Real time RT-PCR analysis of the expression of bone sialoprotein, osteocalcin and bone morphogenetic protein (BMP)-2, levels are normalised to glyceraldehyde-3-phosphate dehydrogenase (GAPDH) and expressed as fold of difference from those measured in cells not stimulated with IL-1β. $n = 5$ experiments with cells from 5 different donors, 10 specimens analysed. (**D**) Effect of ERK and NF-κB inhibition (through 72 h incubation with 10 μm UO126 and 50 nM pyrrolidine dithiocarbamate (PDTC) respectively) on total calcium accumulation and on BMP-2 mRNA expression (see materials and methods for the description of the experimental design). $n = 3$ experiments with cells from 3 different donors, 6 specimens analysed. Data are mean ± SD. * = $p < 0.05$ from IL-1β 0 pg/mL, NS = no significant differences.

isolated bone marrow nucleated cells were then cultured at clonogenic density without IL-1β or in the presence of 50 pg/mL or 1000 pg/mL of IL-1β. IL-1β at the lowest dose significantly enhanced the fraction of CFU-o and CFU-f (1.5- and 1.2-fold respectively, Fig 1A-B). The average colony size was also increased (by 1.2-fold) following exposure to 50 pg/mL IL-1β (Fig. 1C), indicating an enhanced propensity of the cells to proliferate. By grouping the colony diameters in arbitrary size groups we observed a shift in the distribution upon exposure to 50 pg/mL IL-1β (median value from 0.45 cm to 0.55 cm) (Fig. 1D). The presence of FGF-2 during the clonogenic culture of BM-MSC reduced the IL-1β mediated increases of CFU-o, CFU-f and colony size (data not shown).

Effect of IL-1β on the differentiation of BM-MSC

We then investigated whether IL-1β stimulation enhanced the differentiation capacity of BM-MSC when cultured under chondrogenic or osteogenic conditions. Different doses of IL-1β (0 to 1000 pg/mL) were tested.

Osteogenic differentiation

Following culture of BM-MSC in osteogenic medium, the intensity of staining for calcium and hydroxyapatite deposit strongly increased in presence of IL-1β up to 50 pg/mL and remained almost unchanged at higher doses (Fig 2A). Biochemical analyses confirmed the histological trend: calcium contents increased up to 78-fold by IL-1β 50 pg/mL, higher doses of IL-1β induced a further increase in calcium contents that was not statistically significant (Fig. 2B). RT-PCR analyses indicated that IL-1β at both tested concentrations resulted in the up-regulation of the bone sialoprotein, osteocalcin and BMP-2, however statistically significant differences were observed only in the expression of BMP-2 at the lower dose of IL-1β (Fig. 2C). Interestingly, even a short exposure (3 days) of BM-MSC to 50 pg/mL IL-1β induced a significant increase of calcium deposition and expression of BMP-2 mRNA (Fig. 2D). To understand how IL-1β induces enhanced osteogenic differentiation of BM-MSC, cells were pre-treated with U0126 (an ERK inhibitor) or PDTC (an NF-κB inhibitor), exposed or not with 50 pg/mL IL-1β (3 days) and then induced to osteogenic differentiation. We observed that: (i) U0126 specifically inhibited the IL-1β induced calcium deposition and caused a general down-regulation of BMP-2 expression, (ii) PDTC did not affect calcium deposition but specifically inhibited the IL-1β mediated up-regulation of BMP-2 mRNA (Fig. 2D). No significant
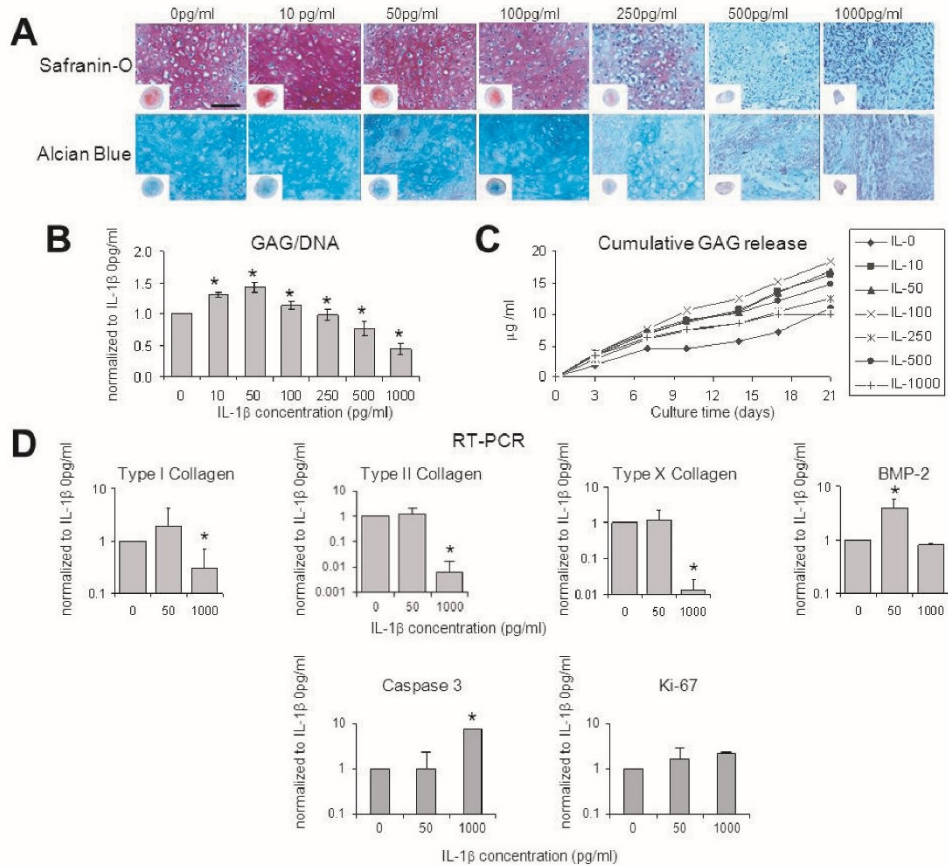
49

IL-1β in BM-MSC-based endochondral bone formation

Fig. 3. Effects of IL-1β on the chondrogenic differentiation of human bone marrow stromal cells (BM-MSC). (**A**) Representative safranin-O (top) and Alcian Blue (bottom) staining of chondrogenic pellets. Bar = 50 μm (**B**) Sulphated glycosaminoglycan (GAG) content normalised to the DNA amount of the pellets. Levels are expressed as difference from those measured in cells not stimulated with IL-1β. $n = 3$ experiments with cells from 3 different donors, 6 specimens analysed. (**C**) GAG released during the chondrogenic culture of a representative BM-MSC donor. (**D**) Real time RT-PCR analysis of the expression of types I, II and X collagen, bone morphogenetic protein (BMP)-2, caspase 3 and Ki67 levels are normalised to glyceraldehyde-3-phosphate dehydrogenase (GAPDH) and expressed as fold of difference from those measured in cells not stimulated with IL-1β. $n = 3$ experiments with cells from 3 different donors, 6 specimens analysed. Data are mean ± SD. * = $p < 0.05$ from IL-1β 0 pg/mL.

differences in the DNA contents were observed between BM-MSC treated or not with U0126 or PDTC (data not shown), suggesting that the inhibitory effects in calcium deposition and BMP-2 expression of these two compounds were not due to a reduction in cell number/survival.

Collectively these results indicate that IL-1β induced an enhanced mineralisation and expression of BMP-2 by BM-MSC more reproducibly when applied at a low dose. Inhibition of ERK but not of NF-κB counteracted both IL-1β mediated mineralisation increase and BMP-2 upregulation.

Chondrogenic differentiation

MSC were also induced to differentiate in pellet in the absence or presence of IL-1β during the entire culture time. Histological analyses indicated that tissues formed by BM-MSC exposed to low doses of IL-1β (10 and 50 pg/mL) were more intensely stained for cartilage specific matrix than tissues formed in absence of IL-1β, while those exposed to high doses (≥ 250 pg/mL) were less intensely stained (Fig. 3A). Biochemical analyses generally confirmed this trend: GAG contents increased up to 1.4-fold (at the IL-1β dose of 50 pg/mL) and decreased up to 2.3-fold at the highest IL-1β dose (Fig. 3B). DNA
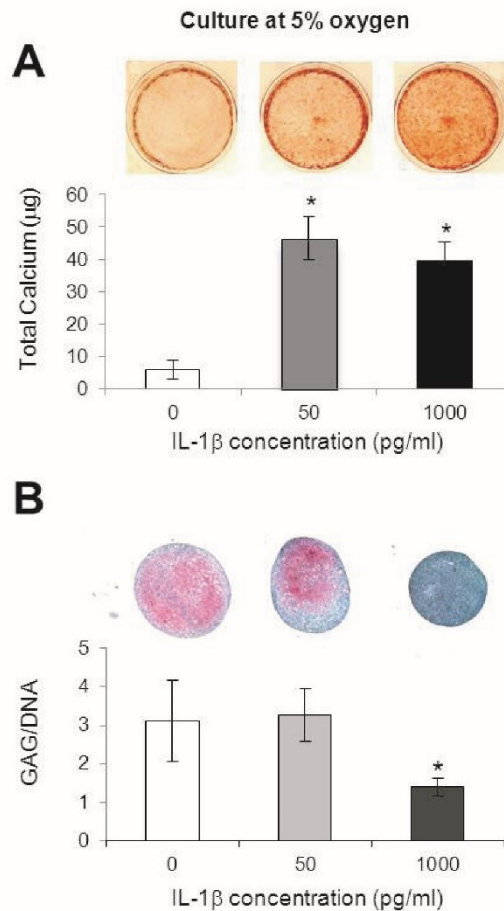
Fig. 4. Effects of IL-1β on the osteogenic and chondrogenic differentiation of human bone marrow stromal cells (BM-MSC) under hypoxic culture. (**A**) Representative alizarin red staining (top) and total calcium contents of osteogenically cultured BM-MSC under 5 % oxygen. (**B**) Representative safranin-O staining (top, scale bar = 500 μm) of and sulphated glycosaminoglycan (GAG) content normalised to the DNA amount of chondrogenic pellets. $n = 3$ experiments with cells from 3 different donors, 6 specimens analysed. Data are mean ± SD. * = $p < 0.05$ from IL-1β 0 pg/mL.

content of pellets gradually decreased with IL-1β, with no statistically significant difference between adjacent groups (data not shown). Biochemical analyses of culture medium harvested at different time of chondrogenic culture indicated that GAG was released to a higher extent by tissues exposed to the lower doses (≥ 100 pg/mL) of IL-1β (Fig. 3C). Cartilaginous tissues generated by BM-MSC not exposed to IL-1β or exposed to low (50 pg/mL) or high (1000 pg/mL) doses of IL-1β were also analysed by RT-PCR. The expression of type I, II and X collagen was not modulated by IL-1β at 50 pg/mL but strongly decreased in samples treated with IL-1β at 1000 pg/mL (3.4-, 170- and 80.1-fold respectively). BMP-2 expression, instead, was enhanced by IL-1β at 50 pg/mL (3.9-fold) but not effected by IL-1β at 1000 pg/mL (Fig. 3D). Interestingly, caspase 3 expression was significantly enhanced by IL-1β at 1000 pg/ mL, possibly explaining the loss of DNA and the reduced pellet size, while Ki67 expression was not significantly modulated by IL-1β (Fig. 3D).

Overall these results indicate that low doses of IL-1β during the chondrogenic culture of BM-MSC enhanced the production (accumulation and release) of GAG and the expression of BMP-2 mRNA. Instead high doses of IL-1β reduced extracellular matrix production and chondrogenesis.

Effects of IL-1β under hypoxic culture
BM-MSC were cultured at reduced oxygen percentages (i.e., 5 % and 2 %) under osteogenic and chondrogenic conditions without IL-1β or with 50 pg/mL or 1000 pg/ mL IL-1β. At 5 % oxygen, (i) calcium deposition of osteogenically cultured BM-MSC was enhanced following exposure to IL-1β (by 8.0- and 6.8-fold respectively for the concentration 50 pg/mL and 1000 pg/mL) (Fig. 4A), (ii) GAG amounts of pellets was not affected by 50 pg/mL IL-1β but reduced following exposure to 1000 pg/mL IL-1β (by 2.3-fold) (Fig. 4B). At 2 % oxygen, IL-1β (i) enhanced ECM mineralisation (at 50 and 1000 pg/mL) but to lower
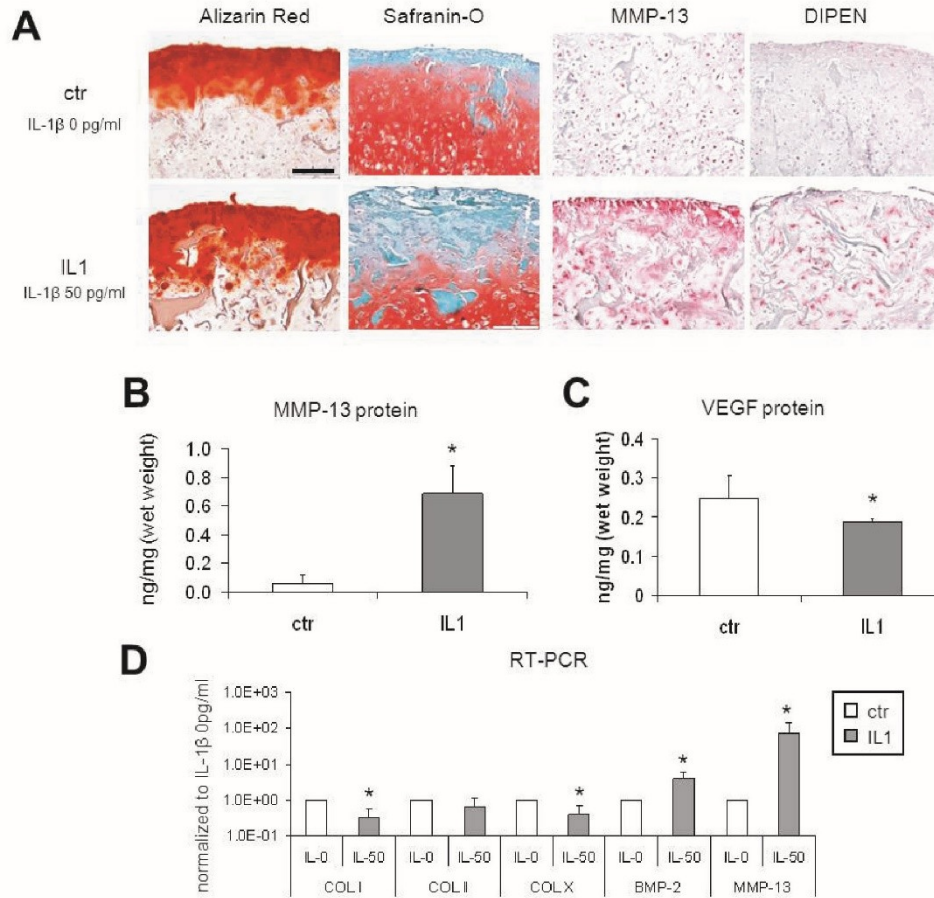
Fig. 5. Effects of IL-1β on *in vitro* formation and remodelling of a newly formed hypertrophic cartilage template by human bone marrow stromal cells (BM-MSC). (**A**) Representative alizarin red, safranin-O, metalloproteinase (MMP)-13 and Aggrecan cryptical epitope (DIPEN) staining of chondrogenic tissues cultured for the last two weeks without or with 50 pg/mL IL-1β. (**B**) MMP-13 protein quantification. (**C**) VEGF protein quantification. (**D**) Real time RT-PCR analysis of the expression of types I, II and X collagens, bone morphogenetic protein (BMP)-2, and MMP-13, levels are normalised to the glyceraldehyde-3-phosphate dehydrogenase (GAPDH) level and expressed as fold of difference from those measured in cells not stimulated with IL-1β. Scale bar = 200 μm; $n = 3$ experiments with cells from 3 different donors, 6 specimens analysed. Data are mean ± SD. * = $p < 0.05$ from IL-1β 0 pg/mL.

---

extents (data not shown), (ii) reduced GAG accumulation by 24.3 % ($p < 0.05$) at 50 pg/mL and to levels close to the limit of detection at 1000 pg/mL.

Effects of IL-1β on the endochondral bone formation
After demonstrating that IL-1β influenced the capacity of BM-MSC to differentiate towards both the chondrogenic and osteogenic lineage, we investigated the effects of this inflammatory chemokine on the maturation/remodelling of hypertrophic cartilage templates and subsequent endochondral bone formation *in vivo*, using our recently published model (Scotti *et al.*, 2010).

***In vitro* hypertrophic cartilage template formation**
Compared to controls, samples exposed to 50 pg/mL IL-1β contained (i) 38 % more calcium (37.95 ±5.47 μg/mg *vs.* 23.42 ±4.02 μg/mg, $p < 0.05$) resulting in a thicker calcified layer (as evidenced by alizarin red, Fig. 5A), (ii) 12 % less GAG (17.72 ±3.98 μg/mg *vs.* 15.59 ±1.6 μg/mg, $p < 0.05$), (iii) 14-fold higher amounts of MMP-13 protein as demonstrated by ELISA. Immunostaining of the extracellular matrix confirmed increased amount of MMP-13 and higher extent of MMP-mediated activity, as assessed by an increased accumulation of the cryptic cleaved fragment of aggrecan (DIPEN) (Fig 5A). MMP-
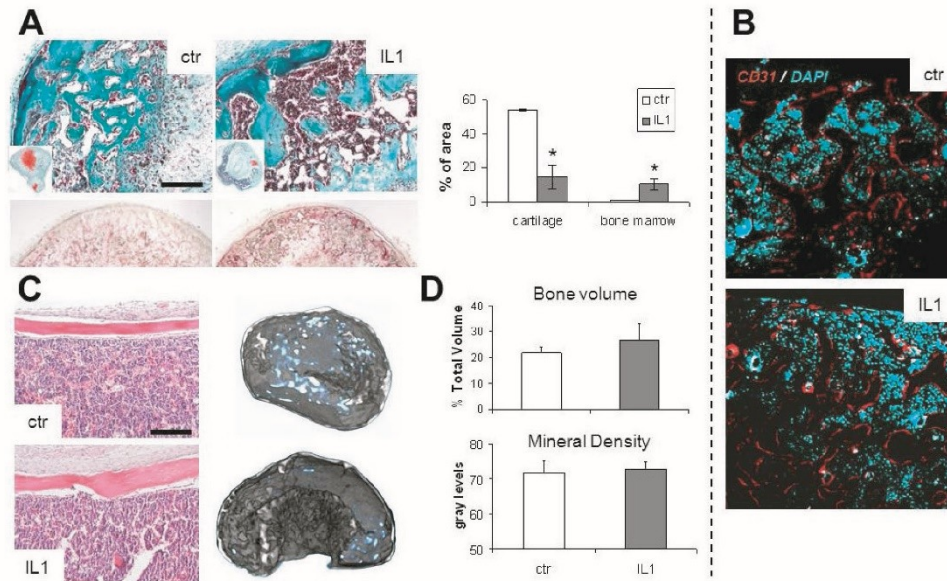
Fig. 6. Effects of IL-1β on the ectopic endochondral bone formation in nude mice of cartilaginous tissues generated with human bone marrow stromal cells (BM-MSC). (**A**) Representative Masson's trichrome and safranin-O (inset) (top) and tartrate-resistant acid phosphatase (TRAP, bottom) stainings and contents of cartilage and bone marrow of tissues harvested after 5 weeks *in vivo*. Scale bar = 200 μm. (**B**) Representative CD31/DAPI staining of constructs after 12 weeks *in vivo*. (**C**) Representative Haematoxylin and Eosin staining (scale bar = 200 μm, left) and 3D reconstructed μCT (right) images of constructs after 12 weeks *in vivo*. (**D**) Quantitative histomorphometric μCT data of constructs after 12 weeks *in vivo*. $n = 2$ experiments with cells from 1 donor, 8 specimens analysed. Data are mean ± SD. * = $p < 0.05$ from IL-1β 0 pg/mL.

13 accumulation within the tissue was also measured and resulted significantly increased in IL-1β treated samples (Fig. 5B). On the contrary, VEGF content was slightly but significantly reduced in IL-1β treated samples (Fig. 5C). Immunostaining for the osteoblastic markers Osterix and osteocalcin increased over time, with no relevant difference between controls and IL-1β treated samples (data not shown). TRAP staining was negative (data not shown). RT-PCR analyses showed that IL-1β treatment did not modify the expression of type II collagen, caused a limited but significant down-regulation of type I collagen (3.2-fold) and type X collagen (2.6-fold), an up-regulation of BMP-2 (3.9-fold) and, in accordance with the biochemical and histological results, a significant and strong up-regulation of MMP-13 mRNA (74.1-fold) (Fig 5D).

Collectively, these results indicated that IL-1β did not enhance the *in vitro* hypertrophic differentiation of BM-MSC but the extent of extracellular matrix calcification and the onset of remodelling of the cartilaginous template at least in part through MMP-13 upregulation.

In vivo tissue development
IL-1β strongly enhanced the remodelling process of the hypertrophic cartilage into bone. In particular, as compared to controls, after 5 weeks *in vivo* IL-1β treated samples showed, (i) reduced safranin-O positive cartilaginous areas

(3.6-fold), (ii) larger bone marrow areas (9.1-fold), and (iii) higher density of multinucleated TRAP-positive cells (Fig. 6A). Interestingly, the decrease in VEGF protein within the tissue, measured with ELISA after IL-1β treatment *in vitro*, did not result in an impaired vascularisation *in vivo* (Fig. 6B). As a matter of fact, vessels quantification, performed on CD31-stained sections, showed no difference between controls and IL-1β -treated samples (data not shown).

At the latest *in vivo* time point (12 weeks), both groups could finalise the endochondral process, showing mature bone formation and bone marrow engrafted within the bone trabeculae (Fig. 6C,D). Human cells survived and could be detected within the newly formed bone with ISH for human Alu repeats (data not shown), confirming our previous report (Scotti *et al.*, 2010). Taken together, these data suggest that IL-1β treatment resulted in an accelerated remodelling of the hypertrophic cartilage, ultimately leading to a bone tissue formation similar to that of controls.

Discussion

In this study, we demonstrated that IL-1β modulates the main stages of endochondral/perichondral bone formation of human adult BM-MSC. In particular we reported that

treatment with low dose of IL-1β (50 pg/mL) resulted in: (i) enhanced proliferation and clonogenicity, (ii) enhanced chondrogenic and osteogenic differentiation, (iii) enhanced *in vitro* MMP13-mediated cartilage remodelling and (v) enhanced cartilage resorption (through recruitment of TRAP-positive cells).

In order to achieve an efficient bone fracture healing, tissue repair-competent MSC have first to be recruited to proliferate within an inflammatory milieu. In our clonogenic culture experiment, we have shown that 50 pg/mL IL-1β enhanced the total number of CFU-f and CFU-o as well as the dimension of the resulting colonies. These effects may be partially due to an IL-1β enhanced production of BMP-2. This factor, known to promote mesenchymal progenitor cell proliferation and osteoblastic commitment (Lou *et al.*, 1999; Katagiri *et al.*, 1990) was in fact enhanced in response to inflammatory signals, consistently with previous works (Hess *et al.*, 2009; Cho *et al.*, 2010). In agreement with our findings, Mohanty *et al.* (2010) in their study aimed at assessing changes in the bone marrow during the onset of inflammatory arthritis, observed an increase in CFU-f and CFU-o in the bone marrow of IL1ra-/- *vs.* wild type mice (Mohanty *et al.*, 2010). Instead, a previous report indicated the inhibitory effects of IL-1β on both the number of BM-MSC derived colonies and colony size (Wang *et al.*, 2002). This discrepancy may be attributed to the modality of IL-1β application (at the time of seeding *vs.* 24 hours after seeding of bone marrow nucleated cells) or the use of different culture medium (DMEM containing 10 % foetal bovine serum *vs.* Iscove's modified Eagle's medium containing 25 % equine serum and hydrocortisone). Indeed, we have also observed in our study that the supplementation of FGF-2 to the culture medium reduced the IL-1β mediated increases of colony numbers and sizes, suggesting the sensitivity of the biological process to accessory signals.

Fracture healing consists of both intramembranous, mainly subperiosteally, and endochondral ossification (Marsell and Einhorn, 2011). We first investigated the effects of IL-1β on the direct osteoblastic differentiation of BM-MSC. Previous studies addressing this issue reported an inhibitory effect of IL-1β as well as of TNF-α on the capacity of *murine* MSC to mineralise the extracellular matrix (Lacey *et al.*, 2009; Lange *et al.*, 2010). The results of our study and of other reports (Hess *et al.*, 2009; Cho *et al.*, 2010), instead, demonstrate that inflammatory cytokines strongly enhanced the mineralisation capacity and the expression of key osteogenic genes by human MSC. Such discrepancy may be due to the inter-species differences in MSC biology (Meisel *et al.*, 2011). Interestingly, we have shown that the IL-1β induced increases of extracellular matrix mineralisation and expression of the osteo-inductive growth factor BMP-2 are caused by the activation of different signalling pathways. While the inhibition of ERK signalling (through the use of U0126) blocked both the IL-1β induced osteogenic responses, the inhibition of NF-κB signalling (through the use of PDTC) blocked significantly only the IL-1β-induced increase of BMP-2 expression. Similarly to our results, Hess *et al.* (2009) showed that a genetic block of the NF-κB pathway inhibits the TNF-α induced increase

of BMP-2 expression, but does not block mineralisation of BM-MSC. In order to more extensively elucidate the molecular mechanism of action of IL-1β on this model, further studies on the pathway-associated kinases would be required.

We then investigated the effects of IL-1β on the chondrogenic differentiation of BM-MSC, as the initial stage towards endochondral ossification. In one previous study it was reported that IL-1β decreased proteoglycan synthesis in a dose-dependent manner starting from the lowest dose used (100 pg/mL) (Wehling *et al.*, 2009). Using a broader range of IL-1β concentrations, we instead observed that GAG accumulation by BM-MSC was significantly enhanced at low doses (50 pg/mL), unaffected at intermediate doses (100-250 pg/mL) and significantly reduced at higher doses ($\geq$ 250 pg/mL) of IL-1β. These differences in the IL-1β dose responses can be due to the different type of tissues from which MSC were isolated (bone marrow aspirate from young patients – year range: 24-49 – *vs.* diaphyseal intramedullary reaming of long bone from old patients – year range: 71-78). We recently reported that even a short exposure of 50 pg/mL IL-1β to articular and nasal chondrocytes caused a significant GAG loss (Scotti *et al.*, 2012). However, MSC are less differentiated cells which have osteogenesis as standard differentiation pathway and can more likely respond positively to signals associated with tissue damage, such as inflammation (Caplan and Correa, 2011). Most importantly, this can also be explained by the upregulation of BMP-2, which is crucial for starting the healing process and the formation of the cartilaginous callus (Tsuji *et al.*, 2006). In contrast, chondrocytes are differentiated cells that typically respond to tissue damage with poor regeneration and further damage through MMP-13 upregulation (Goldring *et al.*, 2011).

Since the bone fracture site is a hypoxic environment, we also investigated the effects of IL-1β in BM-MSC cultured at reduced oxygen percentages. We found that IL-1β (50 and 1000 pg/mL) still enhanced ECM mineralisation by BM-MSC osteogenically cultured at oxygen percentages lower than 19 %, a condition known to inhibit osteogenic differentiation of mesenchymal cells (Malladi *et al.*, 2006; D'Ippolito *et al.*, 2006; Hirao *et al.*, 2006; Pattappa *et al.*, 2010; Wang *et al.*, 2011). Instead, IL-1β 50 pg/mL did not alter GAG accumulation at 5 % and slightly reduced it at 2 % oxygen. The latter finding can be due to a more pronounced production of cartilage matrix degradation agents in response to IL-1β under hypoxic conditions. Mathy-Harter *et al.* (2005), in fact, demonstrated that the IL-1β mediated production of nitric oxide by *in vitro* cultured bovine chondrocytes was more pronounced at low (i.e., 1 %) *vs.* atmospheric (i.e., 21 %) oxygen percentages. It is important however to consider that our experimental condition consisting on the culture of BM-MSC under a continuous hypoxic environment does not fully reproduce the variation in oxygen levels during the different stages of fracture healing (Lu *et al.*, 2011).

Endochondral ossification involves differentiation to hypertrophy followed by remodelling of cartilage into bone. We observed that the supplementation of IL-1β during the hypertrophic culture of human BM-

MSC derived chondrogenic tissues did not significantly enhance the expression of type X collagen but markedly increased MMP-13 expression and activity. The absence of an effect on type X collagen is in accordance with a previously published work which compared the effects of IL-1β, TNF-α and macrophage conditioned medium (MCM) on human chondrocytes seeded on a silk scaffold and reported an upregulation of collagen type X only in MCM-treated samples (Sun *et al.*, 2011). It should also be considered that, in our conditions, cell heterogeneity at the different time points may have masked modulation of type X collagen expression. The fact that Welting *et al.* (2011), instead, did find an effect of cycloxygenase-2 (a canonical IL-1β target gene) on hypertrophic differentiation of chondroprogenitors could be due to the use of cells/ tissues from animal species other than human. The IL-1β mediated increase in MMP-13 expression and activity is particularly relevant for fracture callus remodelling into bone, since MMP-13 is required for proper resorption of hypertrophic cartilage (Behonick *et al.*, 2007) and subsequent endochondral bone development (Stickens *et al.*, 2004; Kosaki *et al.*, 2007).

As a result of the enhanced *in vitro* extracellular matrix (ECM) pre-processing by MMP-13, we described a faster remodelling of the hypertrophic cartilage, with less cartilaginous ECM and more abundant bone marrow engraftment at the intermediate *in vivo* time point. This last experiment was designed as a proof-of-principle of the *in vivo* effect of *in vitro* pre-treatment of hypertrophic cartilage with IL-1β. Our observation that higher amounts of TRAP-positive cells were present in the IL-1β treated samples reinforces a previous observation on the role of inflammation in chondroclastogenesis and cartilage resorption (Ota *et al.*, 2009). Limitations of this study include: (i) the use of expanded BM-MSC which may not reflect normal behaviour of progenitor cells of the bone marrow; (ii) the *in vitro* nature of the first series of experiments, which again limits its relevance to the normal behaviour of BM-MSC; (iii) the ectopic site of implantation for the *in vivo* experiments which is not the physiological site of bone repair.

The results of this study indicate the concentration-dependent role of IL-1β in regulating the chondrogenic and osteogenic differentiation of human BM-MSC and the remodelling of resulting cartilaginous templates into bone and bone marrow elements. A controlled delivery of IL-1β (e.g., by smart scaffolds) could enhance bone healing by resident MSC as well as improve the engineering of implantable tissues. Further studies are needed to extend the system with the presence of inflammatory cells and other cytokines (Liu *et al.*, 2011), in order to more comprehensively study bone regeneration in an immunocompetent animal model.

Acknowledgements

References

Barbero A, Ploegert S, Heberer M, Martin I (2003) Plasticity of clonal populations of dedifferentiated adult human articular chondrocytes. Arthritis Rheum **48**: 1315-1325.

Behonick DJ, Xing Z, Lieu S, Buckley JM, Lotz JC, Marcucio RS, Werb Z, Miclau T, Colnot C (2007) Role of matrix metalloproteinase 13 in both endochondral and intramembranous ossification during skeletal regeneration. PLoS One **2**: e1150.

Bhattacharyya T, Levin R, Vrahas MS, Solomon DH (2005) Nonsteroidal antiinflammatory drugs and nonunion of humeral shaft fractures. Arthritis Rheum **53**: 364-347.

Braccini A, Wendt D, Jaquiery C, Jakob M, Heberer M, Kenins L, Wodnar-Filipowicz A, Quarto R, Martin I (2005) Three-dimensional perfusion culture of human bone marrow cells and generation of osteoinductive grafts. Stem Cells **23**: 1066-1072.

Burd TA, Hughes MS, Anglen JO (2003) Heterotopic ossification prophylaxis with indomethacin increases the risk of long-bone nonunion. J Bone Joint Surg Br **85**: 700-705.

Caplan AI, Correa D (2011) The MSC: an injury drugstore. Cell Stem Cell **9**: 11-15.

Cho HH, Shin KK, Kim YJ, Song JS, Kim JM, Bae YC, Kim CD, Jung JS (2010) NF-kappaB activation stimulates osteogenic differentiation of mesenchymal stem cells derived from human adipose tissue by increasing TAZ expression. J Cell Physiol **223**: 168-177.

Cho TJ, Gerstenfeld LC, Einhorn TA (2002) Differential temporal expression of members of the transforming growth factor beta superfamily during murine fracture healing. J Bone Miner Res **17**: 513-520.

Das R, Jahr H, van Osch GJ, Farrell E (2010) The role of hypoxia in bone marrow-derived mesenchymal stem cells: considerations for regenerative medicine approaches. Tissue Eng Part B Rev **16**: 159-168.

Ding J, Ghali O, Lencel P, Broux O, Chauveau C, Devedjian JC, Hardouin P, Magne D (2009) TNF-alpha and IL-1beta inhibit RUNX2 and collagen expression but increase alkaline phosphatase activity and mineralization in human mesenchymal stem cells. Life Sci **84**: 499-504.

D'Ippolito G, Diabira S, Howard GA, Roos BA, Schiller PC (2006) Low oxygen tension inhibits osteogenic differentiation and enhances stemness of human MIAMI cells. Bone **39**: 513-522.

Farndale RW, Buttle DJ, Barrett AJ (1986) Improved quantitation and discrimination of sulphated glycosaminoglycans by use of dimethylmethylene blue. Biochim Biophys Acta **883**: 173-177.

Frank O, Heim M, Jakob M, Barbero A, Schäfer D, Bendik I, Dick W, Heberer M, Martin I (2002) Real-time quantitative RT-PCR analysis of human bone marrow stromal cells during osteogenic differentiation *in vitro*. J Cell Biochem **85** 737-746.

Gerstenfeld LC, Cullinane DM, Barnes GL, Graves DT, Einhorn TA (2003) Fracture healing as a post-natal

M Mumme   *IL-1β in BM-MSC-based endochondral bone formation*

developmental process: molecular, spatial, and temporal aspects of its regulation. J Cell Biochem **88**: 873-884.

Giannoudis PV, MacDonald DA, Matthews SJ, Smith RM, Furlong AJ, De Boer P (2000) Nonunion of the femoral diaphysis. The influence of reaming and non-steroidal anti-inflammatory drugs. J Bone Joint Surg Br **82:** 655-658.

Goldring MB, Otero M, Plumb DA, Dragomir C, Favero M, El Hachem K, Hashimoto K, Roach HI, Olivotto E, Borzì RM, Marcu KB (2011) Roles of inflammatory and anabolic cytokines in cartilage metabolism: signals and multiple effectors converge upon MMP-13 regulation in osteoarthritis. Eur Cell Mater **21**: 202-220.

Hess K, Ushmorov A, Fiedler J, Brenner RE, Wirth T (2009) TNFalpha promotes osteogenic differentiation of human mesenchymal stem cells by triggering the NF-kappaB signaling pathway. Bone **45**: 367-376.

Hirao M, Tamai N, Tsumaki N, Yoshikawa H, Myoui A (2006) Oxygen tension regulates chondrocyte differentiation and function during endochondral ossification. J Biol Chem **281**: 31079-31092.

Jakob M, Démarteau O, Schäfer D, Hintermann B, Dick W, Heberer M, Martin I (2001) Specific growth factors during the expansion and redifferentiation of adult human articular chondrocytes enhance chondrogenesis and cartilaginous tissue formation *in vitro*. J Cell Biochem **81**: 368-377.

Katagiri T, Yamaguchi A, Ikeda T, Yoshiki S, Wozney JM, Rosen V, Wang EA, Tanaka H, Omura S, Suda T (1990) The non-osteogenic mouse pluripotent cell line, C3H10T1/2, is induced to differentiate into osteoblastic cells by recombinant human bone morphogenetic protein-2. Biochem Biophys Res Commun **172**: 295-299.

Kosaki N, Takaishi H, Kamekura S, Kimura T, Okada Y, Minqi L, Amizuka N, Chung UI, Nakamura K, Kawaguchi H, Toyama Y, D'Armiento J (2007) Impaired bone fracture healing in matrix metalloproteinase-13 deficient mice. Biochem Biophys Res Commun **354**: 846-851.

Krischak GD, Augat P, Sorg T, Blakytny R, Kinzl L, Claes L, Beck A (2007) Effects of diclofenac on periosteal callus maturation in osteotomy healing in an animal model. Arch Orthop Trauma Surg **127**: 3-9.

Lacey DC, Simmons PJ, Graves SE, Hamilton JA (2009) Proinflammatory cytokines inhibit osteogenic differentiation from stem cells: implications for bone repair during inflammation. Osteoarthritis Cartilage **17**: 735-742.

Lange J, Sapozhnikova A, Lu C, Hu D, Li X, Miclau T 3rd, Marcucio RS (2010) Action of IL-1beta during fracture healing. J Orthop Res **28**: 778-784.

Liu Y, Wang L, Kikuiri T, Akiyama K, Chen C, Xu X, Yang R, Chen W, Wang S, Shi S (2011) Mesenchymal stem cell-based tissue regeneration is governed by recipient T lymphocytes via IFN-γ and TNF-α. Nat Med **17**: 1594-1601.

Lou J, Xu F, Merkel K, Manske P (1999) Gene therapy: adenovirus-mediated human bone morphogenetic protein-2 gene transfer induces mesenchymal progenitor cell proliferation and differentiation *in vitro* and bone formation *in vivo*. J Orthop Res **17**: 43-50.

Lu C, Rollins M, Hou H, Swartz HM, Hopf H, Miclau T, Marcucio RS (2008) Tibial fracture decreases oxygen levels at the site of injury. Iowa Orthop J **28**: 14-21.

Lu C, Saless N, Hu D, Wang X, Xing Z, Hou H, Williams B, Swartz HM, Colnot C, Miclau T, Marcucio RS (2011) Mechanical stability affects angiogenesis during early fracture healing. J Orthop Trauma **25**: 494-499.

Malda J, Klein TJ, Upton Z (2007) The roles of hypoxia in the *in vitro* engineering of tissues. Tissue Eng **13**: 2153-2162.

Malladi P, Xu Y, Chiou M, Giaccia AJ, Longaker MT (2006) Effect of reduced oxygen tension on chondrogenesis and osteogenesis in adipose-derived mesenchymal cells. Am J Physiol Cell Physiol **290**: C1139-1146.

Marsell R, Einhorn TA (2011) The biology of fracture healing. Injury **42**: 551-555.

Martin I, Muraglia A, Campanile G, Cancedda R, Quarto R (1997) Fibroblast growth factor-2 supports *ex vivo* expansion and maintenance of osteogenic precursors from human bone marrow. Endocrinology **138**: 4456-4462.

Mathy-Hartert M, Burton S, Deby-Dupont G, Devel P, Reginster JY, Henrotin Y (2005) Influence of oxygen tension on nitric oxide and prostaglandin E2 synthesis by bovine chondrocytes. Osteoarthritis Cartilage **13**: 74-79.

Meisel R, Brockers S, Heseler K, Degistirici O, Bülle H, Woite C, Stuhlsatz S, Schwippert W, Jäger M, Sorg R, Henschler R, Seissler J, Dilloo D, Däubener W (2011) Human but not murine multipotent mesenchymal stromal cells exhibit broad-spectrum antimicrobial effector function mediated by indoleamine 2,3-dioxygenase. Leukemia **25**: 648-654.

Mohanty ST, Kottam L, Gambardella A, Nicklin MJ, Coulton L, Hughes D, Wilson AG, Croucher PI, Bellantuono I (2010) Alterations in the self-renewal and differentiation ability of bone marrow mesenchymal stem cells in a mouse model of rheumatoid arthritis. Arthritis Res Ther **12**: R149.

Ochi H, Hara Y, Asou Y, Harada Y, Nezu Y, Yogo T, Shinomiya K, Tagawa M (2011) Effects of long-term administration of carprofen on healing of a tibial osteotomy in dogs. Am J Vet Res **72**: 634-641.

O'Connor JP, Capo JT, Tan V, Cottrell JA, Manigrasso MB, Bontempo N, Parsons JR (2009) A comparison of the effects of ibuprofen and rofecoxib on rabbit fibula osteotomy healing. Acta Orthop **80**: 597-605.

Ota N, Takaishi H, Kosaki N, Takito J, Yoda M, Tohmonda T, Kimura T, Okada Y, Yasuda H, Kawaguchi H, Matsumoto M, Chiba K, Ikegami H, Toyama Y (2009) Accelerated cartilage resorption by chondroclasts during bone fracture healing in osteoprotegerin-deficient mice. Endocrinology **150**: 4823-4834.

Papadimitropoulos A, Mastrogiacomo M, Peyrin F, Molinari E, Komlev VS, Rustichelli F, Cancedda R (2007) Kinetics of *in vivo* bone deposition by bone marrow stromal cells within a resorbable porous calcium phosphate scaffold: an X-ray computed microtomography study. Biotechnol Bioeng **98**: 271-281.

Pattappa G, Heywood HK, de Bruijn JD, Lee DA (2011) The metabolism of human mesenchymal stem cells during

M Mumme

proliferation and differentiation. J Cell Physiol **226**: 2562-2570.

Scotti C, Tonnarelli B, Papadimitropoulos A, Scherberich A, Schaeren S, Schauerte A, Lopez-Rios J, Zeller R, Barbero A, Martin I (2010) Recapitulation of endochondral bone formation using human adult mesenchymal stem cells as a paradigm for developmental engineering. Proc Natl Acad Sci U S A **107**: 7251-7256.

Scotti C, Osmokrovic A, Wolf F, Miot S, Peretti GM, Barbero A, Martin I (2012) Response of human engineered cartilage based on articular or nasal chondrocytes to interleukin-1â and low oxygen. Tissue Eng Part A **18**: 362-372

Stickens D, Behonick DJ, Ortega N, Heyer B, Hartenstein B, Yu Y, Fosang AJ, Schorpp-Kistner M, Angel P, Werb Z (2004) Altered endochondral bone development in matrix metalloproteinase 13-deficient mice. Development **131**: 5883-5895.

Sun L, Wang X, Kaplan DL (2011) A 3D cartilage – inflammatory cell culture system for the modeling of human osteoarthritis. Biomaterials **32**: 5581-5589.

Tsuji K, Bandyopadhyay A, Harfe BD, Cox K, Kakar S, Gerstenfeld L, Einhorn T, Tabin CJ, Rosen V (2006) BMP2 activity, although dispensable for bone formation, is required for the initiation of fracture healing. Nat Genet **38**: 1424-1429.

Wang L, Mondal D, La Russa VF, Agrawal KC (2002) Suppression of clonogenic potential of human bone marrow mesenchymal stem cells by HIV type 1: putative role of HIV type 1 tat protein and inflammatory cytokines. AIDS Res Hum Retroviruses **18**: 917-931.

Wang Y, Li J, WangY, Lei L, Jiang C, An S, Zhan Y, Cheng Q, Zhao Z, Wang J, Jiang L (2012) Effects of hypoxia on osteogenic differentiation of rat bone marrow mesenchymal stem cells. Mol Cell Biochem **362**: 25-33.

Wehling N, Palmer GD, Pilapil C, Liu F, Wells JW, Müller PE, Evans CH, Porter RM (2009) Interleukin-1beta and tumor necrosis factor alpha inhibit chondrogenesis by human mesenchymal stem cells through NF-kappaB-dependent pathways. Arthritis Rheum **60**: 801-812.

Welting TJ, Caron MM, Emans PJ, Janssen MP, Sanen K, Coolsen MM, Voss L, Surtel DA, Cremers A, Voncken JW, van Rhijn LW (2011) Inhibition of cyclooxygenase-2 impacts chondrocyte hypertrophic differentiation during endochondral ossification. Eur Cell Mater **22**: 420-436.

Discussion with Reviewers

Reviewer I: Given the large increase in caspase-3, it would be interesting to know whether cell death increases in pellets treated with high IL-1β. Please comment!
Authors: We did not perform specific analyses to assess IL-1β mediated cell death in BM-MSC during pellet cultures. However the reduction in size and DNA contents of pellets cultured with increasing IL-1β concentrations, the necrotic appearance of the pellets treated with the highest doses of IL-1β as well as the large increase in caspase-3 suggest that IL-1β (at high concentration) induces cell death of chondrogenically cultured BM-MSC.

Reviewer I: What can be inferred from this study on the relationship between IL-1β, FGF and ERK signalling in modulating endochondral ossification?
Authors: The current work was not aimed at studying the relationship between IL-1β, FGF and ERK signalling in modulating endochondral ossification. Our results however suggest that FGF-2 and ERK signalling might modulate some BM-MSC responses to IL-1β. We have in fact shown that: (i) FGF-2 counteracted the IL-1β-mediated proliferation of osteoprogenitor cells (ii) inhibition of ERK counteracted both IL-1β mediated mineralisation increase and BMP-2 upregulation. Since both IL-1β and FGF-2 are present at a bone fracture site, future studies will have to be undertaken to investigate the interaction between these two factors in the endochondral differentiation of BM-MSC.

Reviewer II: What is the impact of your findings for translational medicine?
Authors: Local inflammation is known to play a pivotal role in tissue regeneration, whereby absence, excess or disregulation of inflammatory processes may negatively affect bone repair. In accordance with this clinical evidence, our experimental data suggest that low levels of inflammatory cytokines may enhance the process of fracture healing by promoting chondrogenesis and the subsequent phases of callus formation/remodelling. A local control of inflammation might therefore improve the results of bone regeneration strategies.

Reviewer III: How do you think these findings relate to natural phenomena such as, for instance, fracture repair? May this constitute evidence that very low local amounts of IL-1 may have a role in priming chondrogenesis in the callus?
Authors: Local inflammation is known to play a pivotal role in tissue regeneration, whereby absence, excess or disregulation of inflammatory processes may negatively affect bone repair. In accordance with this clinical evidence, our experimental data suggest that low levels of inflammatory cytokines may enhance the process of fracture healing by promoting chondrogenesis and the subsequent phases of callus formation/remodelling. The work is in line with the increasing recognition that controlled management of inflammation is a crucial target towards enhancement of fracture healing. Our study on the one hand prompts for further investigations to better dissect the role of IL-1 and other cytokines in the different phases of bone regeneration, and on the other hand proposes the *in vitro*/ectopic replication of endochondral ossification as a model to address those critical processes.

Chapter II

Novel perfused compression

bioreactor system as an in vitro

model to investigate fracture healing

Novel perfused compression bioreactor system as an *in vitro* model to investigate fracture healing

Waldemar Hoffmann[1,2,3], Sandra Feliciano[1,2], Ivan Martin[1,2]*, Michael de Wild[3] and David Wendt[1,2]

[1] Department of Biomedicine, University Hospital Basel, Basel, Switzerland
[2] Department of Surgery, University Hospital Basel, Basel, Switzerland
[3] School of Life Sciences, Institute for Medical and Analytical Technologies, University of Applied Sciences Northwestern Switzerland, Muttenz, Switzerland

Secondary bone fracture healing is a physiological process that leads to functional tissue regeneration via endochondral bone formation. *In vivo* studies have demonstrated that early mobilization and the application of mechanical loads enhances the process of fracture healing. However, the influence of specific mechanical stimuli and particular effects during specific phases of fracture healing remain to be elucidated. In this work, we have developed and provided proof-of-concept of an *in vitro* human organotypic model of physiological loading of a cartilage callus, based on a novel perfused compression bioreactor (PCB) system. We then used the fracture callus model to investigate the regulatory role of dynamic mechanical loading. Our findings provide a proof-of-principle that dynamic mechanical loading applied by the PCB can enhance the maturation process of mesenchymal stromal cells toward late hypertrophic chondrocytes and the mineralization of the deposited extracellular matrix. The PCB provides a promising tool to study fracture healing and for the *in vitro* assessment of alternative fracture treatments based on engineered tissue grafts or pharmaceutical compounds, allowing for the reduction of animal experiments.

Keywords: bioreactor, *in vitro* model, mechanical loading, hypertrophy, fracture healing

INTRODUCTION

Bone fracture healing is a natural, physiological process leading to functional tissue regeneration through a highly orchestrated sequence (Gerstenfeld et al., 2003; Behonick et al., 2007; Marsell and Einhorn, 2011). Primary fracture healing occurs within stable fracture sites when there is direct contact between the fracture ends, re-establishing the anatomically correct and biomechanically competent lamellar bone structure (Marsell and Einhorn, 2011). However, in the majority of cases a gap is present at the fracture site, and therefore indirect or secondary fracture healing occurs.

Secondary fracture healing, a process recapitulating the process of endochondral bone formation, is divided into four main phases: hemorrhage and inflammation, soft callus formation, hard callus formation, and callus remodeling (Sfeir et al., 2005; Schindeler et al., 2008). Following initial hemorrhage and inflammation, a key step during secondary fracture healing is the formation of a soft fracture callus, consisting of cartilaginous extracellular matrix, chondrocytes, and fibroblasts. It provides mechanical support to the fracture and serves as a template for subsequent remodeling into a bony callus (Gerstenfeld et al., 2003; Sfeir et al., 2005; Schindeler et al., 2008). During the subsequent phase of hard callus formation, a mineralized cartilaginous template is gradually replaced with unordered woven bone matrix. The callus becomes vascularized, increasing the oxygen tension, and fostering maturation of osteoblasts (Sfeir et al., 2005; Schindeler et al., 2008). In the final phase, the woven bone is fully remodeled toward cortical and/or trabecular bone in a spatially and temporally choreographed manner (Sfeir et al., 2005; Schindeler et al., 2008).

In vivo models have demonstrated that mechanical stimulation of fractures can improve the secondary fracture healing process and/or alter the biological pathways involved (Rand et al., 1981; Goodship and Kenwright, 1985; Aro et al., 1991; Claes et al., 1997; Park et al., 1998; Rubin et al., 2001; Chao and Inoue, 2003). However, due to the multitude of parameters that play a role in the mechanical environment of the fracture site, these *in vivo* studies did not allow for a systematic study of specific mechanical stimuli nor their influence during the different phases of fracture healing (Gerstenfeld et al., 2003; Schindeler et al., 2008).

As an alternative, *in vitro* model systems facilitate a methodical approach to study the impact of the mechanical stimuli during distinct phases of secondary fracture healing in a controlled manner. However, *in vitro* models have previously been limited to applying mechanical loads on cartilaginous tissues in order to develop more functional tissues or to study the impact of different loading regimes on chondrogenesis (Démarteau et al., 2003; Ballyns and Bonassar, 2010; Sun et al., 2010; Puetzer et al., 2012), but the effect of mechanical loading during the process of hypertrophic cartilage formation and remodeling, critical in fracture healing, has not yet been studied.

Here, were propose an *in vitro* model based on a perfused compression bioreactor (PCB) system to: (i) apply physiological strain/loads, (ii) perfuse a construct allowing for mass transport and simulation of vascularization, and (iii) compress rigid load-bearing scaffolds in a physiological manner. The application of dynamic mechanical loading was validated for both collagen-based and nickel–titanium (NiTi) based tissue constructs, highlighting the broad operational range of

Chapter II – Novel perfused compression bioreactor

the system including the compressive strength (100–200 MPa) of bone (Keaveny et al., 2004; Weiner and Wagner, 1998). In a proof-of-concept study, we hypothesized that physiological compressive loading applied during hypertrophy enhances extracellular matrix mineralization of cartilaginous constructs and triggers the maturation process of MSC toward late hypertrophic chondrocytes.

MATERIALS AND METHODS

PERFUSED COMPRESSION BIOREACTOR SYSTEM

The PCB system consists of two main components: the bioreactor chamber (**Figures 1A,B**) and the power transmission rack (**Figure 1C**). A detailed description of the bioreactor system can be found in Hoffmann et al. (2014b). The bioreactor chamber holds the scaffold in place and ensures hermetic sealing as well as force transmission onto the cell loaded construct. It consists of medium inlets/outlets, flow distributors, a flexible force transmitting disk, and the intended space for scaffold/construct placement. The power transmission rack includes a plunger, a pre-load screw, and a cam-shaft. The chamber is placed on the plunger and fixed via tightening of the pre-load screw. The cam-shaft moves the plunger in order to apply a sinusoidal compression pattern onto the bioreactor chamber.

To minimize the potential for contamination, all electronics and mechanical instrumentation were housed beneath the bioreactor chambers in a closed environment. The overall dimensions were kept sufficiently small (width × height × depth: 9 cm × 25 cm × 35 cm) to fit in a standard CO_2 incubator (**Figure 1C**).

The system is controlled and monitored using a custom-made program based on LabView (NI, 622X, Austin, TX, USA) installed on a dedicated PC. This software controls the motor connected to the cam-shaft (**Figure 1D**) via a belt-drive generating a sinusoidal waveform for compression and simultaneously monitors data from four independent force sensors (**Figure 1D**, FC23 Compression Load Cell®, Measurement Specialties, VA, USA).

CELL CULTURE

Human mesenchymal stromal cells (MSC) were isolated from bone marrow aspirates (Braccini et al., 2005), after informed patient consent and following protocol approval by the local ethical committee (University Hospital Basel; Prof. Dr. Kummer; approval date 26/03/2007 Ref Number 78/07), and cultured as previously described (Frank et al., 2002). MSC were expanded for two to four passages for subsequent experiments. Then MSC were seeded on type I collagen-based OPTIMAIX scaffolds (O3D304030 Matricel, Germany, punched to cylindrical shape, 3 mm height, 8 mm diameter) or NiTi scaffolds (4 mm height, 8 mm diameter, open-porous 3D-printed structure) (Hoffmann et al., 2014a) with a seeding density of 4E + 06 cells/scaffold using a previously developed perfusion bioreactor system (Wendt et al., 2003, 2006). During the seeding phase, bidirectional perfusion was performed using syringe pumps at a perfusion velocity of 3 mL/min.

Open-porous, metallic NiTi scaffolds were included for the initial validation to ensure the broad operational range of the PCB. Further investigations were conducted using OPTIMAIX due to ease of histological assessments.
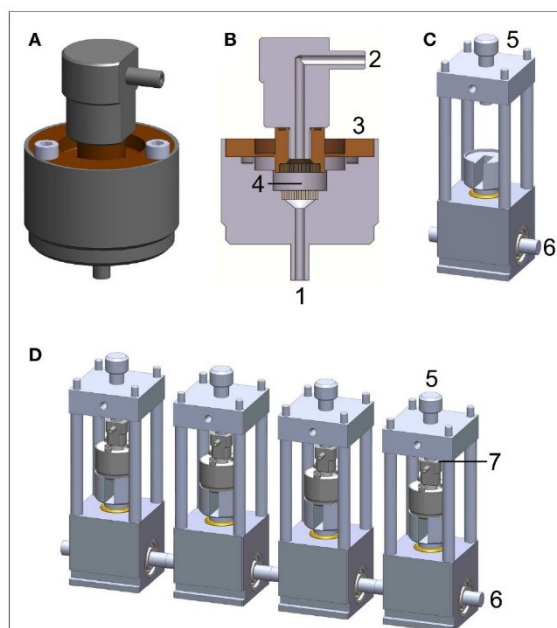

FIGURE 1 | Perfused compression bioreactor (PCB). (A) Bioreactor chamber holding the scaffold in place and ensuring hermetic sealing as well as force transmission toward the cell loaded construct. **(B)** Cross section of bioreactor chamber indicating medium inlets/outlets (1 and 2), flexible force transmitting disk (3), and intended space for scaffold/construct placement (4). **(C)** Power transmission rack including cam-shaft (6), which moves the plunger in order to apply a sinusoidal compression pattern onto the bioreactor chamber. The chamber is held in place with a pre-load screw (5) allowing for defined loading regimes. **(D)** A complete PCB system comprises four bioreactor chambers, four force transmission devices, and four force sensors (placed at position 7, not shown).

CHONDROGENIC CONSTRUCT CULTURE

Mesenchymal stromal cell seeded constructs were cultured for 3 weeks in chondrogenic medium (serum free medium supplemented with 0.1 mM ascorbic acid 2-phosphate, 10 ng/mL TGF-β3 and 10^{-7} M dexamethasone) (Mackay et al., 1998; Barbero et al., 2003). The serum free medium consists of: Dulbecco's modified Eagle's medium (DMEM) supplemented with 1 mM sodium pyruvate, 100 mM HEPES buffer, 100 U/mL penicillin, 100 µg/mL streptomycin, 0.29 mg/mL L-glutamine, ITS (10 µg/mL insulin, 5.5 µg/mL transferrin, 5 ng/mL selenium), 0.5 mg/mL bovine serum albumin, and 4.7 µg/mL linoleic acid. Using peristaltic pumps, unidirectional perfusion was applied to constructs with a perfusion velocity of 0.3 mL/min, with media changes twice per week (Santoro et al., 2011).

HYPERTROPHIC CONSTRUCT CULTURE

In order to withstand dynamic mechanical loading, stable cartilaginous templates are a prerequisite. Therefore, only constructs exhibiting good chondrogenesis were included for further investigations. Following 3 weeks of culture, cartilaginous constructs were then separated in two groups: loaded and non-loaded.

Non-loaded specimens were maintained in the unidirectional perfusion bioreactor whereas loaded specimens were transferred to the PCB system. Hypertrophic differentiation was induced by culturing constructs for 2 weeks in serum free medium supplemented with 50 nM thyroxine, 10 mM β-glycerophosphate, 10^{-8} M dexamethasone, and 0.1 mM L-ascorbic acid-2-phosphate (Scotti et al., 2010). Loaded constructs were exposed to an intermittent loading regime (construct displacement $\Delta z = 100\,\mu m$, frequency of $f = 1$ Hz, three load cycles per day comprising 2 h of loading and 6 h of rest) for 2 weeks with a pre-load ensuring press fit of the construct. During the application of mechanical load, the applied forces were monitored for each bioreactor chamber separately.

QUANTIFICATION OF GLYCOSAMINOGLYCAN AND DNA CONTENTS

Chondrogenic constructs were digested in proteinase K (1 mg/mL proteinase K in 50 mM Tris with 1 mM EDTA, 1 mM iodoacetamide, and 10 mg/mL pepstatin A) at 56°C overnight. The glycosaminoglycan (GAG) content of the cartilaginous constructs was determined spectrophotometrically using dimethylmethylene blue, with chondroitin sulfate as standard (Farndale et al., 1986). The DNA content of the constructs was measured using the CyQuant cell proliferation assay kit (Molecular Probes, Eugene, OR, USA) and used to normalize the GAG content.

REAL-TIME RT-PCR QUANTITATION OF TRANSCRIPT LEVELS

Total RNA was extracted from cells using Trizol® (LuBioScience GmbH, Lucerne, Switzerland) and reverse-transcribed as previously described (Frank et al., 2002). The samples were analyzed using a GeneAmp® PCR System 9600 (Perkin Elmer, www.perkinelmer.com) and the transcription levels of the following genes of interest were quantified: collagen type-I, collagen type-II, aggrecan, cartilage oligomeric matrix protein (COMP), SOX9, and glyceraldehyde 3-phosphate dehydrogenase (GAPDH) as housekeeping gene (Barbero et al., 2003).

HISTOLOGY AND IMMUNOHISTOCHEMISTRY

After *in vitro* cultures, the constructs were fixed in 1.5% paraformaldehyde and embedded in paraffin. Sections (5–10 μm thick) were stained for Safranin-O (Fluka) and Alizarin red after rehydration. Immunohistochemical analyses were performed to characterize the extracellular matrix using the following antibodies: collagen type-II (Col II; MPBiomedicals), collagen type-X (Col X; AbCam), and bone sialoprotein (BSP, 1:2000, A4232.1/A 4232.2, Immundiagnostik AG, Germany). Upon rehydration in ethanol series, sections were treated as previously described for antigen retrieval for Col II and Col X (Dickhut et al., 2009). The immunobinding was detected with biotinylated secondary antibodies and the appropriate Vectastain ABC kits. The red signal was developed with the Vector® Red kit (Linaris AK-5000) and sections counterstained by Hematoxylin. Negative controls were performed during each analysis by omitting the primary antibodies. Histological and immunohistochemical sections were analyzed using an Olympus BX-63 microscope.

RESULTS

PERFUSED COMPRESSION BIOREACTOR SYSTEM

The custom-made PCB system (**Figure 1**) underwent a systematic validation of the cyclic compression regime and the monitoring of the force sensors over a period of 5 weeks. **Figure 2** depicts representative force diagrams for chondrogenic constructs cultured under mechanical loading for 2 weeks. **Figure 2A** displays a force diagram of the daily loading regime consisting of loading (2 h) and resting phases (6 h). The force necessary to compress the chondrogenic constructs remained relatively constant throughout the entire culture period (**Figure 2A**). During the loading phase (**Figures 2B,C**), a sinusoidal waveform can be seen with a periodicity of approximately 1 s leading to the targeted frequency of 1 Hz. Moreover, the PCB showed a broad operational range as both collagen-based constructs (maximal force applied 110 N, **Figure 2B**) and NiTi-based constructs (maximal force applied 900 N, **Figure 2C**) could be stimulated without further modifications of the system.

CHONDROGENIC DIFFERENTIATION

After 3 weeks of chondrogenic culture, MSC cultured on OPTI-MAIX scaffolds could generate cartilaginous tissues. Cells were embedded in lacunae and deposited extracellular matrix positively stained for GAG and collagen type II (**Figure 3A**). GAG contents
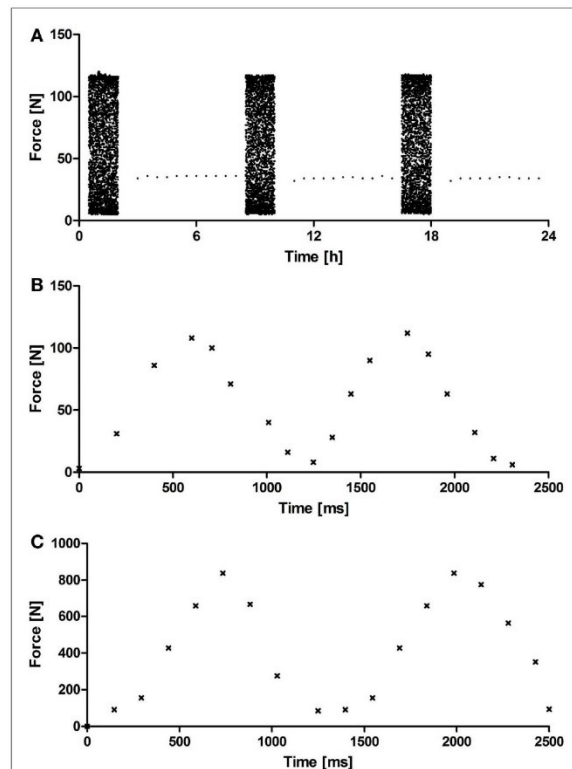
FIGURE 2 | Representative acquisition diagram from a force sensor.
(A) Representative force diagram acquired during 24 h of mechanical loading showing loading (2 h) and resting phases (4 h) for OPTIMAIX-based constructs ($n = 4$). Representative force diagram acquired during 2.5 s of loading showing the frequency (1 Hz) and periodicity of the sinusoidal wave for **(B)** OPTIMAIX- and **(C)** NiTi-based constructs ($n = 4$).

Chapter II – Novel perfused compression bioreactor

FIGURE 3 | Characterization of chondrogenic OPTIMAIX constructs (post 3 weeks of perfusion culture). (A) Representative histological Safranin-O staining for GAG and immunohistochemical staining for type-II collagen indicating cartilaginous tissue formation (n = 4). Scale bar = 1 mm (valid for both panels). **(B)** Gene expression levels for MSC cultured on scaffolds for 3 weeks. Measurements are mean ± SD (n = 3).

were determined to be $14.6 \pm 3.4\,\mu g/\mu g$ (GAG/DNA). **Figure 3B** shows the expression levels of genes associated with chondrogenic differentiation.
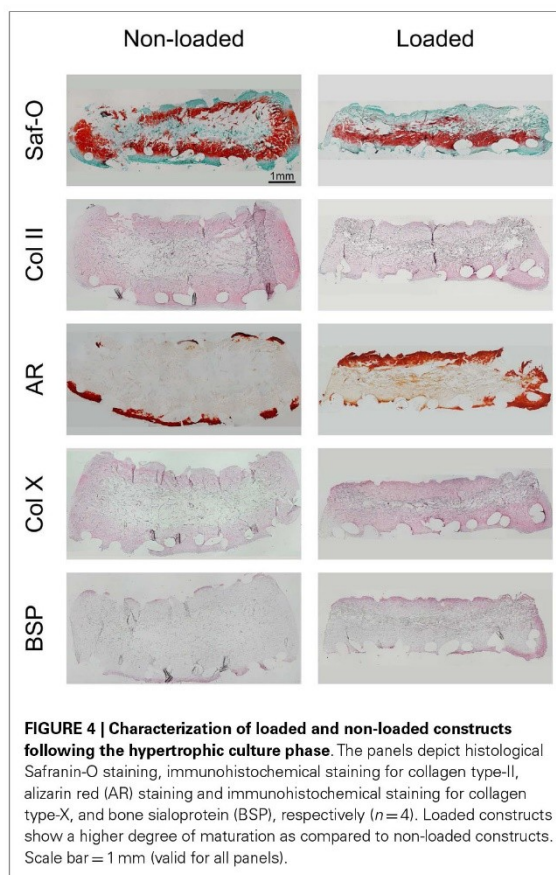
HYPERTROPHIC DIFFERENTIATION

Following 2 weeks of hypertrophic differentiation, constructs exhibited increased GAG deposition (**Figure 4**). Similar to chondrogenic constructs, the scaffold cores of non-loaded hypertrophic constructs were devoid of GAG, yet containing fibrotic tissue and limited amounts of cells. Loaded constructs exhibited a more homogeneous distribution of GAG, but less intense staining than non-loaded constructs indicating ongoing remodeling. Collagen type-II staining of non-loaded hypertrophically differentiated constructs was increased as compared to chondrogenic constructs and loaded hypertrophic constructs.

Alizarin red staining showed that the ECM of both loaded and non-loaded constructs was mineralized preferentially along the scaffold periphery. However, loaded constructs exhibited thicker mineralized borders as compared to non-loaded constructs as well as mineralized islets within the construct. Collagen type-X staining was also observed to be preferentially deposited at the scaffold periphery in both loaded and non-loaded constructs. However, it was enriched throughout the construct in loaded samples, especially in the highly mineralized regions. BSP immunohistochemical staining indicated relatively few positively stained cells in the periphery of the non-loaded scaffolds. Loaded constructs showed high amounts of BSP-positive cells in both the peripheral regions of the constructs and within the internal central region.

DISCUSSION

In this work, we have developed a PCB system to apply physiological dynamic mechanical loads and strains on engineered

FIGURE 4 | Characterization of loaded and non-loaded constructs following the hypertrophic culture phase. The panels depict histological Safranin-O staining, immunohistochemical staining for collagen type-II, alizarin red (AR) staining and immunohistochemical staining for collagen type-X, and bone sialoprotein (BSP), respectively (n = 4). Loaded constructs show a higher degree of maturation as compared to non-loaded constructs. Scale bar = 1 mm (valid for all panels).

constructs to investigate the process of fracture healing. A proof-of-concept study was performed applying dynamic mechanical loads onto cell seeded collagen- and NiTi-based constructs, presenting the broad operational range of the developed system.

The PCB underwent systematic validation revealing safe and reliable functionality to ensure defined dynamic mechanical loading of viable engineered tissues. As compared to previously described systems (Rath et al., 2008; Ballyns and Bonassar, 2010; Sittichokechaiwut et al., 2010; Sun et al., 2010; Lujan et al., 2011; Matziolis et al., 2011; Omata et al., 2012; Petri et al., 2012; Puetzer et al., 2012; Shahin and Doran, 2012), the PCB exhibits a broader operational range. It allows for physiological mechanical compression in a consistent and reliable manner in a range from approximately 10 N up to 1 kN, while maintaining compact dimensions.

Given the fact that the compression applied is displacement driven, a various range of scaffolds and tissues can be easily investigated with dynamic mechanical loading without further adaptation of the system. Additionally, this range can be further enlarged via exchanging the eccentric cam-shaft, thereby adapting the displacement toward the desired range.

Our proof-of-concept study was conducted to assess the effect of physiological compressive loads during hypertrophic differentiation as an *in vitro* model for the transition from a soft to a hard callus. Since the development of a soft cartilaginous callus is a crucial step during secondary fracture healing (Schindeler et al., 2008), during the initial phase of the study, MSC were seeded on OPTIMAIX scaffolds and primed toward chondrogenesis. The resulting engineered constructs showed cartilaginous characteristics including: (i) ECM containing GAGs and collagen type-II, (ii) cells embedded in lacunae, and (iii) chondrocytic gene expression. Moreover, the cartilaginous constructs exhibited stable size and shape, enabling the application of dynamic loading within the PCB.

In our experimental setup, constructs undergoing mechanical loading during hypertrophy exhibited a higher degree of maturation than unloaded constructs. MSC embedded in the cartilaginous extracellular matrix of mechanically loaded constructs displayed enlarged lacunae to a higher extent than in non-loaded constructs. Furthermore, the diminished GAG and collagen type-II staining, as well as the high degree of mineral deposition (Mackie et al., 2008), collagen type-X content (Mackie et al., 2008; Gawlitta et al., 2010), and BSP staining (Sommer et al., 1996; Gawlitta et al., 2010) within loaded constructs underlines the late hypertrophic state of the MSC. Moreover, as BSP has been shown to be the main nucleator of hydroxyapatite crystals and to correlate with the initial phase of matrix mineralization (Bianco et al., 1993), the increased BSP staining in the ECM of mechanically loaded constructs indicates a higher degree of maturation as compared to non-loaded constructs. While this proof-of-concept study provides evidence of loading mediated hypertrophic differentiation, subsequent work should be aimed at further understanding the extent of hypertrophy (e.g., gene expression profiles).

In this study, we present our mechanically loaded hypertrophic constructs as an *in vitro* model of a fracture callus, which is undergoing the transition from soft to hard callus through remodeling and ossification of the soft cartilaginous callus (Gerstenfeld et al., 2003). The results obtained from our *in vitro* model system, i.e., application of dynamic mechanical compression during the hypertrophic differentiation phase, are consistent with previous *in vivo* models (Grundnes and Reikerås, 1991; Buckwalter and Grodzinsky, 1999; Hardy, 2004), which demonstrated that early mobilization and application of mechanical loads enhances the process of fracture healing. These results thus support the use of the PCB as an *in vitro* model for dynamic mechanical loading.

CONCLUSION

In this study, we have demonstrated that the developed PCB system depicts a versatile tool for the *in vitro* application of dynamic physiological mechanical loads onto scaffolding materials with a wide range of mechanical properties. Mechanical loading applied via the developed bioreactor system enhances ECM mineralization during hypertrophy of cartilaginous constructs and triggers the maturation process of MSC toward late hypertrophic chondrocytes as demonstrated through the decrease in GAG and collagen type-II, the thickened mineralized border, the increased amounts of type-X collagen and positive BSP staining. Furthermore, the application of cyclic mechanical loading leads to the maturation

of scaffold-based constructs. In combination with the fracture callus model, the PCB displays an advanced *in vitro* model and a promising tool for further studies testing alternative fracture treatments, based on engineered grafts or pharmaceutical compounds. Additionally, toward implementation of the 3R principles (replace, reduce, and refine) (Goldberg et al., 1996), this system could lead to a reduction of animal experiments within the field.

SUPPLEMENTARY MATERIAL

The Supplementary Material for this article can be found online at http://www.frontiersin.org/Journal/10.3389/fbioe.2015.00010/abstract

REFERENCES

Aro, H. T., Wahner, H. T., and Chao, E. Y. (1991). Healing patterns of transverse and oblique osteotomies in the canine tibia under external fixation. *J. Orthop. Trauma* 5, 351–364. doi:10.1097/00005131-199109000-00016

Ballyns, J. J., and Bonassar, L. J. (2010). Dynamic compressive loading of image-guided tissue engineered meniscal constructs. *J. Biomech.* 44, 509–516. doi:10.1016/j.jbiomech.2010.09.017

Barbero, A., Ploegert, S., Heberer, M., and Martin, I. (2003). Plasticity of clonal populations of dedifferentiated adult human articular chondrocytes. *Arthritis Rheum.* 48, 1315–1325. doi:10.1002/art.10950

Behonick, D. J., Xing, Z., Lieu, S., Buckley, J. M., Lotz, J. C., Marcucio, R. S., et al. (2007). Role of matrix metalloproteinase 13 in both endochondral and intramembranous ossification during skeletal regeneration. *PLoS ONE* 2:e1150. doi:10.1371/journal.pone.0001150

Bianco, P., Riminucci, M., Silvestrini, G., Bonucci, E., Termine, J. D., Fisher, L. W., et al. (1993). Localization of bone sialoprotein (BSP) to Golgi and post-Golgi secretory structures in osteoblasts and to discrete sites in early bone matrix. *J. Histochem. Cytochem.* 41, 193–203. doi:10.1177/41.2.8419459

Braccini, A., Wendt, D., Jaquiery, C., Jakob, M., Heberer, M., Kenins, L., et al. (2005). Three-dimensional perfusion culture of human bone marrow cells and generation of osteoinductive grafts. *Stem Cells* 23, 1066–1072. doi:10.1634/stemcells.2005-0002

Buckwalter, J. A., and Grodzinsky, A. J. (1999). Loading of healing bone, fibrous tissue, and muscle: implications for orthopaedic practice. *J. Am. Acad. Orthop. Surg.* 7, 291–299.

Chao, E. Y. S., and Inoue, N. (2003). Biophysical stimulation of bone fracture repair, regeneration and remodelling. *Eur. Cell. Mater.* 6, 72–84; discussion 84–5.

Claes, L., Augat, P., Suger, G., and Wilke, H. J. (1997). Influence of size and stability of the osteotomy gap on the success of fracture healing. *J. Orthop. Res.* 15, 577–584. doi:10.1002/jor.1100150414

Démarteau, O., Jakob, M., Schäfer, D., Heberer, M., and Martin, I. (2003). Development and validation of a bioreactor for physical stimulation of engineered cartilage. *Biorheology* 40, 331–336.

Dickhut, A., Pelttari, K., Janicki, P., Wagner, W., Eckstein, V., Egermann, M., et al. (2009). Calcification or dedifferentiation: requirement to lock mesenchymal stem cells in a desired differentiation stage. *J. Cell. Physiol.* 219, 219–226. doi:10.1002/jcp.21673

Farndale, R. W., Buttle, D. J., and Barrett, A. J. (1986). Improved quantitation and discrimination of sulphated glycosaminoglycans by use of dimethylmethylene blue. *Biochim. Biophys. Acta* 883, 173–177. doi:10.1016/0304-4165(86)90306-5

Frank, O., Heim, M., Jakob, M., Barbero, A., Schäfer, D., Bendik, I., et al. (2002). Real-time quantitative RT-PCR analysis of human bone marrow stromal cells during osteogenic differentiation in vitro. *J. Cell. Biochem.* 85, 737–746. doi:10.1002/jcb.10174

Gawlitta, D., Farrell, E., Malda, J., Creemers, L. B., Alblas, J., and Dhert, W. J. A. (2010). Modulating endochondral ossification of multipotent stromal cells for

bone regeneration. *Tissue Eng. Part B. Rev.* 16, 385–395. doi:10.1089/ten.TEB.2009.0712

Gerstenfeld, L. C., Cullinane, D. M., Barnes, G. L., Graves, D. T., and Einhorn, T. A. (2003). Fracture healing as a post-natal developmental process: molecular, spatial, and temporal aspects of its regulation. *J. Cell. Biochem.* 88, 873–884. doi:10.1002/jcb.10435

Goldberg, A. M., Zurlo, J., and Rudacille, D. (1996). The three Rs and biomedical research. *Sci.* 272, 1403. doi:10.1126/science.272.5267.1403

Goodship, A. E., and Kenwright, J. (1985). The influence of induced micromovement upon the healing of experimental tibial fractures. *J. Bone Joint Surg. Br.* 67, 650–655.

Grundnes, O., and Reikerås, O. (1991). Mechanical effects of function on bone healing. Nonweight bearing and exercise in osteotomized rats. *Acta Orthop. Scand.* 62, 163–165. doi:10.3109/17453679108999248

Hardy, M. A. (2004). Principles of metacarpal and phalangeal fracture management: a review of rehabilitation concepts. *J. Orthop. Sports Phys. Ther.* 34, 781–799. doi:10.2519/jospt.2004.34.12.781

Hoffmann, W., Bormann, T., Rossi, A., Muller, B., Schumacher, R., Martin, I., et al. (2014a). Rapid prototyped porous nickel-titanium scaffolds as bone substitutes. *J. Tissue Eng.* 5, doi:10.1177/2041731414540674

Hoffmann, W., Döbeli, C., Santoro, R., Wendt, D., and de Wild, M. (2014b). *Reactor Device for Mechanical Loading of Tissue Specimens and/or Engineered Tissues.* European Patent Office Munich, priority application, EP 14/169756.

Keaveny, T. M., Morgan, E. F., Yeh, O. C., Material, C., Bone, C., and Bone, T. (2004). "Bone mechanics," in *Standard handbook of Biomedical Engineering and Design*, 1–24.

Lujan, T. J., Wirtz, K. M., Bahney, C. S., Madey, S. M., Johnstone, B., and Bottlang, M. (2011). A novel bioreactor for the dynamic stimulation and mechanical evaluation of multiple tissue-engineered constructs. *Tissue Eng. Part C Methods* 17, 367–374. doi:10.1089/ten.tec.2010.0381

Mackay, A. M., Beck, S. C., Murphy, J. M., Barry, F. P., Chichester, C. O., and Pittenger, M. F. (1998). Chondrogenic differentiation of cultured human mesenchymal stem cells from marrow. *Tissue Eng.* 4, 415–428. doi:10.1089/ten.1998.4.415

Mackie, E. J., Ahmed, Y. A., Tatarczuch, L., Chen, K.-S., and Mirams, M. (2008). Endochondral ossification: how cartilage is converted into bone in the developing skeleton. *Int. J. Biochem. Cell Biol.* 40, 46–62. doi:10.1016/j.biocel.2007.06.009

Marsell, R., and Einhorn, T. A. (2011). The biology of fracture healing. *Injury* 42, 551–555. doi:10.1016/j.injury.2011.03.031

Matziolis, D., Tuischer, J., Matziolis, G., Kasper, G., Duda, G., and Perka, C. (2011). Osteogenic predifferentiation of human bone marrow-derived stem cells by short-term mechanical stimulation. *Open Orthop. J.* 5, 1–6. doi:10.2174/1874325001105010001

Omata, S., Sonokawa, S., Sawae, Y., and Murakami, T. (2012). Effects of both vitamin C and mechanical stimulation on improving the mechanical characteristics of regenerated cartilage. *Biochem. Biophys. Res. Commun.* 424, 724–729. doi:10.1016/j.bbrc.2012.07.019

Park, S. H., O'Connor, K., McKellop, H., and Sarmiento, A. (1998). The influence of active shear or compressive motion on fracture-healing. *J. Bone Joint Surg. Am.* 80, 868–878.

Petri, M., Ufer, K., Toma, I., Becher, C., Liodakis, E., Brand, S., et al. (2012). Effects of perfusion and cyclic compression on in vitro tissue engineered meniscus implants. *Knee Surg. Sports Traumatol. Arthrosc.* 20, 223–231. doi:10.1007/s00167-011-1600-3

Puetzer, J. L., Ballyns, J. J., and Bonassar, L. J. (2012). The effect of the duration of mechanical stimulation and post-stimulation culture on the structure and properties of dynamically compressed tissue-engineered menisci. *Tissue Eng. Part A* 18, 1365–1375. doi:10.1089/ten.TEA.2011.0589

Rand, J. A., An, K. N., Chao, E. Y., and Kelly, P. J. (1981). A comparison of the effect of open intramedullary nailing and compression-plate fixation on fracture-site blood flow and fracture union. *J. Bone Joint Surg. Am.* 63, 427–442.

Rath, B., Nam, J., Knobloch, T. J., Lannutti, J. J., and Agarwal, S. (2008). Compressive forces induce osteogenic gene expression in calvarial osteoblasts. *J. Biomech.* 41, 1095–1103. doi:10.1016/j.jbiomech.2007.11.024

Rubin, C., Bolander, M., Ryaby, J. P., and Hadjiargyrou, M. (2001). The use of low-intensity ultrasound to accelerate the healing of fractures. *J. Bone Joint Surg. Am.* 83-A, 259–270.

Santoro, R., Krause, C., Martin, I., and Wendt, D. (2011). On-line monitoring of oxygen as a non-destructive method to quantify cells in engineered 3D tissue constructs. *J. Tissue Eng. Regen. Med.* 6, 696–701. doi:10.1002/term.473

Schindeler, A., McDonald, M. M., Bokko, P., and Little, D. G. (2008). Bone remodeling during fracture repair: the cellular picture. *Semin. Cell Dev. Biol.* 19, 459–466. doi:10.1016/j.semcdb.2008.07.004

Scotti, C., Tonnarelli, B., Papadimitropoulos, A., Scherberich, A., Schaeren, S., Schauerte, A., et al. (2010). Recapitulation of endochondral bone formation using human adult mesenchymal stem cells as a paradigm for developmental engineering. *Proc. Natl. Acad. Sci. U. S. A.* 107, 7251–7256. doi:10.1073/pnas.1000302107

Sfeir, C., Ho, L., Doll, B. A., Azari, K., and Hollinger, J. O. (2005). "Fracture repair," in *Bone Regeneration and Repair: Biology and Clinical Applications*, eds J. R. Lieberman and G. E. Friedlaender (New York: Humana Press Inc.), 21–44.

Shahin, K., and Doran, P. M. (2012). Tissue engineering of cartilage using a mechanobioreactor exerting simultaneous mechanical shear and compression to simulate the rolling action of articular joints. *Biotechnol. Bioeng.* 109, 1060–1073. doi:10.1002/bit.24372

Sittichokechaiwut, A., Edwards, J. H., Scutt, A. M., and Reilly, G. C. (2010). Short bouts of mechanical loading are as effective as dexamethasone at inducing matrix production by human bone marrow mesenchymal stem cell. *Eur. Cell. Mater.* 20, 45–57.

Sommer, B., Bickel, M., Hofstetter, W., and Wetterwald, A. (1996). Expression of matrix proteins during the development of mineralized tissues. *Bone* 19, 371–380. doi:10.1016/S8756-3282(96)00218-9

Sun, M., Lv, D., Zhang, C., and Zhu, L. (2010). Culturing functional cartilage tissue under a novel bionic mechanical condition. *Med. Hypotheses* 75, 657–659. doi:10.1016/j.mehy.2010.08.011

Weiner, S., and Wagner, H. D. (1998). THE MATERIAL BONE: structure-mechanical function relations. *Annu. Rev. Mater. Sci.* 28, 271–298. doi:10.1146/annurev.matsci.28.1.271

Wendt, D., Marsano, A., Jakob, M., Heberer, M., and Martin, I. (2003). Oscillating perfusion of cell suspensions through three-dimensional scaffolds enhances cell seeding efficiency and uniformity. *Biotechnol. Bioeng.* 84, 205–214. doi:10.1002/bit.10759

Wendt, D., Stroebel, S., Jakob, M., John, G. T., and Martin, I. (2006). Uniform tissues engineered by seeding and culturing cells in 3D scaffolds under perfusion at defined oxygen tensions. *Biorheology* 43, 481–488.

Conflict of Interest Statement: The authors declare that the research was conducted in the absence of any commercial or financial relationships that could be construed as a potential conflict of interest.

66

Chapter III

Rapid prototyped porous NiTi

scaffolds as bone substitutes

Original Article

Rapid prototyped porous nickel–titanium scaffolds as bone substitutes

Waldemar Hoffmann[1,2], Therese Bormann[2,3], Antonella Rossi[4,5],
Bert Müller[3], Ralf Schumacher[2], Ivan Martin[1], Michael de Wild[2]
and David Wendt[1]

Abstract

While calcium phosphate–based ceramics are currently the most widely used materials in bone repair, they generally lack tensile strength for initial load bearing. Bulk titanium is the gold standard of metallic implant materials, but does not match the mechanical properties of the surrounding bone, potentially leading to problems of fixation and bone resorption. As an alternative, nickel–titanium alloys possess a unique combination of mechanical properties including a relatively low elastic modulus, pseudoelasticity, and high damping capacity, matching the properties of bone better than any other metallic material. With the ultimate goal of fabricating porous implants for spinal, orthopedic and dental applications, nickel–titanium substrates were fabricated by means of selective laser melting. The response of human mesenchymal stromal cells to the nickel–titanium substrates was compared to mesenchymal stromal cells cultured on clinically used titanium. Selective laser melted titanium as well as surface-treated nickel–titanium and titanium served as controls. Mesenchymal stromal cells had similar proliferation rates when cultured on selective laser melted nickel–titanium, clinically used titanium, or controls. Osteogenic differentiation was similar for mesenchymal stromal cells cultured on the selected materials, as indicated by similar gene expression levels of bone sialoprotein and osteocalcin. Mesenchymal stromal cells seeded and cultured on porous three-dimensional selective laser melted nickel–titanium scaffolds homogeneously colonized the scaffold, and following osteogenic induction, filled the scaffold's pore volume with extracellular matrix. The combination of bone-related mechanical properties of selective laser melted nickel–titanium with its cytocompatibility and support of osteogenic differentiation of mesenchymal stromal cells highlights its potential as a superior bone substitute as compared to clinically used titanium.

Introduction

The most widely used scaffold materials for bone tissue engineering applications are calcium phosphate ceramics (e.g., hydroxyapatite and tricalcium phosphate) due to their osteoinductive and osteoconductive properties.[1–4] However, these materials generally lack the tensile strength required for initial load bearing and primary stability and, as bulk material, do not match the mechanical properties of the surrounding bone, limiting their application to non-load-bearing situations or requiring long periods of immobilization during bone healing.

As an alternative to ceramics, metals have been used for prostheses in orthopedics and orthodontics for decades due

[1]Departments of Biomedicine and Surgery, University Hospital Basel, Basel, Switzerland
[2]University of Applied Sciences Northwestern Switzerland, School of Life Sciences, Institute for Medical and Analytical Technologies, Gründenstrasse 40, 4132 Muttenz, Switzerland
[3]Biomaterials Science Center, University of Basel, Basel, Switzerland
[4]Laboratory for Surface Science and Technology, Department of Materials, ETH Zurich, Zurich, Switzerland
[5]Dipartimento di Scienze Chimiche e Geologiche, Università degli Studi di Cagliari, Cagliari, Italy

Corresponding author:
Michael de Wild, University of Applied Sciences Northwestern Switzerland, School of Life Sciences, Institute for Medical and Analytical Technologies, Gründenstrasse 40, 4132 Muttenz, Switzerland.
Email: michael.dewild@fhnw.ch

to their superior mechanical properties. In particular, titanium has traditionally been one of the most commonly used metallic implant materials, demonstrating biocompatibility[5–7] and osseointegration.[8] However, the Young's modulus of Ti (100 GPa) significantly exceeds that of cortical bone (3–20 GPa), which can result in stress-shielding. As the Ti implant absorbs most of the applied mechanical load, the surrounding bone is shielded from the applied stress, ultimately leading to bone resorption.[9]

As compared to pure metals, metallic alloys allow the tuning of the particular mechanical properties toward specific medical needs (e.g., Young's modulus). In particular, nickel–titanium (NiTi) alloys have—for a metallic material—particularly low Young's moduli, which are comparable to that of bone, are pseudo-elastic, have a high damping capacity,[10] and exhibit shape memory properties. Due to this unique combination of mechanical properties, NiTi possesses great promise as a next generation scaffold material for bone repair.

To produce metallic scaffolds with a well-defined geometry, conventional methods (including turning, milling, and drilling) are often impracticable and expensive. Selective laser melting (SLM), an additive manufacturing method, is a promising alternative. Complex-shaped, porous elements or filigree lattices with strut sizes down to 200 μm can be fabricated on the basis of a predefined three-dimensional (3D) dataset.[11,12] Since pore shapes, sizes, and distributions can be controlled, specific scaffold architectures can be tailored to meet the particular needs for cell ingrowth or to match the mechanical environment of the intended implant site.[13–15] Therefore, the flexibility of the SLM technique, combined with the material properties of NiTi, allows for the design of implants with precisely tuned mechanical properties optimized for bone repair applications.

With the ultimate goal of fabricating 3D NiTi implants for spinal, orthopedic, and dental applications, in this work, we aimed to compare the behavior of human bone marrow–derived mesenchymal stromal cells (MSC) cultured on SLM-produced NiTi substrates as compared to the gold standard titanium. We first characterized the topographical and chemical surface properties of non-porous two-dimensional (2D) substrate surfaces fabricated by SLM. We next aimed to assess the proliferation and osteogenic differentiation of MSC cultured on these materials. Finally, we assessed the behavior of MSC seeded and cultured on 3D NiTi scaffolds fabricated by SLM. The cytocompatibility and osteogenic potential of SLM NiTi as demonstrated here, along with its superior mechanical properties (i.e., damping, shape memory), highlight the potential of SLM NiTi as a superior bone substitute as compared to today's Ti implant materials.

Materials and methods

SLM manufacturing of 2D disks

In order to investigate the effect of material surface properties on cell behavior, non-porous "2D" metallic disks of

Table 1. Sample treatment scheme. "Ti ref" is our reference material which is a conventionally manufactured and surface-treated titanium material used in the clinic.[5] A direct comparison of the effects of Ti ref and our SLM produced nickel–titanium ("NiTi") on MSC behavior is nontrivial due to a number of variables: (1) chemistry of the bulk materials, (2) the effect of the SLM manufacturing process, and (3) surface topography. Therefore, titanium disks produced by the SLM process were also fabricated ("Ti"). To account for the surface treatment of Ti ref, two groups of SLM produced disks were also surface treated ("Ti ST" and "NiTi ST") to obtain similar surface topographies..

	Ti ref	Ti	Ti ST	NiTi	NiTi ST
SLM		✓	✓	✓	✓
Sandblasting	✓		✓		
Etching	✓		✓		✓

MSC: mesenchymal stromal cells; SLM: selective laser melting.

both nickel–titanium and titanium ($\varnothing$ 14 mm, 2 mm thickness) were produced using SLM technology with the SLM Realizer 100 and Realizer 250, respectively (SLM Solutions, Lübeck, Germany). Disks were produced from either nickel–titanium with a nominal nickel-content of 55.96 wt% (Memry GmbH, Lübeck, Germany) or grade 2 titanium (SLM Solutions) with particle sizes ranging from 35 to 180 μm. Subsequent to fabrication, nickel–titanium disks were annealed for 20 min at a temperature of 500°C under a protective argon atmosphere. Disks produced by SLM were compared to disks of a conventionally manufactured reference titanium material (grade 2 Ti, non-SLM produced). Reference titanium disks were surface treated by sandblasting (abrasive grit Al_2O_3 particles with a mean grain size of 125 μm and 4 bar blasting pressure for 2 min) and acid etching (mixture of ddH_2O (resistivity 18.2 MΩcm, ELGA Purelab Option-Q DV 25, ELGA LabWater, Celle, Germany): H_2SO_4 (95%, J.T. Baker, Avantor Performance Materials, Inc., Phillipsburg, NJ, USA): HCl (32%, Sigma-Aldrich Chemie GmbH, Buchs, Switzerland) in a volume ratio of 1: 1: 2 at 93 °C for 7 min). The surface-treated reference titanium material ("Ti ref") which has been used clinically for dental implants[5,7] was provided by Thommen Medical AG (Grenchen, Switzerland).

Surface treatment of SLM disks

Considering that Ti ref disks had been surface treated, we aimed to assess the effects of surface treatment. Disks were surface treated according to the conditions outlined in Table 1. "Ti" and "NiTi" disks received no further post-processing surface treatments. Following SLM production, "Ti ST" disks were surface treated to create surfaces similar to Ti ref.[5] Ti ST disks were sandblasted and etched using similar parameters as for Ti ref. Since the titanium etching process is not effective for nickel–titanium, "NiTi ST" disks were alternatively surface treated by etching in
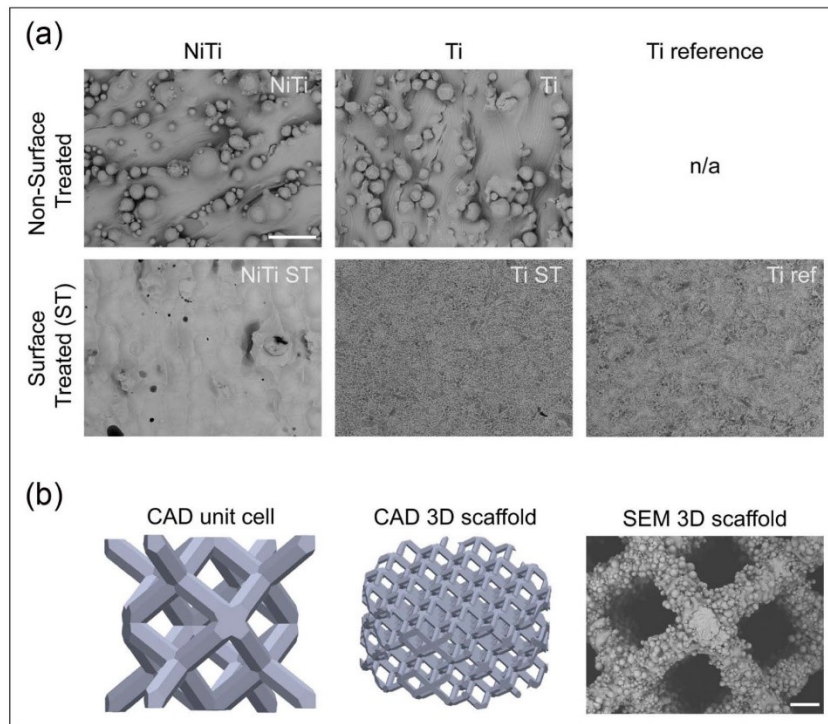
Figure 1. (a) SEM micrographs of 2D metallic disks. Upper panel depicts SLM produced NiTi and Ti disks. Lower panel depicts post-production surface treated (ST, that is, etching, passivation) disks including the clinically used reference (conventional Ti Ref). Scale bar = 100 μm and (b) CAD models of the unit cell (2 mm height), entire cylindrical 3D scaffold (4 mm height, 8 mm diameter) and SEM micrograph of the SLM produced 3D NiTi scaffold. Scale bar = 100 μm.
SEM: scanning electron microscope; 2D: two-dimensional; SLM: selective laser melting; NiTi: nickel–titanium; CAD: computer-aided design; 3D: three-dimensional.

HF at a temperature of 60°C for a duration of 3 min after SLM production.

Cleaning, passivation, and sterilization of disks

Disks were cleaned in a 4% Deconex® 15PF (Beiersdorf Münchenstein, Switzerland) solution at 90°C with ultrasonic agitation for 5 min. Specimens were then rinsed in ultrapure water (resistivity 18.2 MΩcm) for 15 min (3 × 5 min with exchange of water) in an ultrasonic bath. Subsequently, disks were passivated in nitric acid (32.5% HNO$_3$, Sigma-Aldrich Chemie GmbH, Buchs, Switzerland) with ultrasonic agitation for 10 min.[16] Finally, the specimens were high purity oxygen plasma treated (PDC-32G, Harrick, Ithaca, NY, USA, oxygen purity 99.9995%, Carbagas) at 29.7 W for 2 min and sterilized using hot steam (Cominox Sterilclave 24BHD, Cominox S.r.l., Carate B.za, Italia, 121°C for 20 min).

SLM manufacturing of 3D scaffolds

3D scaffolds were manufactured from nickel–titanium powder with a nominal nickel content of 55.96 wt% and particle sizes ranging between 35 and 75 μm. Smaller particles were used to fabricate 3D scaffolds compared to 2D disks to facilitate the production of small diameter filigree struts. Scaffolds were formed using a rhombic dodecahedron unit cell (height × width × depth: 2 mm × 2 mm × 2 mm, Figure 1(b)). Magics software (V15.0.4.2; Materialise, Leuven, Belgium) was used to design a scaffold with a final cylindrical shape (8 mm diameter × 4 mm height) and an overall porosity of 84%.[13] Furthermore, SLM-fabricated scaffolds exhibited a gravimetrically determined porosity of 77.5% ± 0.4% (Mettler Toledo AT261 Delta Range, Mettler-Toledo GmbH, Greifensee, Schweiz) and a porosity of 76% determined by micro-computed tomography,[17] which are slightly lower due to minimal geometric deviations during the melting process and due to residual powder particles. Following SLM production, "3D NiTi scaffolds" were post-processed as 2D NiTi disks (i.e., non-surface-treated), excluding the annealing step.

Surface characterization

Surface characterization was performed on cleaned and passivated, unsterilized samples. Surface topography was

assessed using a scanning electron microscope (SEM; FEI Nova Nano SEM 230; Microscopy Centre University Basel, Switzerland). The surface roughness was measured using 3D Confocal Laser Scanning Microscope (LEXT OLS4000; Olympus, 50× objective, Olympus Schweiz AG, Volketswil, Schweiz). Each substrate was scanned three times at random positions to determine the roughness values: average surface roughness (SR_a), maximal peak to valley height (SR_Z), and roughness spacing parameter (S_m, a measure of the mean spacing between peaks) (cutoff wavelength λ_c = 51.9 µm).[18] Additionally, the developed surface area ratio (Sdr, the ratio of the effective surface area due to the surface roughness and the projected surface area) were measured according to Wennerberg and Albrektsson.[19] Substrate wettability was evaluated by means of water contact angle measurements using a sessile drop set-up (EasyDrop; Krüss, Hamburg, Germany; MilliQ water, Millipore, MA, USA; V = 5 µL) and the corresponding software DSA 100 to calculate contact angles θ.

X-ray photoelectron spectroscopy (XPS) was carried out using a Phi Quantera SXM spectrometer (ULVAC-PHI, Chanhassen, MN, USA) equipped with a monochromatic aluminum K_α x-ray source (hv = 1486.6 eV). Survey and high-resolution spectra were acquired from all 2D disks using a 100 µm beam diameter with the analyzer operated in fixed analyzer transmission (FAT) mode. Survey spectra were acquired setting the pass energy at 280 eV and a step size of 1.0 eV (full-width-at-half-maximum (fwhm) of the peak height for $Ag3d_{5/2}$ = 1.66 eV) while high-resolution spectra were acquired with a pass energy of 26 eV and a step size of 0.05 eV (fwhm for $Ag3d_{5/2}$ = 0.7 eV). Composition versus depth profiles were recorded alternating the etching of the sample surface with an argon source ran at 3 keV and 15 nA. The pass energy was set at 69 eV (fwhm of the peak height for $Ag3d_{5/2}$ = 0.87 eV), and the step size was 0.125 eV. Calibration of the depth scale was performed using a Si/SiO_2 reference sample under the same experimental conditions and was found to be (10.8 ± 0.1) nm/min. For data acquisition, the COMPASS software (v.7.3.4; ULVAC-PHI, Chanhassen, MN, USA) was used. Data processing and quantification of the composition depth profiles was performed using MultiPakTM 8 (V8.1C; ULVAC-PHI). Details on the spectrometer calibration are provided in Crobu et al.[20]

Cytotoxicity assessment

Cytotoxicity was assessed in accordance with ISO 10993-5.[21] Metallic substrates were immersed in complete medium (CM) consisting of alpha–minimum essential medium (MEM) supplemented with 10% fetal bovine serum (FBS), 1% HEPES, 1% sodium pyruvate, and 1% Penicillin-Streptomycin Glutamate (100×) solution (all

from Gibco, Life Technologies Europe, Zug, Switzerland, http://www.invitrogen.com) with a surface to media ratio of 6 cm²/mL for at least 24 h in a cell culture incubator. Additionally, unconditioned CM and CM conditioned with latex were used as positive and negative controls, respectively. Post extraction, metallic substrates were removed and the conditioned media used for the culture of MG-63 osteosarcoma cells. Following 3 and 7 days, the viability of MG-63 cells was determined by incubation with MTT (3-(4,5-dimethylthiazol-2-yl)-2,5-diphenyltetrazolium bromide; Sigma Aldrich) solution at a final concentration of 0.05 mg/mL. The amount of blue/purple-metabolized substrate of MTT was quantified spectroscopically by DMSO (D2650; Sigma-Aldrich Chemie GmbH, Buchs, Switzerland) extraction and absorption measurement at 575 nm wavelength (SpectraMax 190; Bucher Biotec AG, Basel, Switzerland).

Cell culture

Human bone marrow aspirates were harvested during routine iliac crest bone grafting, in accordance with the rules of the local ethical committee (University Hospital Basel, Basel, Switzerland) and after informed consent was obtained. MSC were isolated from the bone marrow aspirates[22] and expanded[23] as previously described. MSC were expanded for two to four passages for subsequent experiments.

2D cultures

For the assessment of cell proliferation, MSC were seeded onto the surfaces of metallic 2D disks and Petri dishes (i.e., tissue culture polystyrene—"TCP") at densities of 3×10^4 cells/cm² and cultured in CM supplemented with fibroblast growth factor–2 (FGF-2) for up to 3 weeks with media changes twice a week.

The osteogenic differentiation of MSC was performed by seeding 3×10^5 cells/cm² onto metallic 2D disks and 6×10^4 cells/cm² on TCP to reach confluence upon seeding, thereby increasing cell-to-cell contacts and accelerating the onset of osteogenic differentiation. Cells were cultured in CM or osteogenesis inducing medium (OM) consisting of CM supplemented with 10 nM dexamethasone, 0.1 mM L-ascorbic acid-2-phosphate, and 10 mM b-glycerophosphate for 2 weeks with media changes performed twice a week.

3D cultures

MSC were seeded, expanded, and differentiated within 3D NiTi scaffolds using a perfusion bioreactor system as previously described.[24,25] The bioreactor system was designed to first perfuse a cell suspension directly through the pores of a 3D scaffold, to seed cells uniformly throughout the

entire scaffold, and subsequently to perfuse culture media, to maintain cell viability during expansion and differentiation. The perfusion flow rate was set to 2.8 mL/min for 24 h during the seeding phase and subsequently changed to 0.28 mL/min for the proliferation and differentiation phases.

The proliferation of MSC on 3D NiTi scaffolds was assessed by seeding 1×10^5 cells/scaffold in the bioreactor. Cell-seeded scaffolds were subsequently cultured within the perfusion bioreactor for 3 weeks with CM supplemented with FGF-2 with media changes twice a week. To compare MSC proliferation in 3D NiTi scaffolds to proliferation on 2D disks, cells derived from one particular donor used in 2D experiments were used in the 3D scaffold experiments (n = 3 scaffold experiments).

The osteogenic differentiation capacity of MSC cultured in the 3D NiTi scaffolds was assessed by seeding 3×10^6 cells/scaffold (surface calculation based on computer-aided design (CAD) data leading to similar seeding density as on 2D metallic substrates) in the bioreactor in three independent experiments (n = 3 different donors). Cell-seeded scaffolds were subsequently cultured within the perfusion bioreactor in either OM or CM supplemented with FGF-2 for up to 3 weeks, with media changes twice a week.

Cell proliferation assay

The CyQUANT® Cell Proliferation Assay was used according to the manufacturer's protocol. Briefly, 2D disks or 3D scaffolds were washed with phosphate-buffered saline (PBS; Gibco, http://www.invitrogen.com) and frozen. Prior to the assay, a phosphate buffer–based (800 mM) enzymatic extraction protocol was carried out in order to liberate the DNA from the substrates.[26]

Imaging techniques

MSC attachment, morphology, spreading, as well as extracellular matrix (ECM) deposition were assessed using SEM (FEI Nova Nano SEM 230) following overnight cell fixation in 4% para-formaldehyde, dehydration, critical point drying, and gold sputtering.

Gene expression

Trizol® (http://www.invitrogen.com) was added to 2D disks and 3D scaffolds to extract RNA. The RNA was isolated using the NucleoSpin® RNA II kit (Macherey-Nagel, Oensingen, Switzerland, http://www.mn-net.com). RNA was eluted in RNase-free water, and transcription into complementary DNA (cDNA) was performed according to the manufacturer's protocol. The samples were analyzed using a GeneAmp® polymerase chain reaction (PCR) System 9600 (Perkin Elmer, Schwerzenbach, Switzerland,

http://www.perkinelmer.com), and the transcription levels of the following genes of interest were quantified: bone sialoprotein (BSP), osteocalcin (OC),[27] and glyceraldehyde 3-phosphate dehydrogenase (GAPDH) as housekeeping gene (Primer R ATG GGG AAG GTG AAG GTC G; Primer F TAA AAG CAG CCC TGG TGA CC; Probe CGC CCA ATA CGA CCA AAT CCG TTG AC).[23]

Calcium staining

Alizarin Red (Sigma Aldrich, A5533) is an organic compound used to stain mineralized matrix in red or light purple color. After a culture period of 3 weeks, 2D disks and TCP were rinsed with PBS and fixed with formalin 4% for 10 min. After an extensive rinse with ddH$_2$O, 2% Alizarin Red staining solution was added to the cell layer for 10 min at room temperature. The staining solution was removed and the cell layer washed twice with pure ethanol. The samples were dried and images acquired.

Statistical analyses

For MSC cultures on metallic 2D disks, averages of four independent experiments (four different donors), with three disks per substrate and assay, were expressed as arithmetic mean ± standard deviation. For MSC cultures on 3D NiTi scaffolds, results from three independent experiments (three donors) are expressed as arithmetic mean ± standard deviation. The data were analyzed by one-way analysis of variance (ANOVA), followed by Bonferroni's post hoc test for multiple comparison (disk experiments). Differences were considered statistically significant at $p < 0.05$.

Results

Substrate characterization

SEM images in Figure 1 show the surface topographies of the metallic disks. Non-surface-treated SLM samples (NiTi and Ti) had macroscopically rough surfaces due to residues of the powder. These powder residues were sintered to the surface layer during the SLM process, and any loose particles were removed during the sonication step of the cleaning procedure. Moreover, these residues led to high arithmetic mean surface roughness values (SR$_a$) and to an increase in the developed surface area ratio (Sdr) (Table 2). In contrast, surface-treated samples appeared much smoother, with no powder residues remaining. The surface roughness parameters SR$_a$, SR$_Z$, Sdr, and S$_m$ were not significantly different among the three surface-treated disks or between the two non-surface-treated disks.

Water contact angle measurements were below 90° for all disks tested (Table 2), indicating hydrophilic properties of the materials.[28] For Ti ref and NiTi, contact angle

Table 2. Measurements of contact angle (CA, static contact angle, sessile drop), arithmetic mean surface roughness (SR$_a$), developed surface area (Sdr), and roughness spacing parameter (S$_m$) of 2D metallic disks.

	Ti ref	Ti	Ti ST	NiTi	NiTi ST
CA (°)	0[a]	61 ± 8	66 ± 16	0[a]	45 ± 23
SR$_a$ (µm)	2.1 ± 0.1	7.3 ± 1.8	3.5 ± 0.5	7.2 ± 0.6	4.3 ± 0.9
SR$_z$ (µm)	12.8 ± 2.7	75.0 ± 36.4	20.7 ± 15.2	65.2 ± 54.6	64.7 ± 38.9
Sdr (%)	151 ± 4	368 ± 82	201 ± 15	333 ± 55	231 ± 78
S$_m$	6.5 ± 2.7	12.3 ± 8.0	8.6 ± 4.9	13.8 ± 6.6	10.5 ± 5.4

2D: two-dimensional; NiTi: nickel–titanium; SD: standard deviation.
[a]No stable droplet formation. Measurements are mean ± SD (n = 3).

measurements of 0° are reported since no stable droplet formation was visible due to immediate droplet elapse, indicating extreme hydrophilicity of these materials.

Analyses of XPS survey (Figure 2(a)) and high-resolution spectra (not shown) indicate the presence of titanium oxide layers on the surface of all disks; the Ti2p$_{3/2}$ was found at 458.9 ± 0.2 eV being a typical binding energy of titanium in titanium oxide. In addition to Ti and O, NiTi ST showed Ni signals. The Ni2p$_{3/2}$ signal is multicomponent: one signal is detected at 852.4 eV and another one, with higher intensity, exhibited the peak maximum at 853.1 eV. The presence of the signal at higher binding energies indicated that the surface film after passivation contains oxidized Ni, but the layer is thin enough to allow for detection of Ni in the metallic state in the NiTi matrix.[29]

Depth profiling of the NiTi substrates showed a titanium oxide layer approximately 96 nm in thickness for NiTi and approximately 5 nm for NiTi ST (Figure 2(b)). Considering that the oxide layer is removed by surface treatment and re-formed through auto-passivation, Ti ST is expected to have an oxide layer thickness similar to NiTi ST. In this work, the oxide layer thickness is estimated to be higher than 6.5 nm using the inelastic mean free path of the signal of titanium oxide (TiO) at 455.1 eV. Surface-treated titanium implants have been shown to exhibit oxide layer thicknesses in the range of 1.5 to 10 nm,[30] consistent with the native oxide layer previously measured on Ti ref.[31] Carbon and sodium were only detected in the outermost layer due to the exposure to the ambient atmosphere. These signals disappeared after the first Ar$^+$ sputtering cycle.

Cytotoxicity assessment

Assessment of the viability of MG-63 cells via MTT staining revealed no cytotoxic effect of NiTi and NiTi ST according to ISO 10993-5. MG-63 metabolic activity on NiTi and NiTi ST were determined to be 1.01 ± 0.10-fold and 0.98 ± 0.10-fold as compared to positive controls; latex negative control was 0.16 ± 0.01-fold compared to positive controls.

2D culture

Proliferation assessment. Proliferation studies were carried out with four independent donors. No significant differences in the growth rate of MSC could be observed for any of the materials as compared to Ti ref or among any of the materials (Figure 3).

Cell morphology. SEM images were acquired after 11 days (depicting an intermediate time point of differentiation; data not shown) of MSC culture on metallic disks in CM and OM. Cell morphology was similar for all metallic substrates. However, morphological differences were observed between MSC cultured in CM as compared to OM. MSC cultured in CM had a randomly oriented, branched, and flat morphology, whereas MSC cultured in OM aligned themselves and branched only into a preferred axis. Interestingly, cells cultured on non-surface-treated disks had adhered to both the underlying substratum as well as the powder residues.

To investigate ECM production by differentiated MSC, SEM images were acquired after 21 days (Figure 4(a)). On all disks, dense cell layers with high amounts of ECM were observed. MSC cultured on surface-treated disks (NiTi ST, Ti ST, and Ti ref) exhibited a spindle-like shape with random orientation in CM and an aligned orientation in OM. MSC cultured on non-surface-treated disks (Ti and NiTi) were almost indistinguishable from the abundant ECM, hindering the assessment of their morphology.

Osteogenic differentiation. BSP gene expression levels were similar for MSC cultured on all materials (p > 0.5 for CM and p > 0.08 for OM) (Figure 4(b)). However, expression of OC was down-regulated for MSC cultured in OM on NiTi (3-fold; p < 0.05) and NiTi ST (6-fold; p < 0.05) as compared to Ti ref. For all materials, BSP expression was significantly higher when MSC were cultured in OM as compared to CM on the respective materials (p < 0.001).

Alizarin Red staining of CM cultured MSC showed similar faint staining for all materials tested. In contrast, with the exception of TCP, high matrix mineralization was observed when MSC were cultured in OM on all of the metallic disks (Figure 4(c)).
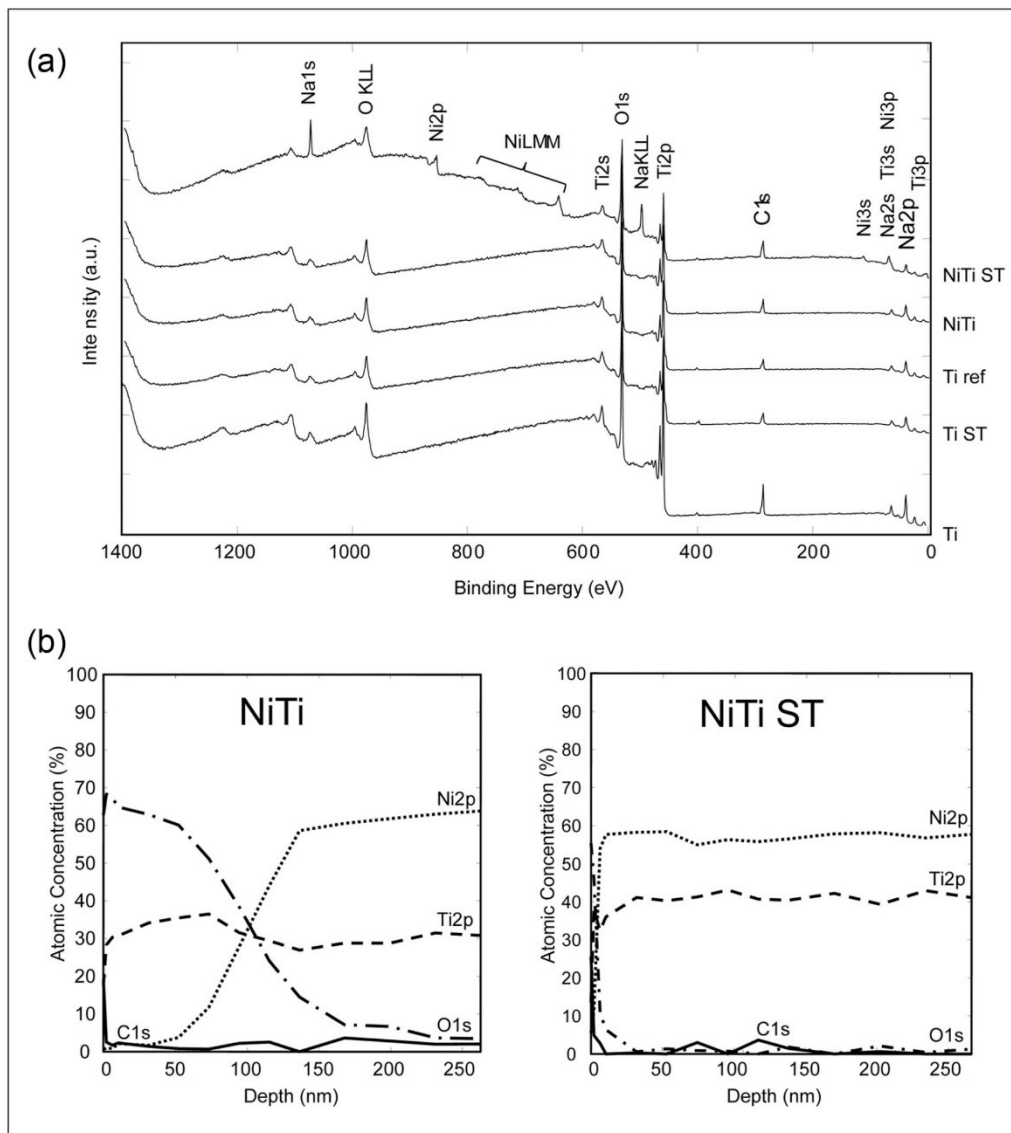
Figure 2. (a) XPS survey spectra of 2D disks indicated the presence of a titanium oxide layer on the surface of the materials. Ni could be detected on the surface of NiTi ST. (b) XPS depth profile for NiTi and NiTi ST revealed oxide layer thicknesses of approximately 96 nm and 5 nm, respectively. Approximate depths were estimated according to the sputter rate on Si/SiO_2 reference sample (10.8 ± 0.1 nm/min).
XPS: x-ray photoelectron spectroscopy; 2D: two-dimensional; NiTi: nickel–titanium.

3D culture

Proliferation and cell morphology assessment. MSC proliferated at similar rates, independent of whether the cells were cultured on porous 3D scaffolds or on 2D disks of SLM NiTi (3D: 0.28 ± 0.04 doublings/day; 2D: 0.32 ± 0.02 doublings/day).

Following 14 days of 3D culture, MSC cultured in CM had colonized the entire scaffold, being homogeneously distributed along the struts of the scaffold at the periphery as well as the struts throughout the internal region (Figure 5(a), upper panel). However, the pore volume remained relatively empty within CM cultured constructs. In contrast, MSC cultured in OM were not only homogeneously distributed along the scaffold struts but were also embedded within ECM filling the volume of the scaffold pores (Figure 5(a), lower panel).
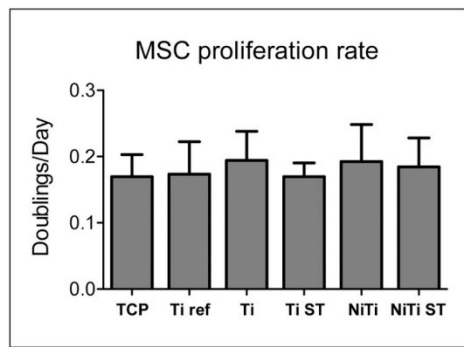
Figure 3. Proliferation rate (doublings/day) of MSC cultured on 2D disks for 1 week.
TCP: tissue culture polystyrene; NiTi: nickel–titanium; MSC: mesenchymal stromal cells; 2D: two-dimensional; SD: standard deviation. No significance differences were observed between the substrates tested. Measurements are mean ± SD (n = 4).

Osteogenic differentiation. BSP gene expression levels were significantly up-regulated when MSC were cultured on 3D NiTi for either 2 or 3 weeks in OM as compared to CM (Figure 5(b)). In contrast to results for 2D cultures, expression of OC was significantly up-regulated when MSC were cultured on 3D NiTi scaffolds in OM as compared to CM. Expression of both BSP and OC was significantly higher when MSC were cultured in osteogenic medium on the 3D NiTi scaffolds as compared to 2D NiTi disks (p < 0.01).

Discussion

In this work, we have demonstrated that the proliferation and osteogenic differentiation capacity of human MSC is similar when cultured on SLM NiTi as compared to a clinically used titanium implant material. We have further shown that when cultured in SLM-produced, porous 3D NiTi scaffolds, MSC colonized the scaffolds, differentiated osteogenically, and filled the pore volume with extracellular matrix.

The surface roughness has been demonstrated to affect cell behavior;[32–35] therefore, we quantitatively and qualitatively assessed the surface topography of the 2D disks. Materials with a higher surface roughness have been demonstrated to favor cell attachment due to enhanced protein binding to the surface,[32] and to increase osteogenic differentiation[33,34] but impair cell proliferation.[33,35] In our study, while non-surface-treated NiTi and Ti had significantly higher values of SR_a than Ti ref, the differences in roughness did not affect MSC proliferation or osteogenic differentiation. It has been demonstrated that bone response was influenced by the implant surface topography at the micro- and nanometer scales. Based on the extent of osseointegration, surface roughness was thus categorized as (1) smooth ($SR_a < 0.5$ μm), (2) minimally rough (SR_a 0.5–1 μm), (3) moderately rough ($SR_a > 1$–2 μm), and (4) rough ($SR_a > 2$ μm) surfaces.[36,37]

Moderately rough and rough surfaces showed the strongest bone response in terms of osseointegration. In our study, all 2D disks, whether surface treated or not, would be classified as "rough," since values of SR_a were larger than 2 μm, possibly explaining the similar response of MSC among the groups.

The surfaces of all disks fabricated in this study were found to have contact angles of θ < 90 °, defining them as hydrophilic.[38] It was previously shown that MSC gene expression of osteogenic markers was generally higher on hydrophilic as compared to hydrophobic surfaces, however at the expense of impaired cell adhesion and proliferation.[38,39] In our study, MSC not only showed signs of osteogenic differentiation but extensively proliferated on all substrates as well.

Although nickel is known to exhibit cytotoxic effects[40] as an intermetallic component of the NiTi alloy, it has been demonstrated to be biocompatible.[41,42] Our study is consistent with others,[43] showing that the SLM processing of NiTi does not impair its cytocompatibility. Moreover, SLM processed NiTi has been demonstrated to be biocompatible.[44] The cytocompatibility and biocompatibility of NiTi arise from auto-passivation,[45] which creates an inert titanium oxide surface layer (Figure 2(b)) that prevents the release of Ni^{2+}.[46] An oxide layer 1.5–10 nm in thickness is also spontaneously formed on Ti substrates when in contact with oxygen.[30] The XPS data shown in Figure 2 confirm the presence of oxide layers on all of our NiTi and Ti disks. Surface oxides are known to spontaneously nucleate calcium phosphate (apatite) when in contact with physiological fluids.[47,48] The nucleated apatite (hydroxyapatite) triggers cell attachment as well as cell differentiation.[49,50] Larsson et al.[51] demonstrated that implants with an oxide layer improved the degree of bone contact area and bone formation. Moreover, the thickness of the oxide layer can also play a crucial role. Electropolished Ti, with a depleted oxide layer of only 2–3 nm in thickness, was associated with decreased bone formation around the implant as compared to auto-passivated Ti.[51] On the other hand, Sul et al.[52] showed that Ti, which was thermally treated to increase the thickness of the oxide layer to 200 and 1000 nm, had significantly stronger bone response with the thickest oxide layer. However, no significant differences were reported for oxide layers generated by auto-passivation and oxide layers up to 200 nm.[52] Therefore, our work appears consistent with Sul et al.,[52] since MSC had similar responses on all disks, which exhibited native oxide layers with thicknesses (ranging from 5–96 nm) below the threshold of 200 nm.

NiTi and Ti substrates incorporated residual metallic powder particles onto their surface, which increased the overall roughness and led to relatively high micrometer-scale peaks. As seen by SEM, these peaks appeared to serve as additional attachment points for cells, possibly imposing pseudo-3D properties to cells, leading to multiple cell layers with increased cell-to-cell and cell-to-ECM contacts. In contrast, cells cultured on the smoother
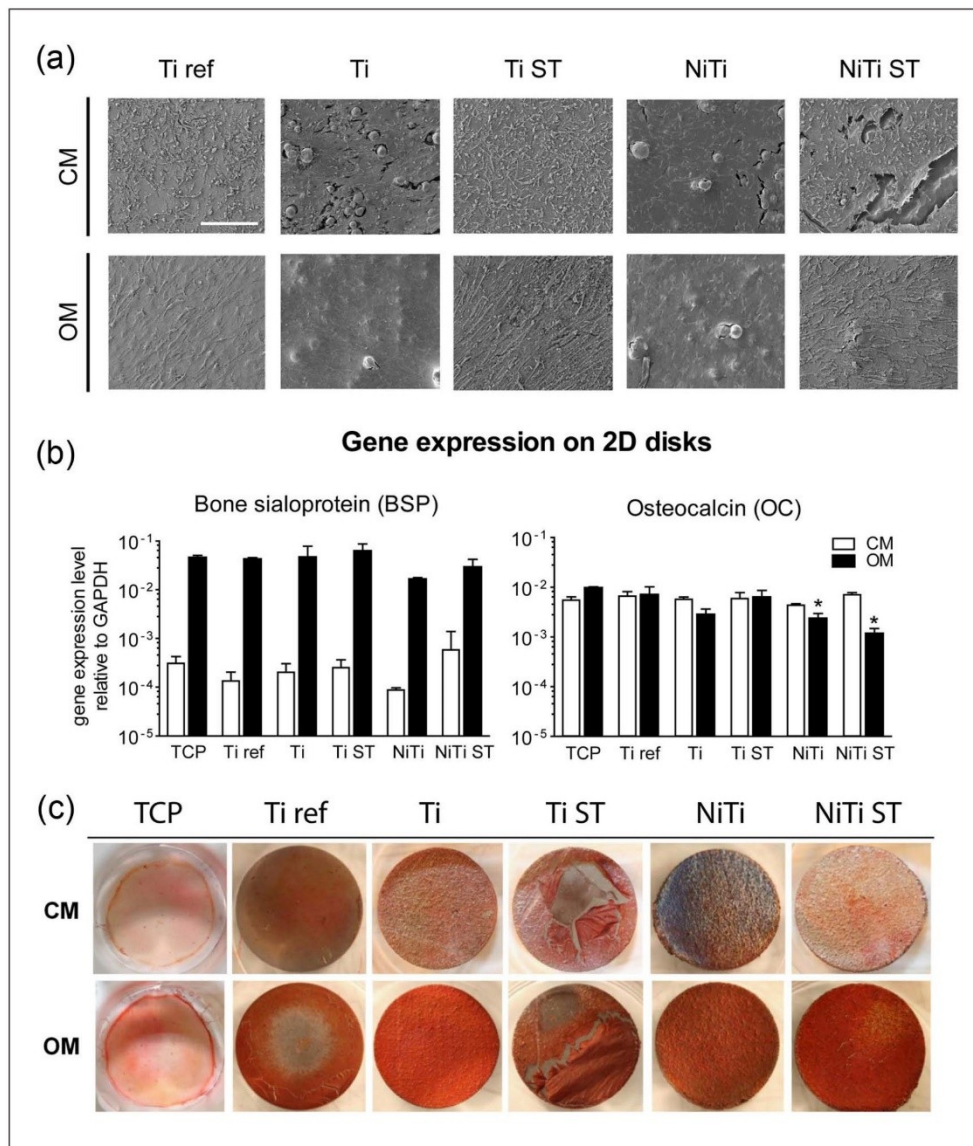
Figure 4. (a) SEM micrographs of MSC cultured on 2D metallic disks for 21 days. MSC colonized the entire substrate surfaces and produced high amounts of extracellular matrix (ECM). Scale bar = 200 μm. (b) Gene expression levels for MSC cultured on 2D disks for 14 days. BSP was up-regulated for MSC cultured in OM. Levels of OC were slightly down-regulated for MSC cultured in OM on Ti, NiTi, and NiTi ST. Measurements are mean ± SD (n = 3).*p<0.05, **p<0.01, as compared to Ti ref in corresponding medium. (c) Alizarin Red Staining of 2D disks following 2 weeks of MSC culture depicting matrix mineralization for MSC cultured in OM on metallic disks.

CM: complete medium; OM: osteogenesis inducing medium; SEM: scanning electron microscope; MSC: mesenchymal stromal cells; 2D: two-dimensional; NiTi: nickel–titanium; SD: standard deviation.

surface-treated samples did not build-up multi-layered colonies as observed with the non-surface-treated samples. Nevertheless, the results show similar proliferation rates and differentiation capacities on surface-treated and non-surface-treated disks, indicating a negligible effect of the residual powder particles.

BSP correlates with the initial phase of matrix mineralization and was proposed to be the main nucleator of hydroxyapatite crystals.[53] OC is the most abundant non-collagenous bone-matrix protein,[54,55] which is synthesized by osteoblasts in the late differentiation state[56] and induced at the onset of extracellular matrix mineralization.[57] High
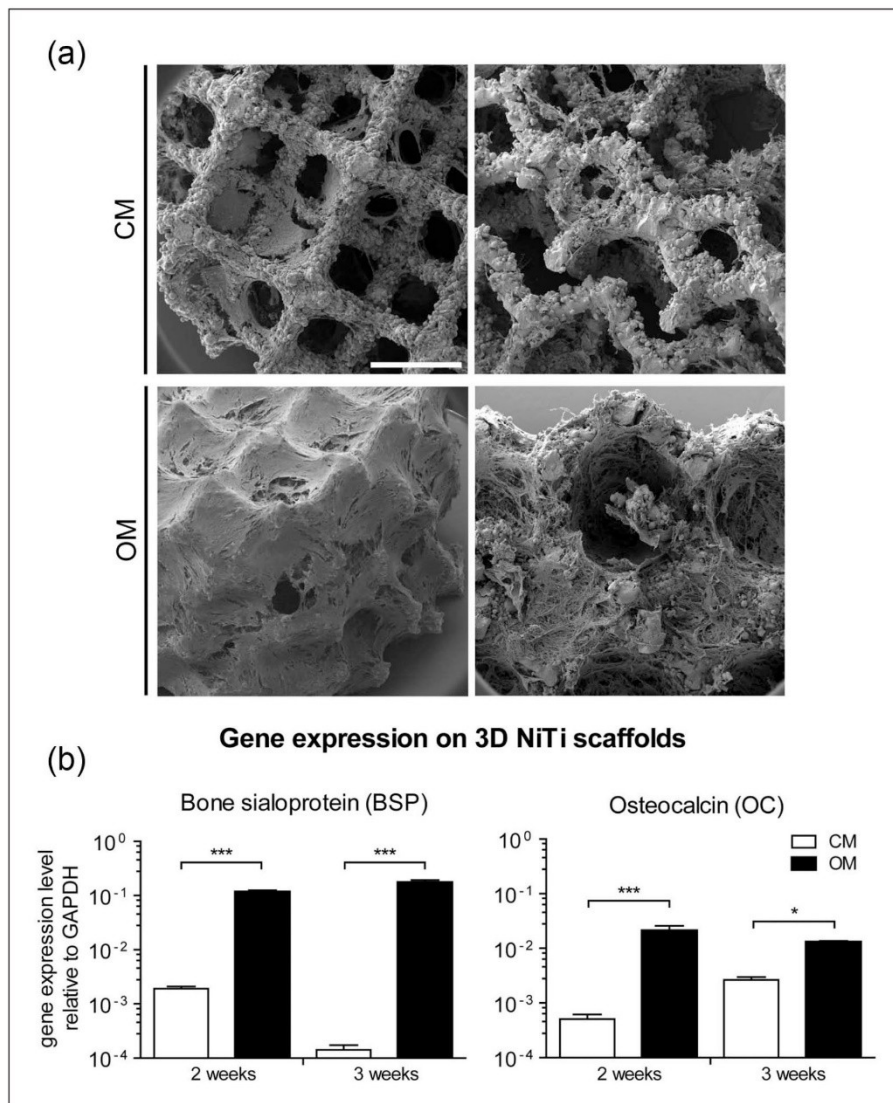
Figure 5. (a) SEM micrographs of cells cultured on 3D NiTi scaffolds in CM or OM, for 14 days. Left panels depict view on the periphery of the scaffolds. Right panels depict the scaffold interior. Scale bar = 1 mm. High amounts of ECM were observed for OM-cultured MSC. (b) Gene expression levels of MSC cultured on 3D NiTi scaffolds for 2 weeks and 3 weeks. Both BSP and OC were up-regulated when MSC were cultured in OM.
SEM: scanning electron microscope; 3D: three-dimensional; NiTi: nickel–titanium; CM: complete medium; OM: osteogenesis inducing medium; ECM: extracellular matrix; MSC: mesenchymal stromal cells; SD: standard deviation.
Measurements are mean ± SD (n = 3).
*$p < 0.05$, ***$p < 0.001$.

expression levels of both BSP and OC on each of the materials tested highlight a similar capacity of MSC to differentiate along the osteogenic lineage when cultured on NiTi as on the conventional Ti ref. Moreover, Alizarin red staining underlines similar levels of matrix mineralization by MSC on NiTi as compared to Ti ref (Figure 4(c)).

After demonstrating that SLM NiTi can support the osteogenic differentiation and matrix mineralization of MSC in our 2D disk model system, we next aimed to investigate the effect of a 3D environment of a SLM NiTi scaffold. Design of the scaffold architecture was based on criteria supporting vascularization and integration of an implant,[58] as well as

finite element modeling of stress/strain profiles within the scaffold under compressive loading.[13] First, we determined that growth rates of MSC cultured in 3D NiTi scaffolds were similar to growth rates on 2D disks. As seen by SEM (Figure 5(a)), MSC colonized the 3D scaffold struts and, when osteogenically induced, filled the porous volume of the scaffold with extracellular matrix. Similar to the 2D disk model system, both BSP and OC were also highly expressed by MSC cultured in the 3D NiTi scaffolds in osteogenic medium. Interestingly, expression of both BSP and OC was significantly higher when MSC were osteogenically differentiated within the 3D environment of the NiTi scaffolds as compared to on the 2D surface of NiTi disks. This is consistent with other studies, which have shown that more osteoinductive constructs could be generated by culturing MSC in a 3D scaffold as compared to culturing MSC in 2D.[22,59] Taken together, the high proliferation rate, differentiation capacity, and high ECM production of MSC on 3D NiTi scaffolds highlight the potential of NiTi as a scaffold for bone tissue engineering applications.

Considering the adhesion, proliferation, and differentiation capacity of MSC on SLM NiTi, this study also presents the possibility to utilize 3D NiTi scaffolds as a cell-free implant material for bone repair. In vivo, small numbers of MSC from the blood or bone marrow in the repair site could infiltrate the scaffolds, adhere to their surface, and proliferate. This could result in the colonization of the scaffold, subsequent differentiation of MSC down the osteogenic linage, and ultimately lead to accelerated osseointegration of the implant.

In addition, porous NiTi scaffolds that are able to switch between defined structural states (shape memory), induced either mechanically or thermally,[13] represent a further approach to study the response of cells and tissues to physiological strains in vitro.[60,61] For example, Strauß et al.[62] determined that static compression of NiTi scaffolds was able to trigger osteogenic differentiation of adipose tissue–derived stem cells. Further investigations might lead to implants that apply physiological strains via shape memory properties that trigger cell differentiation and bone tissue ingrowth. These advanced implants might actively stimulate the surrounding tissue through the application of micro-motions leading to profound reductions in implant integration periods and ultimately to faster patient recoveries.

Conclusion

We have demonstrated that MSC cultured on rapid-prototyped NiTi proliferated and differentiated along the osteogenic lineage to similar extents as on the clinically used reference titanium material. These results highlight the potential of SLM NiTi as a scaffold material for bone tissue engineering applications (i.e., in vitro engineering of osteogenic grafts) as well as regenerative medicine approaches (i.e., as a cell-free implant material). Moreover, the flexibility of the SLM technique, combined with the unique mechanical properties of NiTi, would allow for the design of grafts/implants better matching the mechanical requirements of a bone repair site than conventional Ti implants. Finally, the development of advanced NiTi shape memory implants, capable of applying regenerative mechanical stimuli at the site of implantation, could have profound consequences on implant integration periods leading to faster patient recoveries[63] and to more successful clinical outcomes in the long term.

References

1. Hutmacher DW, Schantz JT, Lam CXF, et al. State of the art and future directions of scaffold-based bone engineering from a biomaterials perspective. *J Tissue Eng Regen Med* 2007; 1(4): 245–260, http://dx.doi.org/10.1002/term.24
2. Salgado AJ, Coutinho OP and Reis RL. Bone tissue engineering: state of the art and future trends. *Macromol Biosci* 2004; 4(8): 743–765, http://dx.doi.org/10.1002/mabi.200400026
3. Rezwan K, Chen QZ, Blaker JJ, et al. Biodegradable and bioactive porous polymer/inorganic composite scaffolds for bone tissue engineering. *Biomaterials* 2006; 27(18): 3413–3431, http://www.sciencedirect.com/science/article/pii/S0142961206001232
4. Albrektsson T and Johansson C. Osteoinduction, osteoconduction and osseointegration. *Eur Spine J* 2001; 10(Suppl. 2): S96–S101, http://link.springer.com/article/10.1007/s005860100282 (accessed 6 November 2013).
5. Tugulu S, Lowe K, Scharnweber D, et al. Preparation of superhydrophilic microrough titanium implant surfaces by

alkali treatment. *J Mater Sci Mater Med* 2010; 21(10): 2751–2763, http://www.ncbi.nlm.nih.gov/pubmed/20725770

6. Germanier Y, Tosatti S, Broggini N, et al. Enhanced bone apposition around biofunctionalized sandblasted and acid-etched titanium implant surfaces. A histomorphometric study in miniature pigs. *Clin Oral Implants Res* 2006; 17(3): 251–257, http://www.ncbi.nlm.nih.gov/pubmed/16672019 (accessed 12 November 2012).

7. Milleret V, Tugulu S, Schlottig F, et al. Alkali treatment of microrough titanium surfaces affects macrophage/monocyte adhesion, platelet activation and architecture of blood clot formation. *Eur Cell Mater* 2011; 21: 430–444, http://www.ncbi.nlm.nih.gov/pubmed/21604243

8. Nag S and Banerjee R. Fundamentals of medical implant materials. In: Narayan R (ed.) *ASM handbook, volume 23: materials for medical devices*. Materials Park, OH: ASM International, 2012, pp. 6–17.

9. Huiskes R, Weinans H and van Rietbergen B. The relationship between stress shielding and bone resorption around total hip stems and the effects of flexible materials. *Clin Orthop Relat Res* 1992; 274: 124–134, http://www.ncbi.nlm.nih.gov/pubmed/1728998 (accessed 19 August 2013).

10. De Wild M, Meier F, Bormann T, et al. Damping of selective-laser-melted NiTi for medical implants. *J Mater Eng Perform* 2014, http://link.springer.com/10.1007/s11665-014-0889-8 (accessed 17 February 2014).

11. Mullen L, Stamp RC, Brooks WK, et al. Selective Laser Melting: a regular unit cell approach for the manufacture of porous, titanium, bone in-growth constructs, suitable for orthopedic applications. *J Biomed Mater Res B Appl Biomater* 2009; 89(2): 325–334, http://www.ncbi.nlm.nih.gov/pubmed/18837456 (accessed 28 February 2014).

12. Pattanayak DK, Fukuda A, Matsushita T, et al. Bioactive Ti metal analogous to human cancellous bone: fabrication by selective laser melting and chemical treatments. *Acta Biomater* 2011, http://www.sciencedirect.com/science/article/B7GHW-51491KH-C/2/408b9a0545d42b82221a0f73be480024

13. Bormann T, Schulz G, Deyhle H, et al. Combining micro computed tomography and three-dimensional registration to evaluate local strains in shape memory scaffolds. *Acta Biomater* 2013; 10(2): 1024–1034, http://www.ncbi.nlm.nih.gov/pubmed/24257506 (accessed 22 November 2013).

14. Sobral JM, Caridade SG, Sousa RA, et al. Three-dimensional plotted scaffolds with controlled pore size gradients: effect of scaffold geometry on mechanical performance and cell seeding efficiency. *Acta Biomater* 2011; 7(3): 1009–1018, http://www.ncbi.nlm.nih.gov/pubmed/21056125 (accessed 14 March 2014).

15. Van Bael S, Chai YC, Truscello S, et al. The effect of pore geometry on the in vitro biological behavior of human periosteum-derived cells seeded on selective laser-melted Ti6Al4V bone scaffolds. *Acta Biomater* 2012; 8(7): 2824–2834, http://www.ncbi.nlm.nih.gov/pubmed/22487930 (accessed 18 February 2014).

16. Zhao G, Zinger O, Schwartz Z, et al. Osteoblast-like cells are sensitive to submicron-scale surface structure. *Clin Oral Implants Res* 2006; 17(3): 258–264, http://www.ncbi.nlm.nih.gov/pubmed/16672020 (accessed 19 August 2013).

17. Bormann T, de Wild M, Beckmann F, et al. Assessing the morphology of selective laser melted NiTi-scaffolds for

a three-dimensional quantification of the one-way shape memory effect. In: (ed NC Goulbourne and HE Naguib), 2013, p. 868914, http://proceedings.spiedigitallibrary.org/proceeding.aspx?doi=10.1117/12.2012245 (accessed 20 May 2014).

18. Olympus. *User's manual: confocal scanning laser microscope LEXT OLS3100*. Hamburg: Olympus Life Science Europa GMBH, 2008.

19. Wennerberg A and Albrektsson T. On implant surfaces: a review of current knowledge and opinions. *Int J Oral Maxillofac Implants* 2009; 25(1): 63–74, http://www.ncbi.nlm.nih.gov/pubmed/20209188

20. Crobu M, Rossi A, Mangolini F, et al. Chain-length-identification strategy in zinc polyphosphate glasses by means of XPS and ToF-SIMS. *Anal Bioanal Chem* 2012; 403(5): 1415–1432, http://www.ncbi.nlm.nih.gov/pubmed/22451170 (accessed 2 April 2014).

21. ISO 10993-5:2009. Biological evaluation of medical devices—part 5: tests for in vitro cytotoxicity.

22. Braccini A, Wendt D, Jaquiery C, et al. Three-dimensional perfusion culture of human bone marrow cells and generation of osteoinductive grafts. *Stem Cells* 2005; 23(8): 1066–1072, http://www.ncbi.nlm.nih.gov/pubmed/16002780 (accessed 12 August 2013).

23. Frank O, Heim M, Jakob M, et al. Real-time quantitative RT-PCR analysis of human bone marrow stromal cells during osteogenic differentiation in vitro. *J Cell Biochem* 2002; 85(4): 737–746, http://www.ncbi.nlm.nih.gov/pubmed/11968014

24. Wendt D, Marsano A, Jakob M, et al. Oscillating perfusion of cell suspensions through three-dimensional scaffolds enhances cell seeding efficiency and uniformity. *Biotechnol Bioeng* 2003; 84(2): 205–214, http://www.ncbi.nlm.nih.gov/pubmed/12966577

25. Wendt D, Stroebel S, Jakob M, et al. Uniform tissues engineered by seeding and culturing cells in 3D scaffolds under perfusion at defined oxygen tensions. *Biorheology* 2006; 43(3–4): 481–488, http://www.ncbi.nlm.nih.gov/pubmed/16912419

26. Piccinini E, Sadr N and Martin I. Ceramic materials lead to underestimated DNA quantifications: a method for reliable measurements. *Eur Cell Mater* 2010; 20: 38–44, http://www.ncbi.nlm.nih.gov/pubmed/20652860 (accessed 22 November 2012).

27. Barbero A, Ploegert S, Heberer M, et al. Plasticity of clonal populations of dedifferentiated adult human articular chondrocytes. *Arthritis Rheum* 2003; 48(5): 1315–1325, http://www.ncbi.nlm.nih.gov/pubmed/12746904

28. Vogler EA. Structure and reactivity of water at biomaterial surfaces. *Adv Colloid Interface Sci* 1998; 74: 69–117, http://www.ncbi.nlm.nih.gov/pubmed/9561719 (accessed 12 November 2012).

29. Addari D, Mignani A, Scavetta E, et al. An XPS investigation on glucose oxidase and Ni/Al hydrotalcite interaction. *Surf Interface Anal* 2011; 43(4): 816–822, http://doi.wiley.com/10.1002/sia.3636 (accessed 2 April 2014).

30. Sul YT, Johansson CB, Jeong Y, et al. Oxidized implants and their influence on the bone response. *J Mater Sci Mater Med* 2001; 12(10–12): 1025–1031, http://www.ncbi.nlm.nih.gov/pubmed/15348359 (accessed 4 March 2014).

31. Kang B-S, Sul Y-T, Oh S-J, et al. XPS, AES and SEM analysis of recent dental implants. *Acta Biomater* 2009; 5(6): 2222–2229, http://www.ncbi.nlm.nih.gov/pubmed/19261554 (accessed 4 March 2014).

32. Deligianni DD, Katsala N, Ladas S, et al. Effect of surface roughness of the titanium alloy Ti-6Al-4V on human bone marrow cell response and on protein adsorption. *Biomaterials* 2001; 22(11): 1241–1251, http://www.ncbi.nlm.nih.gov/pubmed/11336296 (accessed 26 February 2014).

33. Hempel U, Hefti T, Dieter P, et al. Response of human bone marrow stromal cells, MG-63, and SaOS-2 to titanium-based dental implant surfaces with different topography and surface energy. *Clin Oral Implants Res* 2013; 24(2): 174–82, http://dx.doi.org/10.1111/j.1600-0501.2011.02328.x (accessed 12 May 2014).

34. Martin JY, Schwartz Z, Hummert TW, et al. Effect of titanium surface roughness on proliferation, differentiation, and protein synthesis of human osteoblast-like cells (MG63). *J Biomed Mater Res* 1995; 29(3): 389–401, http://www.ncbi.nlm.nih.gov/pubmed/7542245 (accessed 4 February 2013).

35. Ponsonnet L, Comte V, Othmane A, et al. Effect of surface topography and chemistry on adhesion, orientation and growth of fibroblasts on nickel–titanium substrates. *Mater Sci Eng C* 2002; 21(1–2): 157–165, http://linkinghub.elsevier.com/retrieve/pii/S0928493102000978 (accessed 4 February 2013).

36. Wennerberg A and Albrektsson T. Effects of titanium surface topography on bone integration: a systematic review. *Clin Oral Implants Res* 2009; 20(Suppl. 4): 172–184, http://www.ncbi.nlm.nih.gov/pubmed/19663964 (accessed 28 November 2013).

37. Rønold HJ, Lyngstadaas SP and Ellingsen JE. Analysing the optimal value for titanium implant roughness in bone attachment using a tensile test. *Biomaterials* 2003; 24(25): 4559–4564, http://linkinghub.elsevier.com/retrieve/pii/S0142961203002564 (accessed 4 December 2013).

38. Rupp F, Scheideler L, Olshanska N, et al. Enhancing surface free energy and hydrophilicity through chemical modification of microstructured titanium implant surfaces. *J Biomed Mater Res A* 2006; 76(2): 323–334, http://www.ncbi.nlm.nih.gov/pubmed/16270344 (accessed 23 May 2013).

39. Mamalis AA and Silvestros SS. Analysis of osteoblastic gene expression in the early human mesenchymal cell response to a chemically modified implant surface: an in vitro study. *Clin Oral Implants Res* 2011; 22(5): 530–537, http://www.ncbi.nlm.nih.gov/pubmed/21121959 (accessed 23 May 2013).

40. Putters JLM, Kaulesar Sukul DMKS, de Zeeuw GR, et al. Comparative cell culture effects of shape memory metal (Nitinol®), nickel and titanium: a biocompatibility estimation. *Eur Surg Res* 1992; 24(6): 378–382, http://www.karger.com/DOI/10.1159/000129231

41. Habijan T, Bremm O, Esenwein SA, et al. Influence of nickel ions on human multipotent mesenchymal stromal cells (hMSCs). *Materwiss Werksttech* 2007; 38(12): 969–974, http://doi.wiley.com/10.1002/mawe.200700231 (accessed 12 November 2012).

42. Es-Souni MM and Fischer-Brandies H. Assessing the biocompatibility of NiTi shape memory alloys used for medical applications. *Anal Bioanal Chem* 2005; 381(3): 557–567,

http://www.ncbi.nlm.nih.gov/pubmed/15660223 (accessed 12 February 2013).

43. Habijan T, Haberland C, Meier H, et al. The biocompatibility of dense and porous Nickel–Titanium produced by selective laser melting. *Mater Sci Eng C* 2013; 33(1): 419–426, http://linkinghub.elsevier.com/retrieve/pii/S0928493112004407 (accessed 13 November 2012).

44. Shishkovsky IV, Volova LT, Kuznetsov MV, et al. Porous biocompatible implants and tissue scaffolds synthesized by selective laser sintering from Ti and NiTi. *J Mater Chem* 2008; 18(12): 1309–1317, http://xlink.rsc.org/?DOI=b715313a (accessed 30 April 2014).

45. Chan C-M, Trigwell S and Duerig T. Oxidation of an NiTi alloy. *Surf Interface Anal* 1990; 15(6): 349–354, http://dx.doi.org/10.1002/sia.740150602 (accessed 19 May 2014).

46. Shabalovskaya SA, Tian H, Anderegg JW, et al. The influence of surface oxides on the distribution and release of nickel from Nitinol wires. *Biomaterials* 2009; 30(4): 468–477, http://dx.doi.org/10.1016/j.biomaterials.2008.10.014 (accessed 18 February 2013).

47. Li P, Ohtsuki C, Kokubo T, et al. The role of hydrated silica, titania, and alumina in inducing apatite on implants. *J Biomed Mater Res* 1994; 28(1): 7–15, http://dx.doi.org/10.1002/jbm.820280103 (accessed 4 March 2014).

48. Sundgren JE, Bodö P, Lundström I, et al. Auger electron spectroscopic studies of stainless-steel implants. *J Biomed Mater Res* 1985; 19(6): 663–671, http://dx.doi.org/10.1002/jbm.820190606 (accessed 4 March 2014).

49. Habibovic P, Sees TM, van den Doel MA, et al. Osteoinduction by biomaterials—physicochemical and structural influences. *J Biomed Mater Res Part A* 2006; 77(4): 747–762, http://dx.doi.org/10.1002/jbm.a.30712

50. Yoshikawa H and Myoui A. Bone tissue engineering with porous hydroxyapatite ceramics. *J Artif Organs* 2005; 8(3): 131–136, http://www.ncbi.nlm.nih.gov/pubmed/16235028 (accessed 4 March 2014).

51. Larsson C, Thomsen P, Aronsson BO, et al. Bone response to surface-modified titanium implants: studies on the early tissue response to machined and electropolished implants with different oxide thicknesses. *Biomaterials* 1996; 17(6): 605–616, http://www.ncbi.nlm.nih.gov/pubmed/8652779 (accessed 4 March 2014).

52. Sul Y-T, Johansson CB, Jeong Y, et al. Resonance frequency and removal torque analysis of implants with turned and anodized surface oxides. *Clin Oral Implants Res* 2002; 13(3): 252–259, http://www.ncbi.nlm.nih.gov/pubmed/12010155 (accessed 4 March 2014).

53. Bianco P, Riminucci M, Silvestrini G, et al. Localization of bone sialoprotein (BSP) to Golgi and post-Golgi secretory structures in osteoblasts and to discrete sites in early bone matrix. *J Histochem Cytochem* 1993; 41(2): 193–203, http://www.ncbi.nlm.nih.gov/pubmed/8419459 (accessed 12 March 2013).

54. Wolf G. Function of the bone protein osteocalcin: definitive evidence. *Nutr Rev* 1996; 54(10): 332–323, http://doi.wiley.com/10.1111/j.1753-4887.1996.tb03798.x (accessed 12 March 2013).

55. Hauschka PV, Lian JB, Cole DE, et al. Osteocalcin and matrix Gla protein: vitamin K-dependent proteins in bone. *Physiol Rev* 1989; 69(3): 990–1047, http://www.ncbi.nlm.nih.gov/pubmed/2664828 (accessed 28 August 2013).

56. Neve A, Corrado A and Cantatore FP. Osteocalcin: skeletal and extra-skeletal effects. *J Cell Physiol* 2013; 228(6): 1149–1153, http://dx.doi.org/10.1002/jcp.24278

57. Lian JB and Stein GS. Concepts of osteoblast growth and differentiation: basis for modulation of bone cell development and tissue formation. *Crit Rev Oral Biol Med* 1992; 3: 269–305.

58. Hollister SJ. Porous scaffold design for tissue engineering. *Nat Mater* 2005; 4(7): 518–524, http://www.ncbi.nlm.nih.gov/pubmed/16003400 (accessed 12 November 2012).

59. Scherberich A, Galli R, Jaquiery C, et al. Three-dimensional perfusion culture of human adipose tissue-derived endothelial and osteoblastic progenitors generates osteogenic constructs with intrinsic vascularization capacity. *Stem Cells* 2007; 25(7): 1823–1829, http://www.ncbi.nlm.nih.gov/pubmed/17446558 (accessed 20 March 2014).

60. Byrne EM, Farrell E, McMahon LA, et al. Gene expression by marrow stromal cells in a porous collagen-glycosaminoglycan scaffold is affected by pore size and mechanical stimulation. *J Mater Sci Mater Med* 2008; 19(11): 3455–3463, http://www.ncbi.nlm.nih.gov/pubmed/18584120 (accessed 31 January 2013).

61. Van Eijk F, Saris DBF, Creemers LB, et al. The effect of timing of mechanical stimulation on proliferation and differentiation of goat bone marrow stem cells cultured on braided PLGA scaffolds. *Tissue Eng Part A* 2008; 14(8): 1425–1433, http://www.ncbi.nlm.nih.gov/pubmed/18637726 (accessed 30 January 2013).

62. Strauß S, Dudziak S, Hagemann R, et al. Induction of osteogenic differentiation of adipose derived stem cells by microstructured nitinol actuator-mediated mechanical stress. *PLoS One* 2012; 7(12): e51264, http://www.pubmedcentral.nih.gov/articlerender.fcgi?artid=3517541&tool=pmcentrez&rendertype=abstract (accessed 3 January 2013).

63. Leucht P, Kim J, Wazen R, et al. Effect of mechanical stimuli on skeletal regeneration around implants. *Bone* 2007; 40(4): 919–930, http://www.pubmedcentral.nih.gov/articlerender.fcgi?artid=1987325&tool=pmcentrez&rendertype=abstract (accessed 11 March 2013).

84

Conclusions and future perspectives

A. General summary

The processes of bone fracture healing and bone development share certain similarities and are affected by mechanical loads, the local microenvironment and other factors. In this thesis, an established *in vitro* fracture callus model (Scotti et al. 2010; Mumme et al. 2012) was further developed through the introduction of mechanical loading. This system allows for the investigation of the effects of physiological mechanical loads on fracture calluses (engineered endochondral constructs), NiTi-reinforced endochondral constructs and native tissues. Exploring the benefits of rapid-prototyping, shape-memory-alloys and mechanical loading the introduction of a novel, *in vitro* model for mechanically modulated endochondral ossification is intended.

Inflammatory cytokines, which are present in the environment of the fracture site, are important modulators of fracture healing. Thus, in **chapter 1** the effect of IL-1β on glycosaminoglycan (GAG) production and BMP-2 expression during chondrogenesis and ECM calcification during the hypertrophic phase of *in vitro* cultures was investigated. These constructs depict an *in vitro* model for fracture calluses and are therefore used to investigate the effect of IL-1β on the remodeling process, which occurs upon *in vivo* implantation. It has been demonstrated that IL-1β finely modulates early and late events of the endochondral bone formation by MSC. Controlling the inflammatory environment could enhance the success of therapeutic approaches for the treatment of fractures by resident MSC as well as improve the engineering of implantable tissues.

Secondary bone fracture healing is a physiological process, which leads to functional tissue regeneration recapitulating endochondral bone formation. Besides other factors, mechanical loading is known to modulate the process of fracture healing.

Conclusions and future perspectives

Therefore, in **chapter 2** a novel perfused compression bioreactor system (PCB) is demonstrated for the investigation of the effect of dynamic mechanical loading on the mineralization process of engineered, hypertrophic constructs. The results obtained demonstrate that dynamic mechanical loading enhances the maturation process of MSC towards late hypertrophic chondrocytes and the mineralization of the extracellular matrix. Moreover, the system possibly allows for the identification of suitable loading regimes to accelerate the process of fracture healing.

In order to improve primary implant stability and to upscale endochondral constructs, selective laser melting (SLM)-based NiTi constructs are foreseen to be utilized as a backbone for hypertrophic cartilage templates. NiTi alloys possess a unique combination of mechanical properties including a relatively low elastic modulus, pseudoelasticity, and high damping capacity, matching the properties of bone. Hence, in **chapter 3**, we demonstrated biocompatibility of NiTi-based constructs. Moreover, MSC adhesion, proliferation and differentiation along the osteogenic lineage were similar to MSC cultured on clinically used Ti. When seeded and cultured on porous 3D SLM-NiTi scaffolds, MSC homogeneously colonized the scaffold, and following osteogenic induction, filled the scaffold's pore volume with extracellular matrix. The combination of bone-related mechanical properties of SLM-NiTi with its cytocompatibility and support of osteogenic properties by MSC highlights its potential as a superior bone substitute as compared to Ti.

In conclusion, this thesis highlights that MSC based chondrogenic and hypertrophic constructs depict *in vitro* models for soft and hard fracture calluses, respectively. This constructs are responsive to both inflammatory cytokines (IL-1β modulating early and late events of the endochondral bone formation) and dynamic mechanical loading (increased degree of maturation of both MSC and ECM). Moreover, it has been

shown that the PCB serves as a promising tool for further systematic studies in an *in* vitro setting leading to a reduction of animal experiments within the field. Nevertheless, the established models (including mechanically loaded constructs) are not capable of supporting load-bearing fracture sites. Therefore, to overcome the lack of mechanical stability a NiTi-based approach is intended. SLM-NiTi was shown to be biocompatible and MSC do colonize these constructs and differentiate along the osteogenic lineage. Using SLM-NiTi scaffolds as a backbone supporting initial load-bearing, MSC could be used to colonize it and fill the scaffolds pores with a chondrogenic and/or hypertrophic ECM. This construct depicts a NiTi-reinforced, mechanically stable endochondral implant intended for orthotopic implantation.

B.   Future perspectives

As described in Chapter 3, SLM-NiTi constructs depict a promising biomaterial to engineer load-bearing constructs, which might be used in several applications. Nevertheless, Ni release from NiTi implants remains a significant concern limiting the applications due to cytotoxicity (Taira et al. 2000) and hypersensitivity (Jia et al. 1999; Savarino et al. 1999). Therefore, we investigated the Ni release of SLM-NiTi scaffolds in two conditions: loaded (+ML) and non-loaded (-ML). To mimic physiological loading conditions, uniaxial dynamic compression was applied (sinusoidal loading profile, 100 μm displacement amplitude and a frequency of 8 Hz). Samples for Ni release measurements were taken at 24h (690'000 cycles), 1 week (4.8×10^6 cycles) and 2 week time points (9.6×10^6 cycles). The amount of released Ni ions was assessed by atom absorption spectroscopy (AAS, Perkin Elmer, AAnalyst 800, graphite furnace, 232 nm) and is depicted in figure 11.
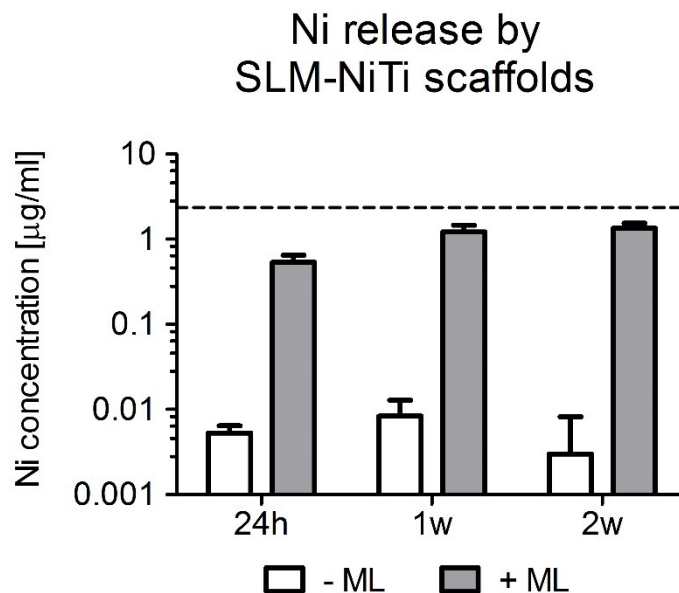

Figure 11 Ni release by SLM-NiTi scaffolds.

Ni release for non-loaded (-ML) and loaded (+ML) NiTi scaffolds. Dashed line depicts cytotoxic Ni ion level: 2.35 μg/mL (Taira et al. 2000).

Non-loaded SLM-NiTi constructs show minimal Ni ion release. The mechanically loaded NiTi scaffolds demonstrated a significantly higher Ni ion release within the first 24h. Thereafter only small, time-dependent increases were detected. Upon application of physiological loads, cracks may form in the titanium oxide layer on the NiTi surface. Due to the rupture of the protective oxide layer, Ni ions are released into the surrounding environment. The Ni ion concentrations determined in this study remain under the cytotoxic level of 2.35 µg/mL (Taira et al. 2000). Surface treatments could further improve the inertness of NiTi constructs. Moreover, under *in vivo* conditions, NiTi implants are continuously flushed by the bloodstream minimizing local Ni ion concentrations even further. Likewise, MSC have been shown to colonize loaded SLM-NiTi scaffolds with no signs of cytotoxicity (Habijan et al. 2011).
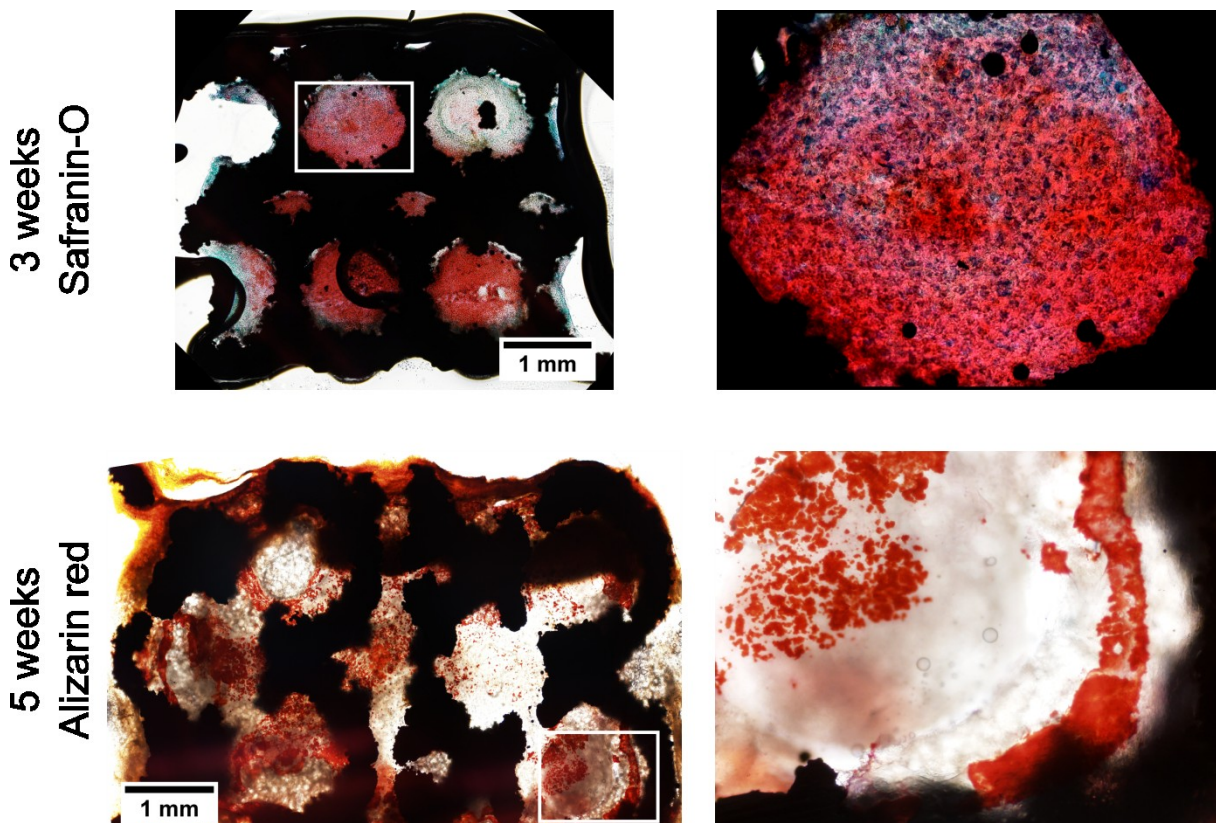

Figure 38 MSC cultured on NiTi scaffolds.

The upper panel depicts glycosaminoglycans stained with Safranin-O after 3 weeks of chondrogenic MSC culture. The lower panel displays mineralized matrix stained with Alizarin Red after 5 weeks of hypertrophic MSC culture.

Conclusions and future perspectives

To further prove the possibility to use SLM-NiTi constructs as biomaterial, the differentiation potential of MSC along the endochondral route was investigated. Figure 12 demonstrates the capacity of MSC seeded on 3D NiTi scaffolds to undergo the process of endochondral ossification. Post chondrogenic induction, MSC depicted chondrogenic features including positive Safranin-o staining for GAG and large cells in typical lacunae. Following the induction of hypertrophic differentiation, the ECM displayed a high degree of mineralization. These observations suggest that SLM-NiTi scaffolds as a reinforcing backbone for endochondral constructs depict a promising approach to engineer load-bearing, up-scaled constructs enriched with a fracture callus-like ECM.

Moreover, the *in vivo* bone forming capacity of SLM-NiTi reinforced endochondral constructs was assessed. Following an *in vitro* culture consisting of three weeks of chondrogenesis and two weeks of hypertrophic induction, endochondral NiTi constructs were implanted ectopically into nude mice. After 12 weeks *in vivo*, bone formation capacity was assessed by means of Hematoxylin and Eosin (H&E) staining.
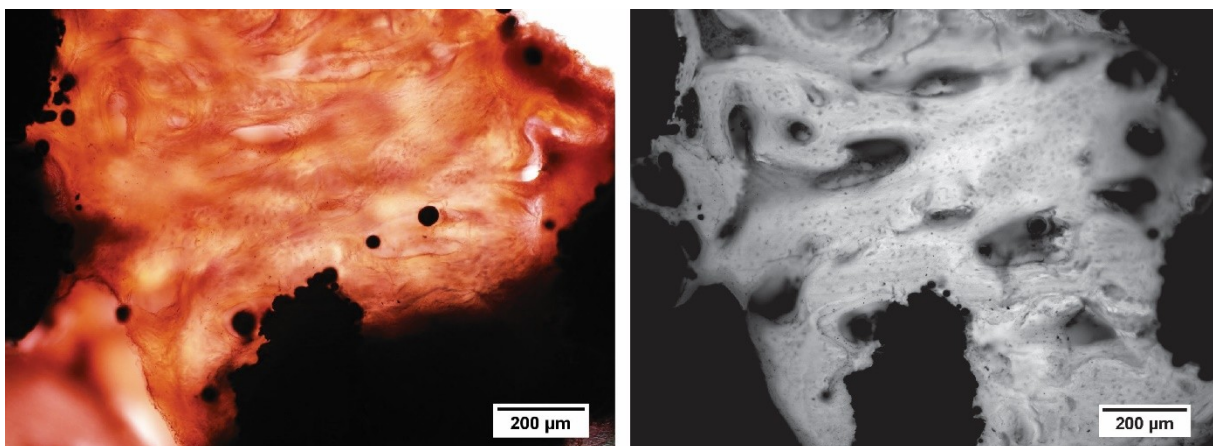

Figure 64 In vivo bone formation capacity of endochondral NiTi constructs.

Left image: H&E staining after 12 weeks *in vivo* period depicting the formation of woven bone within the pores of the SLM-NiTi scaffold. Right image: Fluorescence image of the eosin stain. Osteocytes are visible as dark spots within the bright woven bone.

Formation of woven bone within the pores of the NiTi scaffolds is depicted (Figure 13). Due to the thickness of the histological sections, the acquisition of high resolution bright filed images is not trivial. Therefore, fluorescence microscopy was performed to further investigate the bone formation. *In vivo* bone formation occurred within the NiTi scaffolds leading to osseointegration (bone formation along the implant), dense bone matrix formation (white areas), and osteocyte formation (dark spots). The results emphasize the potential of SLM-NiTi as a load-bearing bone implant.

Further possible applications arising from the data presented in the context of this thesis are summarized in Figure 14:

A. The production of personalized SLM-NiTi implants is facilitated through the use of computer-tomography data to design patient-specific implant geometries and autologous adult mesenchymal stem cells from adipose tissue or bone marrow. The cells are cultured on the implants with the application of physiological mechanical loads using the compression bioreactor system to accelerate the process of matrix production and maturation. This will lead to a personalized, load-bearing implant intended for dental and/or orthopedic applications.

B. Using a cell engineering approach, functionalized MSC can be generated, which deposit a defined and reproducible matrix and simultaneously carry an inducible death cassette (Bourgine et al. 2014). In combination with SLM-NiTi, load-bearing off-the-shelf products can be generated. In this regard the engineered MSC are intended to produce high amounts of chondrogenic/hypertrophic matrix aided by the application of physiological mechanical loads. Subsequently, MSC apoptosis is induced leaving behind

an implant covered with a defined ECM matrix. This ECM-enriched implants can be further processed (e.g. lyophilization) to enable long-term storage.

C. The compression bioreactor system, developed, validated and patented (Hoffmann et al. 2014) in the scope of this work, depicts a promising tool for several applications not only related to the field of tissue engineering. As mentioned previously, it can serve as method used to generate mature engineered tissues *in vitro* using diverse scaffolds with wide ranges of mechanical properties. Besides, quality control of engineered and native tissues can be performed comparing the mechanical properties to healthy, pathological and native tissues. Moreover, the system allows for systematic investigations of the influence of mechanical loading on engineered and native tissues. This approach could lead to further investigations of the underlying mechanisms during mechanically triggered fracture healing and tissue maturation processes.

Figure 84 Future perspectives.

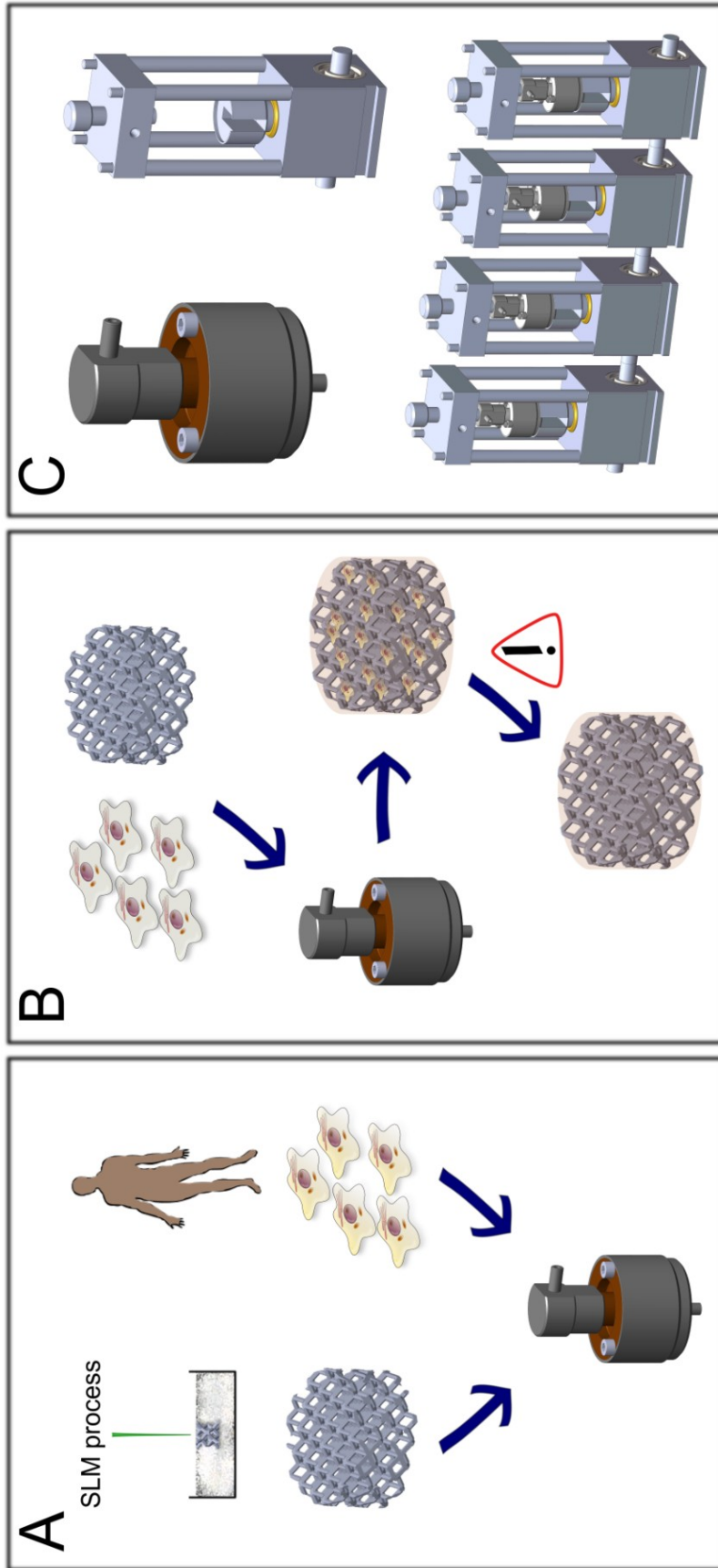A: Patient specific implant generation using SLM, autologous adult MSC and physiological mechanical loads. B: Off-the-shelf load-bearing implants generated with engineered, functionalized MSC, physiological mechanical loads and induction of apoptosis. C: Compression bioreactor system depicting a versatile tool for tissue engineering, quality control and *in vitro* model applications.

References

Abdelaal, O.M. & Darwish, S.H., 2013. Review of Rapid Prototyping Techniques for Tissue Engineering Scaffolds Fabrication. In A. Öchsner, L. F. M. Silva, & H. Altenbach, eds. *Characterization and Development of Biosystems and Biomaterials SE - 3*. Advanced Structured Materials. Springer Berlin Heidelberg, pp. 33–54.

Albrektsson, T. & Johansson, C., 2001. Osteoinduction, osteoconduction and osseointegration. *European spine journal : official publication of the European Spine Society, the European Spinal Deformity Society, and the European Section of the Cervical Spine Research Society*, 10 Suppl 2, pp.S96–101.

Altman, G.H. et al., 2002. Cell differentiation by mechanical stress. *FASEB journal : official publication of the Federation of American Societies for Experimental Biology*, 16(2), pp.270–2.

Alvarez-Barreto, J. & Sikavitsas, V.I., 2007. Tissue Engineering Bioreactors. In J. P. Fisher, A. G. Mikos, & J. D. Bronzino, eds. *Tissue Engineering*.

Amini, A.R., Laurencin, C.T. & Nukavarapu, S.P., 2012. Bone Tissue Engineering: Recent Advances and Challenges. *Critical Reviews™ in Biomedical Engineering*, 40(5), pp.363–408.

Anil, S. & Anand, P., 2011. Dental implant surface enhancement and osseointegration. In I. Turkyilmaz, ed. *Implant Dentistry: A Rapidly Evolving Practice*.

Anon, 2014. Bone Remodeling. *Encyclopaedia Britannica Online*.

Aro, H.T., Wahner, H.T. & Chao, E.Y., 1991. Healing patterns of transverse and oblique osteotomies in the canine tibia under external fixation. *Journal of orthopaedic trauma*, 5(3), pp.351–64.

Aubin, J.E., 1998. Bone stem cells. *Journal of cellular biochemistry. Supplement*, 30-31, pp.73–82.

Balemans, W. & Van Hul, W., 2002. Extracellular regulation of BMP signaling in vertebrates: a cocktail of modulators. *Developmental biology*, 250(2), pp.231–50.

Bancroft, G.N. et al., 2002. Fluid flow increases mineralized matrix deposition in 3D perfusion culture of marrow stromal osteoblasts in a dose-dependent manner. *Proceedings of the National Academy of Sciences of the United States of America*, 99(20), pp.12600–5.

Behonick, D.J. et al., 2007. Role of matrix metalloproteinase 13 in both endochondral and intramembranous ossification during skeletal regeneration. *PloS one*, 2(11), p.e1150.

Bergmann, C.P. & Stumpf, A., 2013. *Dental Ceramics*, Berlin, Heidelberg: Springer Berlin Heidelberg.

References

Bianco, P. et al., 2001. Bone marrow stromal stem cells: nature, biology, and potential applications. *Stem cells (Dayton, Ohio)*, 19(3), pp.180–92.

Bobbio, A., 1972. The first endosseous alloplastic implant in the history of man. *Bulletin of the history of dentistry*, 20(1), pp.1–6.

Bonewald, L.F., 2011. The amazing osteocyte. *Journal of bone and mineral research : the official journal of the American Society for Bone and Mineral Research*, 26(2), pp.229–38.

Bormann, T. et al., 2012. Tailoring Selective Laser Melting Process Parameters for NiTi Implants. *Journal of Materials Engineering and Performance*, 21(12), pp.2519–2524.

Bostrom, M.P. et al., 1995. Immunolocalization and expression of bone morphogenetic proteins 2 and 4 in fracture healing. *Journal of orthopaedic research : official publication of the Orthopaedic Research Society*, 13(3), pp.357–67.

Bourgine, P. et al., 2014. Combination of immortalization and inducible death strategies to generate a human mesenchymal stromal cell line with controlled survival. *Stem cell research*, 12(2), pp.584–98.

Brighton, C.T. et al., 2001. Signal transduction in electrically stimulated bone cells. *The Journal of bone and joint surgery. American volume*, 83-A(10), pp.1514–23.

Browne, D., 2013. Skeletal System Module 5: Bone Formation and Development.

Caetano-Lopes, J. et al., 2011. Upregulation of inflammatory genes and downregulation of sclerostin gene expression are key elements in the early phase of fragility fracture healing. *PloS one*, 6(2), p.e16947.

Chao, E.Y.S. & Inoue, N., 2003. Biophysical stimulation of bone fracture repair, regeneration and remodelling. *European cells & materials*, 6, pp.72–84; discussion 84–5.

Chen, J.-H. et al., 2010. Boning up on Wolff's Law: Mechanical regulation of the cells that make and maintain bone. *Journal of Biomechanics*, 43(1), pp.108–118.

Chua, C., Leaong, K. & Lim, C., 2010. *Rapid Prototyping: Principles and Applications* 3rd ed., World Scientific Publishing Co. Pte. Ltd.

Claes, L. et al., 1997. Influence of size and stability of the osteotomy gap on the success of fracture healing. *Journal of orthopaedic research : official publication of the Orthopaedic Research Society*, 15(4), pp.577–84.

Claes, L.E. & Heigele, C. a, 1999. Magnitudes of local stress and strain along bony surfaces predict the course and type of fracture healing. *Journal of biomechanics*, 32(3), pp.255–66.

Clarke, B., 2008. Normal bone anatomy and physiology. *Clinical journal of the American Society of Nephrology : CJASN*, 3 Suppl 3, pp.S131–9.

Daculsi, G. et al., 1989. Transformation of biphasic calcium phosphate ceramics in vivo: ultrastructural and physicochemical characterization. *Journal of biomedical materials research*, 23(8), pp.883–94.

Davies, J.E., 2003. Understanding peri-implant endosseous healing. *Journal of dental education*, 67(8), pp.932–49.

Davisson, T., Sah, R.L. & Ratcliffe, A., 2002. Perfusion increases cell content and matrix synthesis in chondrocyte three-dimensional cultures. *Tissue engineering*, 8(5), pp.807–16.

Démarteau, O. et al., 2003. Development and validation of a bioreactor for physical stimulation of engineered cartilage. *Biorheology*, 40(1-3), pp.331–6.

Dimitriou, R., Tsiridis, E. & Giannoudis, P. V, 2005. Current concepts of molecular aspects of bone healing. *Injury*, 36(12), pp.1392–404.

Dong, J. et al., 2009. Response of mesenchymal stem cells to shear stress in tissue-engineered vascular grafts. *Acta pharmacologica Sinica*, 30(5), pp.530–6.

Elsinger, E.C. & Leal, L., 1996. Coralline hydroxyapatite bone graft substitutes. *The Journal of foot and ankle surgery : official publication of the American College of Foot and Ankle Surgeons*, 35(5), pp.396–9.

Ethier, C.R. & Simmons, C.A., 2007. *Introductory Biomechanics from Cells to Organisms*, Cambridge University Press, New York.

Ferrara, N. & Gerber, H.P., 2001. The role of vascular endothelial growth factor in angiogenesis. *Acta haematologica*, 106(4), pp.148–56.

Franz-Odendaal, T.A., 2011. Induction and patterning of intramembranous bone. *Frontiers in bioscience (Landmark edition)*, 16, pp.2734–46.

Van Gaalen, S. et al., 2008. Tissue Engineering of bone. In *Tissue engineering*. Elsevier Inc.

Gawlitta, D. et al., 2010. Modulating endochondral ossification of multipotent stromal cells for bone regeneration. *Tissue engineering. Part B, Reviews*, 16(4), pp.385–95.

Gentleman, E., Ball, M.D. & Stevens, M.M., 2009. Medical Sciences - Vol. II - Biomaterials. In *in Encyclopedia of Life Support Systems (EOLSS), Developed under the Auspices of the UNESCO, Eolss Publishers, Paris, France, [http://www.eolss.net]*.

Gerstenfeld, L.C. et al., 2003. Fracture healing as a post-natal developmental process: molecular, spatial, and temporal aspects of its regulation. *Journal of cellular biochemistry*, 88(5), pp.873–84.

References

Goldstein, A.S. et al., 2001. Effect of convection on osteoblastic cell growth and function in biodegradable polymer foam scaffolds. *Biomaterials*, 22(11), pp.1279–88.

Gomes, M.E. et al., 2003. Effect of flow perfusion on the osteogenic differentiation of bone marrow stromal cells cultured on starch-based three-dimensional scaffolds. *Journal of biomedical materials research. Part A*, 67(1), pp.87–95.

Goodship, A.E. & Kenwright, J., 1985. The influence of induced micromovement upon the healing of experimental tibial fractures. *The Journal of bone and joint surgery. British volume*, 67(4), pp.650–5.

Gray, H., Goss, C. & Alvarado, D., 1973. *Anatomy of the human body*,

Habibovic, P. et al., 2006. Relevance of osteoinductive biomaterials in critical-sized orthotopic defect. *Journal of orthopaedic research : official publication of the Orthopaedic Research Society*, 24(5), pp.867–76.

Habijan, T. et al., 2011. Can human mesenchymal stem cells survive on a NiTi implant material subjected to cyclic loading? *Acta biomaterialia*, 7(6), pp.2733–9.

Hauge, E.M. et al., 2001. Cancellous bone remodeling occurs in specialized compartments lined by cells expressing osteoblastic markers. *Journal of bone and mineral research : the official journal of the American Society for Bone and Mineral Research*, 16(9), pp.1575–82.

Hente, R. et al., 2004. The influence of cyclic compression and distraction on the healing of experimental tibial fractures. *Journal of orthopaedic research : official publication of the Orthopaedic Research Society*, 22(4), pp.709–15.

Hoffmann, W. et al., 2014. Reactor device for mechanical loading of tissue specimens and/or engineered tissues.

Hollister, S.J., 2005. Porous scaffold design for tissue engineering. *Nature materials*, 4(7), pp.518–24.

Hutmacher, D.W. et al., 2007. State of the art and future directions of scaffold-based bone engineering from a biomaterials perspective. *Journal of Tissue Engineering and Regenerative Medicine*, 1(4), pp.245–260.

Jagodzinski, M. et al., 2008. Influence of perfusion and cyclic compression on proliferation and differentiation of bone marrow stromal cells in 3-dimensional culture. *Journal of biomechanics*, 41(9), pp.1885–91.

Janssen, F.W. et al., 2006. A perfusion bioreactor system capable of producing clinically relevant volumes of tissue-engineered bone: in vivo bone formation showing proof of concept. *Biomaterials*, 27(3), pp.315–23.

Jeffrey, H. et al. eds., 2005. *Bone Tissue Engineering*,

Jia, W. et al., 1999. Nickel release from orthodontic arch wires and cellular immune response to various nickel concentrations. *Journal of biomedical materials research*, 48(4), pp.488–95.

Jukes, J. et al., 2008. Stem cells. In *Tissue engineering*. Elsevier Inc.

Karaplis, A.C., 2008. Chapter 3 - Embryonic Development of Bone and Regulation of Intramembranous and Endochondral Bone Formation. In J. P. Bilezikian, L. G. Raisz, & T. J. B. T.-P. of B. B. (Third E. Martin, eds. San Diego: Academic Press, pp. 53–84.

Keaveny, T.M. et al., 2004. Bone Mechanics. In *Standard handbook of Biomedical Engineering and Design*. pp. 1–24.

Knothe Tate, M.L. et al., 2008. Mechanical modulation of osteochondroprogenitor cell fate. *The international journal of biochemistry & cell biology*, 40(12), pp.2720–38.

Knothe Tate, M.L. et al., 2004. The osteocyte. *The International Journal of Biochemistry & Cell Biology*, 36(1), pp.1–8.

Kronenberg, H.M., 2003. Developmental regulation of the growth plate. *Nature*, 423(6937), pp.332–6.

Lacroix, D. et al., 2002. Biomechanical model to simulate tissue differentiation and bone regeneration: application to fracture healing. *Medical & biological engineering & computing*, 40(1), pp.14–21.

Lacroix, D., 2000. *Simulation of tissue differentiation during fracture healing*.

Lacroix, D., Planell, J.A. & Prendergast, P.J., 2009. Computer-aided design and finite-element modelling of biomaterial scaffolds for bone tissue engineering. *Philosophical Transactions of the Royal Society A: Mathematical, Physical and Engineering Sciences*, 367(1895), pp.1993–2009.

Lange, J. et al., 2010. Action of IL-1beta during fracture healing. *Journal of orthopaedic research : official publication of the Orthopaedic Research Society*, 28(6), pp.778–84.

Langer, R. & Vacanti, J.P., 1993. Tissue engineering. *Science (New York, N.Y.)*, 260(5110), pp.920–6.

Lanza, R., Langer, R. & Vacanti, J., 2000. *Principles of Tissue Engineering* Second Edi., Academic Press.

LaRochelle, W.J. et al., 1991. A novel mechanism regulating growth factor association with the cell surface: identification of a PDGF retention domain. *Genes & development*, 5(7), pp.1191–9.

Loboa, E.G. et al., 2005. Mechanobiology of mandibular distraction osteogenesis: finite element analyses with a rat model. *Journal of orthopaedic research : official publication of the Orthopaedic Research Society*, 23(3), pp.663–70.

References

Lujan, T.J. et al., 2011. A Novel Bioreactor for the Dynamic Stimulation and Mechanical Evaluation of Multiple Tissue-Engineered Constructs. *Tissue Engineering Part C: Methods*, 17(3), pp.367–74.

Mackie, E.J. et al., 2008. Endochondral ossification: how cartilage is converted into bone in the developing skeleton. *The international journal of biochemistry & cell biology*, 40(1), pp.46–62.

Mackie, E.J., Tatarczuch, L. & Mirams, M., 2011. The skeleton: a multi-functional complex organ: the growth plate chondrocyte and endochondral ossification. *The Journal of endocrinology*, 211(2), pp.109–21.

Manolagas, S.C. & Jilka, R.L., 1995. Bone Marrow, Cytokines, and Bone Remodeling — Emerging Insights into the Pathophysiology of Osteoporosis. *New England Journal of Medicine*, 332(5), pp.305–311.

Marsell, R. & Einhorn, T.A., 2011. The biology of fracture healing. *Injury*, 42(6), pp.551–5.

Martin, I. et al., 1999. Method for quantitative analysis of glycosaminoglycan distribution in cultured natural and engineered cartilage. *Annals of biomedical engineering*, 27(5), pp.656–62.

Martin, I., Wendt, D. & Heberer, M., 2004. The role of bioreactors in tissue engineering. *Trends in biotechnology*, 22(2), pp.80–6.

Matziolis, D. et al., 2011. Osteogenic predifferentiation of human bone marrow-derived stem cells by short-term mechanical stimulation. *The open orthopaedics journal*, 5, pp.1–6.

Matziolis, G. et al., 2006. Simulation of cell differentiation in fracture healing: mechanically loaded composite scaffolds in a novel bioreactor system. *Tissue engineering*, 12(1), pp.201–8.

Maul, T.M. et al., 2011. Mechanical stimuli differentially control stem cell behavior: morphology, proliferation, and differentiation. *Biomechanics and modeling in mechanobiology*, 10(6), pp.939–53.

Van der Meulen, M.C.H. & Huiskes, R., 2002. Why mechanobiology? A survey article. *Journal of biomechanics*, 35(4), pp.401–14.

Mizuno, S. et al., 2002. Hydrostatic Fluid Pressure Enhances Matrix Synthesis and Accumulation by Bovine Chondrocytes in Three-Dimensional Culture. , 327(January 2001), pp.319–327.

Mohan, S. & Baylink, D.J., 2002. IGF-binding proteins are multifunctional and act via IGF-dependent and -independent mechanisms. *The Journal of endocrinology*, 175(1), pp.19–31.

Mumme, M. et al., 2012. Interleukin-1β modulates endochondral ossification by human adult bone marrow stromal cells. *European cells & materials*, 24, pp.224–36.

Muschler, G.F. & Midura, R.J., 2002. Connective tissue progenitors: practical concepts for clinical applications. *Clinical orthopaedics and related research*, (395), pp.66–80.

Neidlinger-Wilke, C., Wilke, H.J. & Claes, L., 1994. Cyclic stretching of human osteoblasts affects proliferation and metabolism: a new experimental method and its application. *Journal of orthopaedic research : official publication of the Orthopaedic Research Society*, 12(1), pp.70–8.

NIH Consens Statement, N., 1982. Clinical Applications of Biomaterials. , pp.4(5):1–19.

Niklason, L. & Langer, R., 1997. Advances in tissue engineering of blood vessels and other tissues. *Transplant immunology*, pp.303–306.

Niklason, L.E. et al., 1999. Functional arteries grown in vitro. *Science (New York, N.Y.)*, 284(5413), pp.489–93.

Noble, B.S., 2008. The osteocyte lineage. *Archives of biochemistry and biophysics*, 473(2), pp.106–11.

Nordin, M. & Frankel, V. eds., 2001. *Basic biomechanics of the musculoskeletal system* 2nd ed.,

Nunes, I. et al., 1997. Latent transforming growth factor-beta binding protein domains involved in activation and transglutaminase-dependent cross-linking of latent transforming growth factor-beta. *The Journal of cell biology*, 136(5), pp.1151–63.

OpenStax College, 2014. Bone Structure.

OpenStaxCollege, 2014. Fractures: Bone Repair.

Park, S.H. et al., 1998. The influence of active shear or compressive motion on fracture-healing. *The Journal of bone and joint surgery. American volume*, 80(6), pp.868–78.

Phillips, A.M., 2005. Overview of the fracture healing cascade. *Injury*, 36 Suppl 3, pp.S5–7.

Pittenger, M.F. et al., 1999. Multilineage potential of adult human mesenchymal stem cells. *Science (New York, N.Y.)*, 284(5411), pp.143–7.

Post, T.M. et al., 2010. Bone physiology, disease and treatment: towards disease system analysis in osteoporosis. *Clinical pharmacokinetics*, 49(2), pp.89–118.

References

Postlethwaite, A.E. et al., 1987. Stimulation of the chemotactic migration of human fibroblasts by transforming growth factor beta. *The Journal of experimental medicine*, 165(1), pp.251–6.

Prendergast, P.J., 1997. Finite element models in tissue mechanics and orthopaedic implant design. *Clinical biomechanics*, 12(6), pp.343–366.

Protoshape, 2014. 3D metal printing.

Puetzer, J.L., Ballyns, J.J. & Bonassar, L.J., 2012. The effect of the duration of mechanical stimulation and post-stimulation culture on the structure and properties of dynamically compressed tissue-engineered menisci. *Tissue engineering. Part A*, 18(13-14), pp.1365–75.

Pugh, C.W. & Ratcliffe, P.J., 2003. Regulation of angiogenesis by hypoxia: role of the HIF system. *Nature medicine*, 9(6), pp.677–84.

Raheja, L.F. et al., 2011. Hypoxic regulation of mesenchymal stem cell migration: the role of RhoA and HIF-1α. *Cell biology international*, 35(10), pp.981–9.

Rand, J.A. et al., 1981. A comparison of the effect of open intramedullary nailing and compression-plate fixation on fracture-site blood flow and fracture union. *The Journal of bone and joint surgery. American volume*, 63(3), pp.427–42.

Rath, B. et al., 2008. Compressive forces induce osteogenic gene expression in calvarial osteoblasts. *Journal of biomechanics*, 41(5), pp.1095–103.

Ratner, B. et al., 1996. *Biomaterials science: an introduction to materials in medicine*,

Rauch, F. et al., 2000. Temporal and spatial expression of bone morphogenetic protein-2, -4, and -7 during distraction osteogenesis in rabbits. *Bone*, 26(6), pp.611–7.

Rauh, J. et al., 2011. Bioreactor systems for bone tissue engineering. *Tissue engineering. Part B, Reviews*, 17(4), pp.263–80.

Rezwan, K. et al., 2006. Biodegradable and bioactive porous polymer/inorganic composite scaffolds for bone tissue engineering. *Biomaterials*, 27(18), pp.3413–3431.

Rifkin, D.B. et al., 1999. Proteolytic control of growth factor availability. *APMIS : acta pathologica, microbiologica, et immunologica Scandinavica*, 107(1), pp.80–5.

Ritchie, R.O., 2011. The conflicts between strength and toughness. *Nature materials*, 10(11), pp.817–22.

Rubin, C. et al., 2001. The use of low-intensity ultrasound to accelerate the healing of fractures. *The Journal of bone and joint surgery. American volume*, 83-A(2), pp.259–70.

Rubin, J., Rubin, C. & Jacobs, C.R., 2006. Molecular pathways mediating mechanical signaling in bone. *Gene*, 367, pp.1–16.

Sahni, A. & Francis, C.W., 2000. Vascular endothelial growth factor binds to fibrinogen and fibrin and stimulates endothelial cell proliferation. *Blood*, 96(12), pp.3772–8.

Sahni, A., Odrljin, T. & Francis, C.W., 1998. Binding of basic fibroblast growth factor to fibrinogen and fibrin. *The Journal of biological chemistry*, 273(13), pp.7554–9.

Salgado, A.J., Coutinho, O.P. & Reis, R.L., 2004. Bone Tissue Engineering: State of the Art and Future Trends. *Macromolecular Bioscience*, 4(8), pp.743–765.

Sanchez, C. et al., 2009. Mechanical loading highly increases IL-6 production and decreases OPG expression by osteoblasts. *Osteoarthritis and cartilage / OARS, Osteoarthritis Research Society*, 17(4), pp.473–81.

Santoro, R. et al., 2010. Bioreactor based engineering of large-scale human cartilage grafts for joint resurfacing. *Biomaterials*, 31(34), pp.8946–52.

Santoro, R. et al., 2011. On-line monitoring of oxygen as a non-destructive method to quantify cells in engineered 3D tissue constructs. *Journal of tissue engineering and regenerative medicine*, 6(9), pp.696–701.

Sato, M. et al., 1999. Mechanical Tension-Stress Induces Expression of Bone Morphogenetic Protein (BMP)-2 and BMP-4, but Not BMP-6, BMP-7, and GDF-5 mRNA, During Distraction Osteogenesis. *Journal of Bone and Mineral Research*, 14(7), pp.1084–1095.

Savarino, L. et al., 1999. Effects of metal ions on white blood cells of patients with failed total joint arthroplasties. *Journal of biomedical materials research*, 47(4), pp.543–50.

Schätti, O. et al., 2011. A combination of shear and dynamic compression leads to mechanically induced chondrogenesis of human mesenchymal stem cells. *European cells & materials*, 22, pp.214–25.

Schindeler, A. et al., 2008. Bone remodeling during fracture repair: The cellular picture. *Seminars in cell & developmental biology*, 19(5), pp.459–66.

Schmidmaier, G. et al., 2003. Synergistic effect of IGF-I and TGF-beta1 on fracture healing in rats: single versus combined application of IGF-I and TGF-beta1. *Acta orthopaedica Scandinavica*, 74(5), pp.604–10.

Scotti, C. et al., 2010. Recapitulation of endochondral bone formation using human adult mesenchymal stem cells as a paradigm for developmental engineering. *Proceedings of the National Academy of Sciences of the United States of America*, 107(16), pp.7251–6.

Segal, A.W., 2005. How neutrophils kill microbes. *Annual review of immunology*, 23(2), pp.197–223.

References

Seliktar, D. et al., 2000. Dynamic mechanical conditioning of collagen-gel blood vessel constructs induces remodeling in vitro. *Annals of biomedical engineering*, 28(4), pp.351–62.

Sfeir, C. et al., 2005. Fracture Repair. In J. R. Lieberman & G. E. Friedlaender, eds. *Bone Regeneration and Repair:Biology and Clinical Applications*.

Shahin, K. & Doran, P.M., 2012. Tissue engineering of cartilage using a mechanobioreactor exerting simultaneous mechanical shear and compression to simulate the rolling action of articular joints. *Biotechnology and bioengineering*, 109(4), pp.1060–73.

Shapiro, F., 1988. Cortical bone repair. The relationship of the lacunar-canalicular system and intercellular gap junctions to the repair process. *The Journal of Bone & Joint Surgery*, 70(7), pp.1067–1081.

Shen, F.H. et al., 2002. Systemically administered mesenchymal stromal cells transduced with insulin-like growth factor-I localize to a fracture site and potentiate healing. *Journal of orthopaedic trauma*, 16(9), pp.651–9.

Sikavitsas, V.I. et al., 2005. Flow perfusion enhances the calcified matrix deposition of marrow stromal cells in biodegradable nonwoven fiber mesh scaffolds. *Annals of biomedical engineering*, 33(1), pp.63–70.

Sittichokechaiwut, A. et al., 2010. Short bouts of mechanical loading are as effective as dexamethasone at inducing matrix production by human bone marrow mesenchymal stem cell. *European cells & materials*, 20, pp.45–57.

Smith-Adaline, E.A. et al., 2004. Mechanical environment alters tissue formation patterns during fracture repair. *Journal of orthopaedic research : official publication of the Orthopaedic Research Society*, 22(5), pp.1079–85.

Stanford, C.M. & Schneider, G.B., 2004. Functional behaviour of bone around dental implants. *Gerodontology*, 21(2), pp.71–7.

Sun, M. et al., 2010. Culturing functional cartilage tissue under a novel bionic mechanical condition. *Medical Hypotheses*, 75(6), pp.657–659.

Tabata, T., 2001. Genetics of morphogen gradients. *Nature Reviews Genetics*, 2(8), pp.620–630.

Taichman, R.S., 2005. Blood and bone: two tissues whose fates are intertwined to create the hematopoietic stem-cell niche. *Blood*, 105(7), pp.2631–9.

Taira, M. et al., 2000. Studies on cytotoxicity of nickel ions using C3H10T1/2 fibroblast cells. *Journal of oral rehabilitation*, 27(12), pp.1068–72.

Thompson, C.A. et al., 2002. A Novel Pulsatile , Laminar Flow Bioreactor for the Development of Tissue-Engineered Vascular Structures. , 8(6), pp.1083–1088.

Tsiridis, E., Upadhyay, N. & Giannoudis, P., 2007. Molecular aspects of fracture healing: which are the important molecules? *Injury*, 38 Suppl 1, pp.S11–25.

De Vernejoul, M.C., Cohen-Solal, M. & Orcel, P., 1993. Bone cytokines. *Current opinion in rheumatology*, 5(3), pp.332–8.

Vunjak-Novakovic, G. et al., 1999. Bioreactor cultivation conditions modulate the composition and mechanical properties of tissue-engineered cartilage. *Journal of orthopaedic research : official publication of the Orthopaedic Research Society*, 17(1), pp.130–8.

Wan, C. et al., 2008. Role of hypoxia inducible factor-1 alpha pathway in bone regeneration. *Journal of musculoskeletal & neuronal interactions*, 8(4), pp.323–4.

Wang, Y. et al., 2007. The hypoxia-inducible factor α pathway couples angiogenesis to osteogenesis during skeletal development. , 117(6).

Weiner, S. & Wagner, H.D., 1998. THE MATERIAL BONE: Structure-Mechanical Function Relations. *Annual Review of Materials Science*, 28(1), pp.271–298.

Wendt, D. et al., 2008. Bioreactors for Tissue Engineering. In *Tissue engineering*. Elsevier Inc.

Wendt, D. et al., 2003. Oscillating perfusion of cell suspensions through three-dimensional scaffolds enhances cell seeding efficiency and uniformity. *Biotechnol Bioeng*, 84(2), pp.205–214.

Wendt, D. et al., 2006. Uniform tissues engineered by seeding and culturing cells in 3D scaffolds under perfusion at defined oxygen tensions. *Biorheology*, 43(3-4), pp.481–488.

De Wild, M. et al., 2014. Damping of Selective-Laser-Melted NiTi for Medical Implants. *Journal of Materials Engineering and Performance*.

Williams, D.F., 1999. *The Williams Dictionary of Biomaterials*, Liverpool: Liverpool University Press.

Willie, B.M. et al., 2010. Cancellous bone osseointegration is enhanced by in vivo loading. *Tissue engineering. Part C, Methods*, 16(6), pp.1399–406.

Winter, L.C. et al., 2003. Intermittent versus continuous stretching effects on osteoblast-like cells in vitro. *Journal of biomedical materials research. Part A*, 67(4), pp.1269–75.

Wolff, J., 1892. Das gesetz der transformation der knochen. *DMW-Deutsche Medizinische Wochenschrift*, 19(47), pp.1222–1224.

Wong, K. V. & Hernandez, A., 2012. A Review of Additive Manufacturing. *ISRN Mechanical Engineering*, 2012, pp.1–10.

References

Yeong, W.-Y. et al., 2004. Rapid prototyping in tissue engineering: challenges and potential. *Trends in biotechnology*, 22(12), pp.643–52.

Yim, E.K. & Sheetz, M.P., 2012. Force-dependent cell signaling in stem cell differentiation. *Stem cell research & therapy*, 3(5), p.41.

Yonemori, K., Matsunaga, S. & Ishidou, Y., 1996. Early effects of electrical stimulation on osteogenesis. *Bone*, 19(2), pp.173–180.

Yusoff, N., Abu Osman, N.A. & Pingguan-Murphy, B., 2011. Design and validation of a bi-axial loading bioreactor for mechanical stimulation of engineered cartilage. *Medical engineering & physics*, 33(6), pp.782–8.

Curriculum vitae

Waldemar Hoffmann

Sonnefäld 17
8197 Rafz
Switzerland
Phone: +41 52 53 33 025
E-Mail: w_h_@gmx.de

	Education

06/ 2010 – 08/2014	PhD Thesis: **Biomedical Engineering** *Medical Faculty, University Basel*, Tissue Engineering Laboratory (Prof. Ivan Martin) **Regulation of mesenchymal stromal cell culture in 3D collagen and NiTi scaffolds by inflammatory and biomechanical factors**
06/2010	Diploma in Bioengineering (corresponding to Master of Engineering in Bioengineering) University of Karlsruhe, Karlsruhe Institute of Technology (KIT)
11/2009 – 05/2010	Master Thesis, *Institute for Surgical Research and Hospital Management (ICFS), University Hospital Basel* Tissue Engineering Laboratory (Prof. Ivan Martin) **The osteogenic effect of BMP-2 on freshly isolated human adipose tissue derived stem cells: an in-vitro and in-vivo study**
10/2004 – 05/2010	Studies at the University of Karlsruhe Branch of studies: Bioengineering Area of concentrations: - Purification of Biomolecules - BioMEMS (micro-electro-mechanical systems)
06/2004	High school diploma at the "Kepler – Gymnasium" in *Freiburg, Germany*

Curriculum vitae

Work Experience

08/2014 - present	R&D Manager Regeneratives & Biologics, Nobel Biocare Services AG, Balz-Zimmermann-Strasse 7, 8302 Kloten, Switzerland
11/2008- 06/2009 & 03/2006- 09/2007	Student assistant at the Institute for Mechanical Process Engineering and Mechanics, University of Karlsruhe
04/2008 – 09/2008	Student research project, *University of Almeria, Spain* **Influence of dilution rate and irradiance on the production of biodiesel with Chlorella vulgaris in continuous cultivation**
10/2007 – 03/2008	Internship at zeta Bio - and Process technology, Alte Jonastraße 83, 8640 *Rapperswil, Switzerland*. Product line: Bioreactors
09/2005 – 02/2006	Student assistant at the Engler-Bunte-Institute, *University of Karlsruhe*

Skills and competences

IT	Adobe Photoshop and Illustrator, SolidWorks, COMSOL, LabView, SAP-DMS, Processing for Arduino, C++, ImageJ and the Microsoft Office suite.
Laboratory	In-vivo experimentation, PCR, SEM, EDX, confocal microscopy, histology, biochemistry, bioreactors, cell culture
Languages	German mother tongue English fluent Spanish basic knowledge

Awards

Annual Meeting of the Swiss Society for Biomaterials, 2013, *Davos, Switzerland*. Student Award Poster Presentation: *FEM analysis of porous titanium bone scaffolds.*

Patents

"Reactor device for mechanical loading of tissue specimens and/or engineered tissues"

Filing Date: 23 May 2014; Filing Number: EP 14/169756

Inventors: Waldemar Hoffmann; Conradin Döbeli; Rosaria Santoro; David Wendt; Michael de Wild

Academic activities

Publications	**Hoffmann W** et al., 2015, *Novel perfused compression bioreactor system as an in vitro model to investigate fracture healing.* Front Bioeng Biotechnol. 2015 Feb 2;3:10. doi:10.3389/fbioe.2015.00010
	Hoffmann W et al., 2014, *Rapid prototyped porous NiTi scaffolds as bone substitutes.* J Tissue Eng. 2014; doi:10.1177/2041731414540674
	Bormann T, **Hoffmann** W et al., 2014, *Combining micro computed tomography and three-dimensional registration to evaluate local strains in shape memory scaffolds.* Acta Biomater; 10(2):1024-34.
	Mumme M, **Hoffmann W** et al., 2012, *Interleukin-1β modulates endochondral ossification by human adult bone marrow stromal cells.* Eur Cell Mater.24:224-36.
	Mehrkens A, **Hoffmann W** et al., 2012 *Intra-operative engineering of osteogenic grafts combining freshly harvested, human adipose-derived cells and physiological doses of bone morphogenetic protein-2.* Eur Cell Mater.24:308-19.
Conferences	20th Swiss Conference on Biomaterials and Regenerative Medicine (SSBRM 2014), May 7th and 8th, 2014, Basel, Switzerland. *Ni release from rapid prototyped 3D NiTi scaffolds* (Oral Presentation).
	Asia Pacific Chapter of the Tissue Engineering and Regenerative Medicine International Society (TERMIS-AP), 23 - 26 October 2013, Shanghai, China. *Load-bearing scaffold for MSC-based endochondral tissue engineering based on rapid-prototyped NiTi* (Oral Presentation).

19th Swiss Conference on Biomaterials (SSB2013), 25 – 26 June 2013, Davos, Switzerland. *FEM analysis of porous titanium bone scaffolds* (Poster).

[MEET THE EXPERT] Implants, 22 – 23 April 2013, Interlaken, Switzerland. *Smart NiTi constructs for 3D cell culture applications* (Poster).

4th International Symposium Interface Biology of Implants (IBI) 2012, 09 - 11 May 2012 at Kurhaus Warnemünde, Rostock, Germany. *The Interplay of NiTi-SMA and human Bone Marrow-derived Mesenchymal Stromal Cells* (Poster).